STRUCTURE, PROPERTIES, AND POTENTIAL APPLICATIONS OF POLYDOPAMINE MATERIALS

A Dissertation
Submitted to
The Temple University Graduate Board

In Partial Fulfillment
of the Requirement for the Degree
DOCTOR OF PHILOSOPHY

By
Haoqi Li
Diploma Date August 2019

Examining committee members:
Dr. Fei Ren, Mechanical Engineering, Temple University
Dr. Jie Yin, Mechanical Engineering, Temple University
Dr. Dmitriy A. Dikin, Mechanical Engineering, Temple University
Dr. Joseph T. Coe, Civil Engineering, Temple University

ABSTRACT

Polydopamine (PDA) as a novel polymer material has attracted much attention in recent years owing to its unique universal adhesive behavior and easy fabrication through self-assembly. Its monomer form (dopamine, DA) contains catechol and amine groups, which both contribute to the adhesive properties. Since 2007, PDA has been investigated extensively by materials research communities. Application wise, most recent researches focused on utilizing PDA as surface chemistry modifiers and secondary platforms. Moreover, by heat treating PDA films in inert or reductive environments, they can carbonize and transform into a conductive form, cPDA (carbonized PDA). It has been found that cPDA has a comparable property to reduced graphene oxide (rGO). The hypothesis is that cPDA also process a layered structure with interlayer distances similar to rGO. Furthermore, with amine groups present in dopamine, cPDA can be regarded as an N-doped rGO after carbonization.

However, even with a decade of research on this topic, the structure of PDA has not yet been fully understood. In my work, the structural evolution of PDA and cPDA with different heat treatment temperature was investigated by a series of techniques including Raman spectroscopy and neutron diffraction, which revealed the progress of nanocrystal carbon growth with respective to temperature. Crystallization of the nanoscale graphitic phase also explained the electrical conductivity increase observed in our measurements.

With catechol groups in DA, PDA is capable of forming coordination bonds with metal ions. These bonds will pin the metal ions within PDA and form a metal-PDA complex (M-PDA). In the second part of my work, the effect of doping on structure and properties of PDA and cPDA was investigated. It was found that the thickness of the

doped film was thinner than the undoped film, which implied that the crosslinking mechanism of PDA was affected by the metal ion dopants. In addition, the pinned metal ions in M-PDA matrix could be reduced into their metal state after thermal annealing in a protective environment. These findings also explained the properties change in the thin film and lead us to further investigation on the mechanism of the metal reduction. Using *in situ* TEM, metal nanoparticles were observed to precipitate from M-PDA complex under irradiation of electrons. It is believed that the TEM beam directly supplied abundant electrons to facilitate the reduction of metal cations which then formed metal nanoparticles. With different metal cations, the nucleation and growth behavior and the formed nanoparticles are very different in size and shape.

This work also discovered that heating M-PDA powders or films can be used as a method for synthesis of self-supported metal nanoparticles, which has many potential future applications, such as catalysis. The performance of the synthesized metal nanoparticles as carbon-supported catalysis was tested for hydrogen generation in acid solution. It has shown that Pt nanoparticles supported on PDA substrates exhibited similar HER catalytic activity to commercial Pt/C paste, while the processing method of the PDA/Pt electrode was less time-consuming than the conventional technique.

The mechanical properties of PDA and cPDA thin films were also studied using nanoindentation. It was discovered that the elastic modulus (Young's modulus) increased with heat treatment temperature. Doping PDA with chelatable metal ions, e.g. Cu^{2+}, could also induce an increase in its elastic modulus. Meanwhile, heat treatment and metal doping seemed to reduce the viscoelasticity of PDA, which was likely related to the increase of the bonding strength.

ACKNOWLEDGMENT

I am deeply grateful for the guidance from my Ph.D. advisor Prof. Fei Ren throughout the years both academically and mentally. He has been a very good tutor and friend since 2013. In addition, throughout the years of my research, I had received countless advice and instrumental training from Dr. Dmitri A. Dikin who had supported my research in a great deal, especially in material characterization methods and techniques. I would also like to address my appreciation to Prof. Jie Yin of my dissertation committee for his discussions and suggestions during the completion of the dissertation.

Furthermore, I would also like to acknowledge my collaborators, who had helped enable my research and published articles together. This includes Mr. Yao Zhao, Dr. Zhuolei Zhang from Prof. Ren's group; Dr. Yaroslav V. Aulin, Dr. Laszlo Fraser, Mr. Tim Marshall from Prof. Eric Borguet's group, and Dr. Akila C. Thenuwara from Prof. Daniel R. Strongin's group, which both group from Chemistry department, Temple University; Ms. Adrienne Donaghue from Prof. Erica R. McKenzie's group; Dr. Gangadhar Andaluri from Civil Engineering Department; Mr. Rohit Kakodkar and Prof. Joseph Feser from University of Delaware; Dr. Ke An and Dr. Yan Chen from Oak Ridge National Laboratory. Special thanks are also given to Miss Jiaxin Xi, an undergraduate research assistant in our group for helping me on sample preparations and measurements.

Also, the author would like to give thanks to Dr. Ke Chen for training me the TEM and AFM; Prof. Xiaoxing Xi for sharing lab equipment generously; Mr. James Gannon, and Mr. John Jemison for technical support on machining and tooling of mechanical parts.

Finally, I would like to show my appreciation to both of my parents M. Li, J. Ma, and my girlfriend M. Wang for continues being supportive both in mental and material.

TABLE OF CONTENTS

ABSTRACT ii

ACKNOWLEDGMENT iv

LIST OF TABLES x

LIST OF FIGURES xi

CHAPTER 1: INTRODUCTION TO POLYDOPAMINE 1

1.1 Polydopamine (PDA) and related materials 1

1.2 Chemistry and properties 2

1.2.1 Unique properties of polydopamine 2

1.2.2 Growth, and the structure of PDA 3

1.2.3 Carbonized polydopamine (cPDA) 5

1.2.4 Metal-chelated PDA 7

1.3 Emerging applications of PDA and cPDA 8

1.4 Scope of current and future research 10

CHAPTER 2: EXPERIMENTAL METHOD 19

2.1 Overview 19

2.2 Material synthesis 20

2.2.1 PDA and M-PDA synthesis 20

2.2.2 cPDA heat treatment 22

2.2.3 Preparation of SiO_2 nanoparticles 23

2.3 Sample fabrication 24

2.3.1 CPDA/M-cPDA films for thermoelectric perperty measurements...... 24

2.3.2 Electron-beam induced metal ion reduction....................................... 25

2.3.3 Metal ion doped PDA/cPDA particle for catalytic measurement........ 25

2.4 Morphological, chemical, and compositional characterization 26

2.4.1 Scanning electron microscopy (SEM) and energy dispersive X-ray spectroscopy (EDX)... 26

2.4.2 TEM and electron diffraction 26

2.4.3 AFM... 27

2.4.4 Thin film and Powder XRD.. 27

2.4.5 Neutron scattering.. 28

2.4.6 Raman spectroscopy 28

2.4.7 XPS 29

2.4.8 BET.. 29

2.4.9 ICP-MS 29

2.5 Mechanical property characterization.. 30

2.6 Thermoelectrical property characterization 30

2.6.1 Electrical conductivity... 30

2.6.2 Seebeck coefficient.. 30

2.7 Characterization of electrocatalytical properties 31

CHAPTER 3: STRUCTURAL EVOLUTION OF CARBONIZED POLYDOPAMINE (CPDA) AND ITS THERMOELECTRIC PROPERTIES 34

3.1 Introduction... 36

3.2 Experimental method 38

3.3 Results and discussion 39

3.4 Conclusions 48

CHAPTER 4: STRUCTURE AND THERMOELECTRIC PROPERTIES OF METAL ION DOPED POLYDOPAMINE (PDA) 52

4.1 Introduction 54

4.2 Experimental Method 56

4.3 Results and discussion 58

4.4 Conclusions 65

CHAPTER 5: ELECTRON-BEAM INDUCED IN-SITU GROWTH OF SELF-SUPPORTED METAL NANOPARTICLES IN ION-CONTAINING POLYDOPAMINE 70

5.1 Introduction 72

5.2 Experimental method 74

5.2.1 Preparation of PDA powder 74

5.2.2 Preparation of PDA coated SiO_2 nanoparticles 74

5.2.3 Transmission electron microscopy experiment 75

5.3 Results and discussion 75

5.4 Conclusions 83

CHAPTER 6: MECHANICAL PROPERTIES OF POLYDOPAMINE (PDA) THIN FILMS 87

6.1 Introduction 89

6.2 Experimental details 91

6.3 Results and discussions 92

6.4 Conclusions 99

CHAPTER 7: POLYDOPAMINE (PDA) INDUCED SURFACE FUNCTIONALIZATION AND SYNTHESIS OF SELF-SUPPORTED NANO-CATALYSIS FOR HYDROGEN EVOLUTION REACTION (HER) 102

7.1 Introduction 104

7.2 Experimental Methods 106

7.2.1 Synthesis of metal NPs on PDA thin film and powder 106

7.2.2 Structural characterization 106

7.2.3 Catalytic performance 107

7.3 Results and discussions 108

7.4 Conclusions 114

CHAPTER 8: CONCLUSIONS AND FUTURE WORK 117

BIBLIOGRAPHY 120

LIST OF TABLES

Table 4.1: Room temperature electrical conductivity (σ) and Seebeck coefficient (S) of PDA thin films. 65

Table 6.1: Average film thickness measured by AFM and fitting parameters to the general Kelvin creep model. 98

LIST OF FIGURES

Figure 1.1: Chemical formula of dopamine 1

Figure 1.2: Current theories on polydopamine structure and polymerization process. Adapted from ref. 8 with permission. 4

Figure 1.3: A proposed structure of cPDA with pyridinic nitrogen and graphitic nitrogen. [after reference 11] 6

Figure 1.4: Electrical conductivity of cPDA respective to annealing temperature. [Reproduced from ref. 12 with permission.].. 6

Figure 1.5: Schematic of a (a) thermoelectric module layout, and (b) individual unit working principle. Reproduced from ref. 32 with permission from The Royal Society of Chemistry (RSC)... 11

Figure 1.6: Schematic of water hydrolysis reaction.. 13

Figure 1.7: Volcano curve of catalysis activity for hydrogen evolution reaction in acid medium. Reproduced from ref. 31 with permission. 13

Figure 2.1: PDA color at different time of synthesis, starting from left to right. 21

Figure 2.2: cPDA heat treatment temperature profile... 22

Figure 2.3: SEM image of SiO2 of 400nm diameter used in coating process............ 23

Figure 2.4: Process schematic of cPDA thin film for thermoelectric measurement... 24

Figure 2.5: Example of PDA at different stages and (d) custom-made sample holder. 24

Figure 2.6: Experimental setup for Seebeck coefficient measurement....................... 31

Figure 2.7: Schematic for electrocatalytical measurement 32

Figure 3.1: Schematics showing (a) the dopamine molecule, (b) a proposed PDA structure based on covalently bonded linear oligomers [5]. (c) a hypothetical structure of carbonized PDA [9]. Reproduced with permission from reference 5. Copyright 2013 American Chemical Society. Reproduced with permission from reference 9. Copyright 2012 John Wiley and Sons. 37

Figure 3.2: (a) SEM image of PDA film, inset is the energy dispersive spectrum. (b) TEM image of carbonized PDA powder, inset is electron diffraction. (c) Neutron pair distribution functions (PDFs) of PDA and carbonized PDA powders at different temperatures and (d) fitting of PDF of cPDA-900^{o}C using the graphite structure. The blue dots, pink line and green line are the observed data, fit data and the difference, respectively. The inset shows the average particle diameters as function of annealing temperature, which were extracted from the PDF fitting. 40

Figure 3.3: (a) Selected Raman spectra of PDA and cPDA samples with various heat treatment temperatures. (b) G peak position and I_D/I_G as a function of heat treatment temperature. (c) Migration of the G band position with respect to the crystallization degree [13] and (d) change of the I_D/I_G ratio as a function of the crystallization degree [13]. The solid lines in (c) and (d) indicate the paths for pure graphite, while the dash lines indicate the ordering trajectories of graphite with impurities. Reproduced with permission from reference 13. Copyright 2004 The Royal Society. 44

Figure 3.4: (a) Seebeck coefficient, electrical conductivity, and power factor respective to annealing temperature. (b) thermal conductivity measured by TDTR and Figure of merit respective to annealing temperature. 47

Figure 4.1: SEM image of (a) Cu-PDA, (b) Mg-PDA, and (c) Na-PDA thin films coated on Si/SiO_2 substrates. Insets show the EDS spectra obtained from areal scans.... 59

Figure 4.2: TEM images and selected area electron diffraction (SAED) of cPDA powder samples. (a) TEM image of Na-PDA powder after heat treatment at 800^{o}C. (b)&(c) TEM image and SAED of Mg-PDA powder after heat treatment at 800^{o}C. (d) & (e) TEM image and SAED of CU-PDA powder after heat treatment at 700^{o}C. (f) TEM image of Cu-PDA powder after heat treatment at 1000^{o}C. 62

Figure 4.3: Comparison of XPS spectra of (a) Cu^{2+} doped PDA (b) Mg^{2+} doped PDA before and after heat treatment at 800˚C.. 62

Figure 4.4: Effect of annealing temperature on (a) the position of the G band, and (b) intensity ratio between the D band and the G band. The increasing trends in the two sets of data indicate the conversion from amorphous carbon to nanocrystalline graphite [2, 25, and 26] in all metal ion doped samples.. 63

Figure 5.1: (a) TEM image of undoped PDA particles; (b) TEM image of Cu-PDA before electron beam treatment and (c) its diffraction pattern; (d)&(e) TEM images of Cu-PDA after electron beam treatment showing growth of nanoparticles; (f) selected area electron diffraction pattern showing diffraction rings corresponding to Cu; (g)&(h) TEM images showing Cu nano rods; (i) selected area electron diffraction pattern obtained from a Cu nanorod... 77

Figure 5.2: TEM images of (a) Ni-PDA and (b) Co-PDA after electron beam irradiation, selected area electron diffraction patterns of (c) Ni-PDA and (d) Co-PDA, (e) a single crystal Ni nanoparticle and (f) its electron diffraction pattern. 79

Figure 5.3: TEM image of (a) SiO2 particles without PDA coating, (b)&(c) SiO2 particles with PDA coating and electron beam irradiation, and (d) selected area electron diffraction pattern.. 82

Figure 6.1: Images of PDA thin films. (a) Optical images of fused silica substrate (left), PDA coating on silica (middle), and carbonized PDA on silica substrate (right). (b) SEM image of PDA freestanding film collected on silicon substrate. (c) SEM image of PDA freestanding film after heat treatment at 300˚C. 93

Figure 6.2: SEM images of freestanding Cu-PDA thin film collected on silicon substrate (a) before and (b) after heat treatment at 300˚C. (c) after heat treatment at 600˚C. (d)TEM image of Cu-PDA powder heat treated at 300˚C; and (e) selected area electron diffraction pattern of heat-treated Cu-PDA powder 95

Figure 6.3: Heat flow during the heating of pristine and Cu doped PDA powders determined by differential scanning calorimetry. 97

Figure 6.4: (a) Typical loading and unloading curve for PDA films with different treatment temperatures; (b) Young's modulus of pristine and Cu doped PDA film as a function of heat treatment temperature; (c) Typical time-dependent load and penetration curves during nanoindentation tests; (d) a selected curve showing time-dependent indentation depth during the hold period at peak load, and its fitting to the Generalized Kelvin model.. 97

Figure 7.1: (a) SEM image of Pt-PDA coated on graphite rod; (b) catalytic performance of various samples (Pt-PDA, thermally annealed Pt-PDA, and commercial Pt/C) in pH=0 sulfuric acid solution against Ag/AgCl electrode. 108

Figure 7.2: TEM images of Cu-PDA thermally annealed at (a) 600ºC, (b) 800 ºC, (c) 1000˚C; Ni-PDA thermally annealed at (d) 600 ºC, (e) 800 ºC, (f) 1000˚C; and CuNi-PDA thermally annealed at (g) 600 ºC, (h) 800 ºC, (i)1000 ˚C. SEM images of M-PDA samples containing (j) Cu, (k) Ni, and (l) Cu-Ni NPs. 110

Figure 7.3: In-situ XRD waterfall plot for (a) Cu-PDA, (b) Ni-PDA, and (c) CuNi-PDA. (d) XRD peak of Cu, Ni, and CuNi-PDA annealed at 800 ˚C. 112

Figure 7.4: catalytic performance of (a) Pt-PDA, (b) Cu-PDA, (c) Ni-PDA, (d) CuNi-PDA, coated graphite rod annealed at different temperature in pH 0 sulfuric acid against Ag/AgCl electrode. 113

CHAPTER 1: INTRODUCTION TO POLYDOPAMINE

1.1 Polydopamine (PDA) and related materials

The study of dopamine (DA, Figure 1.1) has been going on for a century starting from 1910 when dopamine was first synthesized. But it is not until mid-1950 that biologists realized its independent function in the human brain, and blood as neurotransmitter and messenger [1]. With years of studies, researchers now have a better understanding of DA in human bodies, and it is also often referred in literacy as a representative of happiness as it controls the release of multiple hormones [2]. However, the research scope on DA had not limited to biology. In 2007, DA's polymer form, polydopamine (PDA) was studied by Lee et al. as a surface chemistry modifier. Inspired by the adhesive protein secreted by the mussel foot byssus, dopamine is the smallest molecule compound that contains both catechol and amine groups, which are crucial building blocks for its surface adhesive properties [3]. PDA was the first material reported to functionalize any surface chemistry including both organic and inorganic materials [4]. Since then, PDA has been one of the focused materials in a broad range of research fields including medical, energy, biological, engineering, chemical, and environmental.

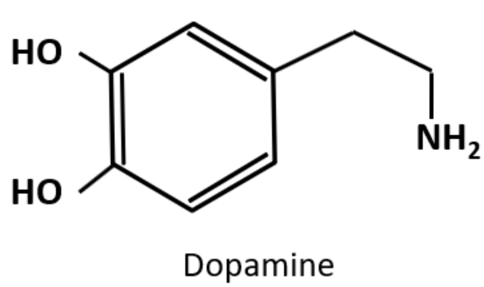

Figure 1.1: Chemical formula of dopamine

Polydopamine is a dopamine-derived melanin polymer, synthesized from tyrosine or levo-3,4-dihydroxyphenylalanine (DOPA) [5]. Melanin represents a board spectrum of both synthetic and natural pigment, and plays an essential role in the biosphere, which provides extensive protection from external stresses such as UV radiation, oxidative chemicals, high temperatures, and heavy metal, etc. In many pathogenic microbes, melanin is used to protect against immune responses from the host. And some fungi have used melanin as photosynthesis pigment to harvest light for energy [6]. In the marine environment, many squid fish also use large quantities of melanin as a 'smoke screen' to escape from the threat. In the human body, melanin is found mostly in skin and hair, which serves as a natural pigment for UV protection [7]. PDA is one of the components of the synthetic melanin, which shares similar functions and properties of melanin.

PDA's monomer form, dopamine, however, serves mostly as a neurotransmitter in neurons within the areas of the midbrain. It is believed that dopamine plays a significant role in controlling the motivational component of reward-motivated behavior. Besides, dopamine is also involved in motor controls and release of various hormones. All in all, dopamine and melanin both are vastly exist in human bodies and act in essential roles in everyone's everyday life. Their non-toxicity gives scientists and engineers possibilities of usage in medication and medical devices.

1.2 Chemistry and properties

1.2.1 Unique properties of polydopamine

Starting from 2007, after the journal article from Lee et al. has published in *Science* [3], polydopamine has attracted much attention in chemistry, and material engineering communities owing to its meritorious properties. It all begins from mimicking the chemical produced by mussel foot, which kept this marine creature sticking to the solid surface. Researchers found that the catechol and amine functional groups both are fundamental building blocks in providing this unique behavior, in fact, dopamine is regarded as the smallest molecule that contains both catechol and amine groups.

Polydopamine, as a synthetic polymer, only requires a mild alkaline condition and an oxidizer to promote its auto-polymerization. Also, polydopamine can form a thin film coating on surfaces of almost any kind of materials. The coating thickness grown from solution could reach up to 50 nm with auto polymerization. The PDA films are usually uniform, smooth, and crack free. The produced film can also be taken out and regrow on a newly made solution to reach a higher thickness through a layer-by-layer (LbL) assembly process. This universal coating property has opened up plenty of potential surface engineering applications such as control of hydrophobicity, tuning of surface chemistry, and protective coating, etc.

In summary, there are two significant properties that attracted the most attention to this material: the simplicity of fabrication; and universal thin film coating formation.

1.2.2 Growth, and the structure of PDA

Although the study on PDA in material science has been going on for over a decade, there has been no governing reaction formula that fully describes the reaction process and the exact structure of PDA. Some proposed structures of PDA are shown in Figure 1.2 [8]. Dopamine undergoes an oxidation process, which becomes quinone and could be further oxidized into 5,6-dihydroxyindole (DHI) by the cyclization of amine. Those three monomers coexist in solution and will all be contributing to stacking and polymerizing. Pi-pi stacking and hydrogen bonding could be formed between layers of monomers; while covalent bonding could be formed between monomers at various sites. Typically, to create a long chain of the polymer backbone, monomers are linked through the binding site located on benzene rings. As shown in Figure 1.2, in the PDA backbone, several forms of building monomers exist. In addition, crosslinking between polymers could also form on indole group, which could potentially build up the side chain or elongate the backbone. Furthermore, research has also suggested that during the polymerization process, two dopamine monomers tend to clamp one DHI through physical interaction cross plane, forming a physical trimer. This result reveals that this is the only physical absorption pathway to form PDA [9].

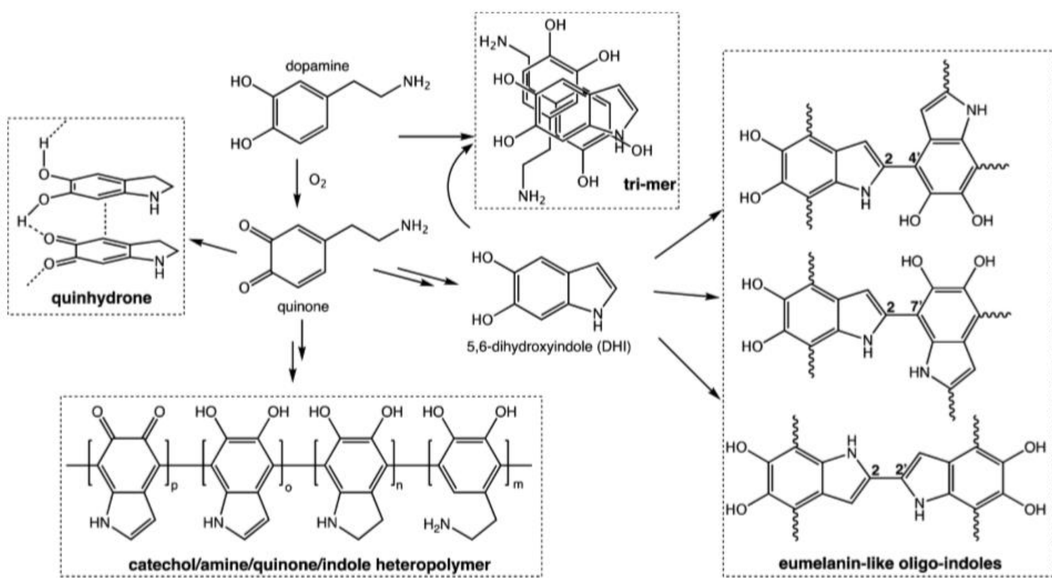

Figure 1.2: Current theories on polydopamine structure and polymerization process. Adapted from ref. 8 with permission.

1.2.3 Carbonized polydopamine (cPDA)

By annealing the thin film or collected powder under an inert atmosphere, PDA undergoes a transformation from an electrical insulator to a semiconductor. As mentioned previously, PDA is composed of primarily benzene ring and indole rings. CPDA can successfully inherit nitrogen from its precursor. As shown in the XPS result from Ai et al. [10], in cPDA system, there is roughly 1/3 amount of pyridinic nitrogen and 2/3 graphitic nitrogen (Figure 1.3). In addition, the carbonization process also removes the oxygen from the PDA system by a significant amount. A proposed structure of cPDA is shown in Figure 1.3, which is considered similar to N-doped graphene. The level of carbonization is directly related to the heat treatment temperature. As shown in Figure 1.4, the electrical conductivity of cPDA increases with the increasing annealing temperature. Finally, after carbonization at 1000˚C, cPDA exhibit an electrical conductivity of 1.2×10^5 S/m, which is even higher than the reduced graphene oxide (Figure 1.4).

TEM study of carbonized PDA has revealed some more detailed information on the structure of cPDA. Kong et al. [11] observed a layered structure of cPDA coated on SiO_2 particles and found cPDA possessed a multilayered structure. This result was confirmed by Yu et al. [13], who found the interlayer spacing of cPDA to be 0.34 nm. Both researchers have found an XRD peak of cPDA at $2\theta = 22^\circ$, which corresponds to the d-spacing of 0.34 nm. Raman spectroscopic study, which is sensitive to carbon structures, D and G peak at roughly 1300 cm^{-1} and 1550cm^{-1} both intensified after heat treatment [14,15]. It is also worth mentioning that the ratio between the D and G peak decreased with heat treatment, which implies an increase in the crystallization degree.

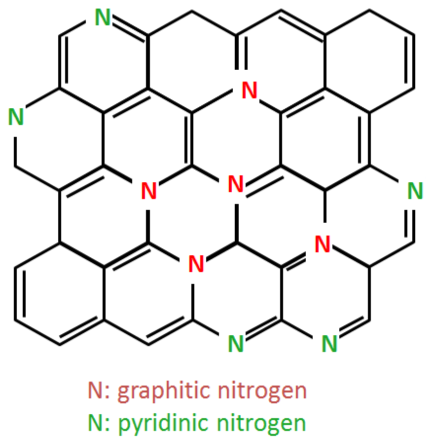

Figure 1.3: A proposed structure of cPDA with pyridinic nitrogen and graphitic nitrogen. [after reference 11]

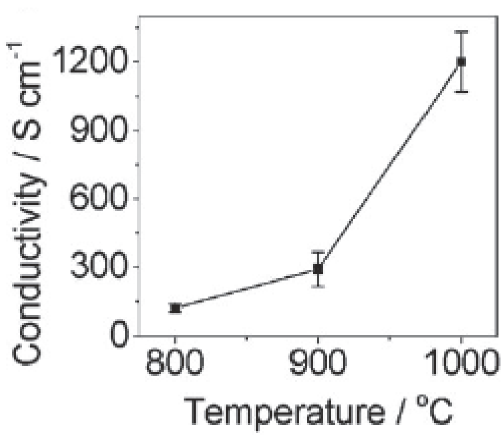

Figure 1.4: Electrical conductivity of cPDA respective to annealing temperature. [Reproduced from ref. 12 with permission.]

1.2.4 Metal-chelated PDA

PDA's ability of adhesion is enabled by its catechol and amine groups, which can form dative ligands with other elements. It has been well studied that transition metals are able to form strong coordination covalent bonds with catechol groups. Doping of PDA can be achieved by direct addition of metal ions into either unpolymerized dopamine solution or the PDA-buffer mixture. This simple one-pot synthesis has been utilized to study the chelation between PDA and a wide range of metal ions, including Cr^{3+}, Mn^{2+}, Fe^{3+}, Fe^{2+}, Co^{2+}, Ni^{2+}, Cu^{2+}, Zn^{2+}, Hg^{2+}, Ag^{+}, Pt^{2+}, Au^{3+}, W^{6+}, Ga^{2+}, Ge^{2+} [16-20].

Several applications have been developed based on this property of PDA. For example, the ability to form a coordination bond is used by water filtration and purification [21]. A heavy metal pollutant can be absorbed by PDA nanoparticles and remove from solution. Also, some metal ions can be directly pinned by coordination bonding without further processing. The M-PDA system could potentially be used in MRI imaging [22]. For Ag^{+}, and Au^{3+}, dopamine can reduce them into its metal forms. Therefore, PDA film is used in surface chemical modification. On the surfaces where Ag or Au is needed to form nanoparticles, a thin layer of PDA could be pre-coated and by simple immersion of the sample into $AgNO_3$ or $AuCl_3$ solutions, uniformly distributed Ag or Au metal nanoparticles can form on the substrate [23]. In the research field of hydrolysis catalysis [24-25], M-PDA is also used to form metal nanoparticles or metal oxide particles within a PDA matrix. The PDA could be carbonized in an inert environment, which convert into electrically conductive N-doped carbon form.

1.3 Emerging applications of PDA and cPDA

Owing to their many interesting properties and behaviors of PDA and cPDA, there are several applications proposed using PDA and cPDA [5,26-28]. Most of those applications utilize the ability of PDA to form chelation with metal ions such as water treatment and target drug delivery while others use the conducting property of cPDA after heat treatment.

In water purification, bonding strength and number of active sites are two crucial parameters for the absorbents, where PDA is excellent in both aspects. Since PDA is mainly composed of catechol groups and amine groups, it offers plenty of active sites for metal capturing through chelation, hydrogen bonding, or pi-pi interactions. As an example, Cu is one of the elements that widely existed in the environment. It plays an essential role in the human body’s functionality. However, exceeding amount of Cu intake will damage human cells and cause multiple diseases. PDA offers large amount of binding site and strong absorption to remove Cu from water. The maximum absorption capacity is 34.4mg/g in 5h. Although the absorption is not high enough to be industrialized as this moment, there are potential to increase the surface area and enhance this purification ability [21].

Although stand-alone PDA might not offer sufficient absorption of metal ions, by combining PDA and other magnetic particles, it offers a unique capability in the water purification applications. PDA coated magnetic nanoparticles not only can absorb the metal ion contaminations from water, but also enable easily removal from solution by applying a magnetic field [30]. This prevents secondary contamination and provides a simple solution for separation. In addition, PDA coating can also be used as a secondary reaction platform. With the chemical reduction property of PDA, Ag nanoparticles could be directly reduced and evenly decorated on the PDA thin film by submerging PDA coating in AgCl solution. The reduced Ag NPs could be used for anti-biotics [29].

Regarding potential applications of cPDA, Li and coworker [12] had successfully fabricated wafer-scaled cPDA thin film and demonstrated its potential in flexible transparent conductive electrodes. CPDA circuits were made by first masking the substrate and exposing circuit pattern for coating. Then PDA was coated on copper foil followed by removal of the mask, and pyrolysis. CPDA could then be transported onto flexible PDMS with a simple peel-off method. The transferred cPDA remained conductive when being bended, and its resistance could be changed by changing the bending curvature or application of light. The potential of the cPDA as flexible electrodes is far beyond making simple strain gauges or light sensors.

PDA could also be used to modify surface chemistry and serve as interfacial fillers or binders. With following thermal annealing, carbonized PDA offers superior interfacial electrical conductivity. Ryu et al. [30] submerged carbon nanotubes (CNTs) into dopamine solution. The adhesion of the PDA coating on the CNTs helped to bind the CNTs. After pyrolysis in H_2 environment at 1050 ˚C for 2h, the interfacial cPDA resulted in high conductivity while holding CNTs together. The use of PDA interfacial binder results in ~ 400% increase in mechanical strength and ~ 630% increase in electrical conductivity. A more recent research by Zou et al. [31] utilized the PDA nanoparticle as a filler between graphene oxide (GO) sheets and underwent pyrolysis at 3000 ˚C. This work resulted in a densely packed graphene paper with cPDA, which increased the mechanical strength, the electrical conductivity, and the thermal conductivity to 47 MPa, 0.89×10^6 S/m, and 1584 W/mK, respectively.

1.4 Scope of current and future research

This dissertation aimed to obtain a deeper understanding of structures of PDA and its related materials, primarily the carbonized PDA and the metal-ion doped PDA. The first part of my studies were focused on the structural characterization in response to thermal annealing and metal ion doping, the effect of processing conditions on the mechanical properties, and the catalytic performance of M-PDA. Furthermore, this work explored the potential of PDA and cPDA in energy related applications, primarily thermoelectrics and electrochemical water splitting (hydrogen evolution reaction).

Thermoelectricity refers to the direct conversion between electric energy and thermal energy. Thermoelectric elements/devices (Figure 1.5) can generate a thermovoltage when subject to a temperature gradient (the Seebeck effect), or they can be used to pump heat using electrons or holes as the energy carrier (the Peltier effect). A key property characterizing the material's thermoelectric performance is the dimensionless Figure of merit, ZT, which is defined as

$$ZT = \frac{S^2}{\rho\lambda}T \qquad \text{(Eq. 1.1)}$$

where T is the temperature, ρ is the electrical resistivity, λ is the thermal conductivity, and S is the Seebeck coefficient that can be calculated from the ratio between the thermovoltage, ΔV and the temperature different ΔT,

$$S = \frac{\Delta V}{\Delta T} \qquad \text{(Eq. 1.2)}$$

Thermoelectric properties of carbon-based nanoscale materials have drawn much attention in recent years, with potential use in wearable devices and where thin film electrodes and fine prints are needed. In this work, the electrical and thermal conductivity, and the Seebeck coefficient of PDA and cPDA materials were measured at room temperature. Effects of heat treatment and metal ion doping were studied, which provided a comprehensive understanding of the thermoelectric performance of the PDA materials at ambient condition.

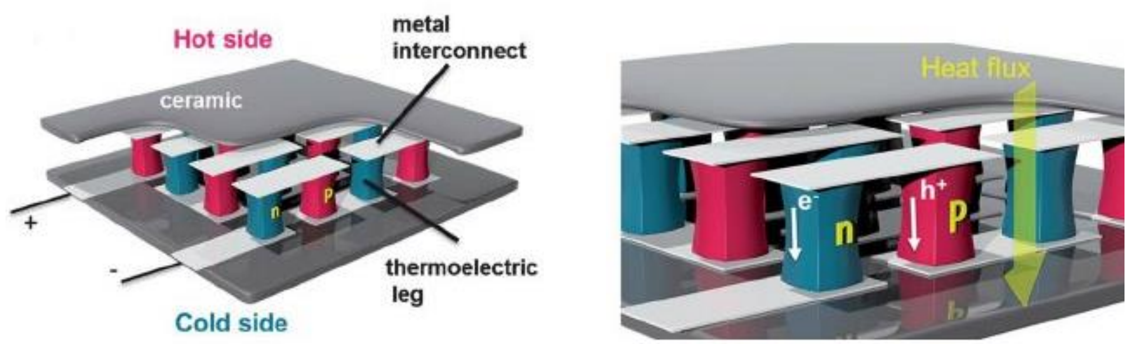

(a) (b)

Figure 1.5: Schematic of a (a) thermoelectric module layout, and (b) individual unit working principle. Reproduced from ref. 32 with permission from The Royal Society of Chemistry (RSC).

Hydrogen is considered one of the ideal candidates for energy storage owing to its high gravimetric energy density, high elemental abundance, and zero emission after combustion. The harvested renewable energy could be stored in hydrogen by water hydrolysis using wind power or solar energy. Storage of the harvested energy in the form of chemical fuel make it easy to transport and storage. A simple schematic of this reaction is shown in Figure 1.6. This process benefits from abundance of water and high reaction yield owing to the high selectivity of the reaction.

Water splinting reaction is described by following equations,

Overall: $H_2O = H_2 \uparrow + O_2 \uparrow$ (Eq. 1.3.)

Oxygen evolution: $H_2O = \frac{1}{2}O_2 + 2H^+ + 2e^-$ (Eq. 1.4)

Hydrogen evolution: $2H^+ + 2e^- = H_2$ (Eq. 1.5)

Hydrogen evolution reaction, or HER, is a half reaction of the water splitting. Even though the reaction only involves two electrons for each generated hydrogen molecule, the multiple elemental reaction induces an accumulation of energy barriers and result in slow kinetic. A variety of HER catalysts has been found to play significant role in expediting the reactions. Through years of study on hydrolysis catalysis, the well-known volcano curve (Figure 1.7) represents the exchange current density of HER in acid solutions [33]. This curve could serve as a comprehensive guideline when designing catalysis. Platinum based materials have shown highest conversion activity. However, due to the low abundance of elemental Pt in the Earth crust, its application has been limited by the high cost. Alternative, low-cost, high activity catalysts for HER are highly demanded.

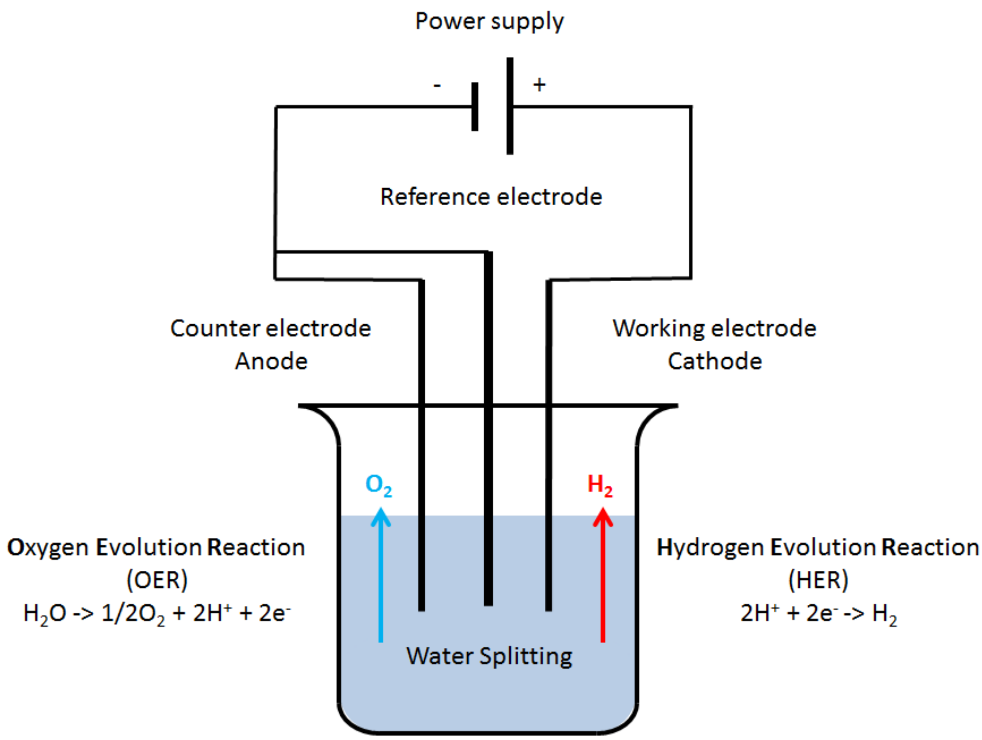

Figure 1.6: Schematic of water hydrolysis reaction

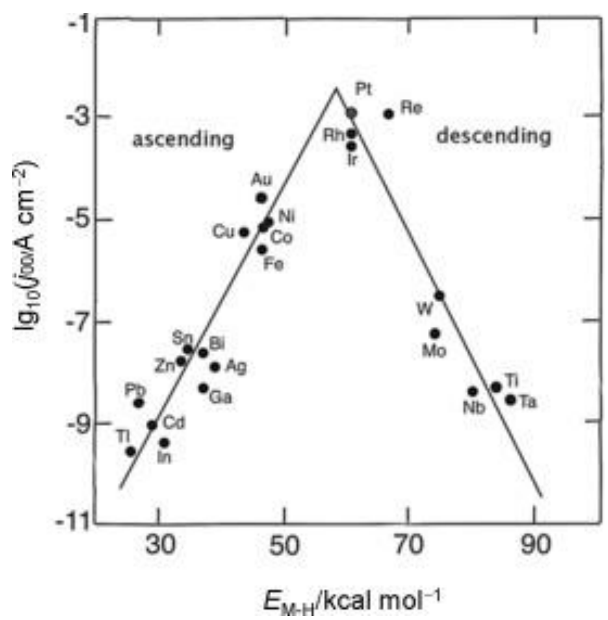

Figure 1.7: Volcano curve of catalysis activity for hydrogen evolution reaction in acid medium. Reproduced from ref. 31 with permission.

The second group with high reaction activity including Ni, Co, Cu, and Fe, which are all non-precious metals. To partially or entirely replace Pt by those metals while maintaining the activity is one of the goals in current catalytic research. Recently, nickel based eletrocatalysts in the shape of nickel foam, alloys, nitrides, phosphides, oxides and metal organic frameworks [34-39] have exhibited very promising activity and stability towards HER. Ni is in the same group in the periodic table as Pt and it has some similar chemical properties to Pt. Furthermore, Ni is much cheaper and more abundant than Pt [40]. Therefore, many researchers are inspired to utilize Ni-based eletrocatalysts in clean energy production as an alternative to Pt, which typically involves incorporating Ni based derivatives with newly developed material with high surface area.

In this work, the HER performance of Pt decorated PDA material was studied by measuring the current vs. voltage curve (I-V curve) in acidic conditions, which was compared to commonly used Pt/C material. Other PDA-metal nanoparticle materials containing Ni, Cu, and Ni-Cu, were also examined as potential HER catalysts. For any applications, the mechanical properties play an pivotal role in the device integrity. In this work, the mechanical properties of PDA and cPDA films were evaluated using nanoindentation as a function of heat treatment and metal ion doping.

REFERENCE

[1] C. A. Marsden, "Dopamine: the rewarding years," *Br J Pharmacol,* vol. 147 Suppl 1, pp. S136-44, Jan 2006.

[2] K. C. Berridge, T. E. Robinson, and J. W. Aldridge, "Dissecting components of reward: 'liking', 'wanting', and learning," *Curr Opin Pharmacol,* vol. 9, no. 1, pp. 65-73, Feb 2009.

[3] H. Lee, S. M. Dellatore, W. M. Miller, and P. B. Messersmith, "Mussel-Inspired Surface Chemistry for Multifunctional Coatings " *science*, vol. 318, p. 5, 2007.

[4] K. S. Schanze, H. Lee, and P. B. Messersmith, "Ten Years of Polydopamine: Current Status and Future Directions," *ACS Appl Mater Interfaces,* vol. 10, no. 9, pp. 7521-7522, Mar 7 2018.

[5] M. E. Lynge, R. van der Westen, A. Postma, and B. Stadler, "Polydopamine - a nature-inspired polymer coating for biomedical science," *Nanoscale,* vol. 3, p. 13, 2011.

[6] b. l. G. A.J. Hamilton, "Melanins in fungal pathogens," *Journal of Medical Microbiology*, vol. 51, 2002.

[7] N. Kollias, "the spectroscopy of human melanin pigmentation," *Melanin: its role in human photoprotection,* 1995.

[8] J. H. Ryu, P. B. Messersmith, and H. Lee, "Polydopamine Surface Chemistry: A Decade of Discovery," *ACS Appl Mater Interfaces,* vol. 10, no. 9, pp. 7523-7540, Mar 7 2018.

[9] Y. Ding *et al.*, "Insights into the aggregation/deposition and structure of a polydopamine film," *Langmuir,* vol. 30, no. 41, pp. 12258-69, Oct 21 2014.

[10] K. Ai, Y. Liu, C. Ruan, L. Lu, and G. M. Lu, "Sp2 C-dominant N-doped carbon sub-micrometer spheres with a tunable size: a versatile platform for highly efficient oxygen-reduction catalysts," *Adv Mater,* vol. 25, no. 7, pp. 998-1003, Feb 20 2013.

[11] J. Kong *et al.*, "Highly electrically conductive layered carbon derived from polydopamine and its functions in SnO2-based lithium ion battery anodes," *Chem Commun (Camb),* vol. 48, no. 83, pp. 10316-8, Oct 25 2012.

[12] R. Li, K. Parvez, F. Hinkel, X. Feng, and K. Mullen, "Bioinspired wafer-scale production of highly stretchable carbon films for transparent conductive electrodes," *Angew Chem Int Ed Engl,* vol. 52, no. 21, pp. 5535-8, May 17 2013.

[13] X. Yu, H. Fan, Y. Liu, Z. Shi, and Z. Jin, "Characterization of carbonized polydopamine nanoparticles suggests ordered supramolecular structure of polydopamine," *Langmuir*, vol. 30, no. 19, pp. 5497-505, May 20 2014.

[14] A. C. Ferrari and J. Robertson, "Raman spectroscopy of amorphous, nanostructured, diamond-like carbon, and nanodiamond," *Philos Trans A Math Phys Eng Sci*, vol. 362, no. 1824, pp. 2477-512, Nov 15 2004.

[15] A. C. Ferrari, "Raman spectroscopy of graphene and graphite: Disorder, electron–phonon coupling, doping and nonadiabatic effects," *Solid State Communications*, vol. 143, no. 1-2, pp. 47-57, 2007.

[16] K. M. Im, T.-W. Kim, and J.-R. Jeon, "Metal-Chelation-Assisted Deposition of Polydopamine on Human Hair: A Ready-to-Use Eumelanin-Based Hair Dyeing Methodology," *ACS Biomaterials Science & Engineering*, vol. 3, no. 4, pp. 628-636, 2017.

[17] T.-L. Chang, X. Yu, and J. F. Liang, "Polydopamine-enabled surface coating with nano-metals," *Surface and Coatings Technology*, vol. 337, pp. 389-395, 2018.

[18] X. Guo *et al.*, "Fabrication of Co@SiO2@C/Ni submicrorattles as highly efficient catalysts for 4-nitrophenol reduction," *Dalton Trans*, vol. 46, no. 35, pp. 11598-11607, Sep 12 2017.

[19] Y. Liang *et al.*, "Metal-polydopamine frameworks and their transformation to hollow metal/N-doped carbon particles," *Nanoscale*, vol. 9, no. 16, pp. 5323-5328, Apr 20 2017.

[20] C. Liu *et al.*, "Noble-metal-free tungsten oxide/carbon (WOx/C) hybrid manowires for highly efficient hydrogen evolution," *Nanotechnology*, vol. 28, no. 44, p. 445403, Nov 3 2017.

[21] N. Farnad, K. Farhadi, and N. H. Voelcker, "Polydopamine Nanoparticles as a New and Highly Selective Biosorbent for the Removal of Copper (II) Ions from Aqueous Solutions," *Water, Air, & Soil Pollution*, vol. 223, no. 6, pp. 3535-3544, 2012.

[22] Z. Wang *et al.*, "Tunable, Metal-Loaded Polydopamine Nanoparticles Analyzed by Magnetometry," *Chemistry of Materials*, vol. 29, no. 19, pp. 8195-8201, 2017.

[23] Z. Wang *et al.*, "High Relaxivity Gadolinium-Polydopamine Nanoparticles," *Small*, vol. 13, no. 43, Nov 2017.

[24] D. Zhou *et al.*, "Fe/N/C hollow nanospheres by Fe(iii)-dopamine complexation-assisted one-pot doping as nonprecious-metal electrocatalysts for oxygen reduction," *Nanoscale*, vol. 7, no. 4, pp. 1501-9, Jan 28 2015.

[25] Y. Zhao, C. Wang, J. Liu, and F. Wang, "PDA-assisted formation of ordered intermetallic CoPt3 catalysts with enhanced oxygen reduction activity and stability," *Nanoscale,* vol. 10, no. 19, pp. 9038-9043, May 17 2018.

[26] C. E. Brubaker and P. B. Messersmith, "The present and future of biologically inspired adhesive interfaces and materials," *Langmuir,* vol. 28, no. 4, pp. 2200-5, Jan 31 2012.

[27] Y. Liu, K. Ai, and L. Lu, "Polydopamine and its derivative materials: synthesis and promising applications in energy, environmental, and biomedical fields," *Chem Rev,* vol. 114, no. 9, pp. 5057-115, May 14 2014.

[28] D. R. Dreyer, D. J. Miller, B. D. Freeman, D. R. Paul, and C. W. Bielawski, "Perspectives on poly(dopamine)," *Chemical Science,* vol. 4, no. 10, 2013.

[29] R. Cai *et al.*, "One-Step Synthesis of Silver Nanoparticles on Polydopamine-Coated Sericin/Polyvinyl Alcohol Composite Films for Potential Antimicrobial Applications," *Molecules*, vol. 22, no. 5, Apr 30 2017.

[30] S. Ryu *et al.*, "Direct Insulation-to-Conduction Transformation of Adhesive Catecholamine for Simultaneous Increases of Electrical Conductivity and Mechanical Strength of CNT Fibers," *Adv Mater,* vol. 27, no. 21, pp. 3250-5, Jun 3 2015.

[31] R. Zou *et al.*, "Carbonized polydopamine nanoparticle reinforced graphene films with superior thermal conductivity," *Carbon,* vol. 149, pp. 173-180, 2019.

[32] O. Bubnova and X. Crispin, "Towards polymer-based organic thermoelectric generators," *Energy & Environmental Science,* vol. 5, no. 11, 2012.

[33] P. Quaino, F. Juarez, E. Santos, and W. Schmickler, "Volcano plots in hydrogen electrocatalysis - uses and abuses," *Beilstein J Nanotechnol,* vol. 5, pp. 846-54, 2014.

[34] D. He *et al.*, "Amorphous nickel boride membrane on a platinum-nickel alloy surface for enhanced oxygen reduction reaction," *Nat Commun,* vol. 7, p. 12362, Aug 9 2016.

[35] B. Zhang, C. Xiao, S. Xie, J. Liang, X. Chen, and Y. Tang, "Iron–Nickel Nitride Nanostructures in Situ Grown on Surface-Redox-Etching Nickel Foam: Efficient and Ultrasustainable Electrocatalysts for Overall Water Splitting," *Chemistry of Materials,* vol. 28, no. 19, pp. 6934-6941, 2016.

[36] P. W. Menezes *et al.*, "Uncovering the Nature of Active Species of Nickel Phosphide Catalysts in High-Performance Electrochemical Overall Water Splitting," *ACS Catalysis,* vol. 7, no. 1, pp. 103-109, 2016.

[37] M. P. Browne *et al.*, "The goldilocks electrolyte: examining the performance of iron/nickel oxide thin films as catalysts for electrochemical water splitting in various aqueous NaOH solutions," *Journal of Materials Chemistry A,* vol. 4, no. 29, pp. 11397-11407, 2016.

[38] V. Vij *et al.*, "Nickel-Based Electrocatalysts for Energy-Related Applications: Oxygen Reduction, Oxygen Evolution, and Hydrogen Evolution Reactions," *ACS Catalysis,* vol. 7, no. 10, pp. 7196-7225, 2017.

[39] J. Duan, S. Chen, and C. Zhao, "Ultrathin metal-organic framework array for efficient electrocatalytic water splitting," *Nat Commun,* vol. 8, p. 15341, Jun 5 2017.

[40] M. Gong *et al.*, "Nanoscale nickel oxide/nickel heterostructures for active hydrogen evolution electrocatalysis," *Nat Commun,* vol. 5, p. 4695, Aug 22 2014.

CHAPTER 2: EXPERIMENTAL METHOD

2.1 Overview

This Chapter discusses the major experimental methods used in this study in detail, including materials and instruments used in the experiments, PDA synthesis and post-synthesis processing, and all different characterization methods.

Both thin film and powder PDA materials were synthesis in tris(hydroxymethyl)aminomethane (TRIS) buffer of pH 8.5 via a self-assembly process. All synthesis of PDA (powder or film) was conducted under ambient pressure and temperature. Carbonized PDA (cPDA) was obtained by thermal annealing PDA in a tube furnace under inner atmosphere.

Morphology of samples was characterized by scanning electron microscopy (SEM, 10 kV, FEI Quanta450 FEG SEM, FEI Inc. Hillsboro, OR), transmission electron microscopy (TEM, 120 kV, JEM-1400, JEOL, Tokyo, Japan), and atomic force microscopy (AFM, MMAFMLN-AM, Veeco Metrology, Horsham, PA). Selected area electron diffraction (SAED, in TEM), X-ray diffraction (XRD, Bruker D8 Discover diffractometer, Bruker, Billerica, MA; X'Pert Pro, Malvern PANalytical Ltd., Malvern, United Kingdom), and neutron diffraction were used to examine the structures of the PDA materials. Raman spectroscopy was conducted to characterize the carbon phase in PDA. X-ray photoelectron spectrum (XPS, VG Scientific 100 mm hemispherical analyzer and a Physical Electronics Mg Ka X-ray source operating at 300 W, Thermo Fisher Scientific Inc., Walthan, MA) was performed to examine the chemical states of various metals in the M-PDA. Neutron diffraction conducted at Oak Ridge National Laboratory was used to examine the structure of PDA and cPDA. Surface area and porous size of the powder sample were tested using Brunauer-Emmett-Teller (BET) method. For detailed compositional analysis of the metal ion concentration in doped PDA (M-PDA), inductively coupled plasma mass spectroscopy (ICP-MS, Agilent 7900, Agilent Technologies, Santa Clara, CA) was conducted.

Electrical conductivity of cPDA thin film was calculated based on the film dimension and the resistance measured by digital multi-meter (DMM, Model 2700, Keithley, Cleveland, OH). To measure the Seebeck coefficient, a temperature gradient was applied across the sample while a thermovoltage was recorded. The temperatures of the sample was measured using thermocouples connected to a digital data logger. The Young's modulus, hardness, and viscoelastic behavior of PDA/cPDA/M-PDA films were measured by nano-indentation (Triboindenter TI980, Bruker, Billerica, MA) with a conical tip. Electrocatalysis measurements, including over potential of catalysis during hydrolysis and Tafel slope were conducted on electrochemical workstation (Versastat 3, Ametek, Berwyn, PA).

2.2 Material synthesis

2.2.1 PDA and M-PDA synthesis

Tris buffer (BP1761, Thermo Fisher Scientific Inc., Walthan, MA), was diluted from 2M to 50 mM, and pH adjusted to 8.5 by hydrochloride acid (SA48, Thermo Fisher Scientific Inc., Walthan, MA). To synthesis PDA, 2mg/mL of the commercially available dopamine hydrochloride (Alfa Aesar, Haverhill, MA) was added into tris buffer. For powder sample synthesis, the mixture was agitated with a magnetic stir for 24 hours to ensure the completion of the reaction. Figure 2.1 shows the color change during the synthesis. The PDA powders were then centrifuged at 3500g for 10min. Sediment was separated and washed with D.I. water. This centrifuge-wash process was repeated for at least three times, followed by drying in an oven at 50˚C for overnight. For thin film coating, the substrates were submerged into the solution before the reaction started and the mixture was commonly remained still during the process to minimize any disturbance to the film growth. Substrates were then taken out and rinsed with deionized water and dried in the oven at 50˚C overnight. If thicker film was needed, a new patch of solution shall be made to repeat the coating process for additional coating.

Metal-ion doped PDA was made by addition of selected metal before the polymerization reaction happened. In this study, metal cations used included Na^{+}, Mg^{2+}, Cu^{2+}, Ni^{2+}, and Co^{2+}. For bi-metallic doping, two metal cations were introduced. The molar ratio between DA and metal cations was controlled to ensure the repeatability. The rest of the fabrication and collection process was the same as described in the previous paragraph. PDA/M-PDA coating on SiO_2 nanoparticle (NP) of 400 nm diameter was also prepared using the similar method. Coated SiO_2 powder was then collected by centrifuge-wash method and finally dried in the oven at 50˚C.

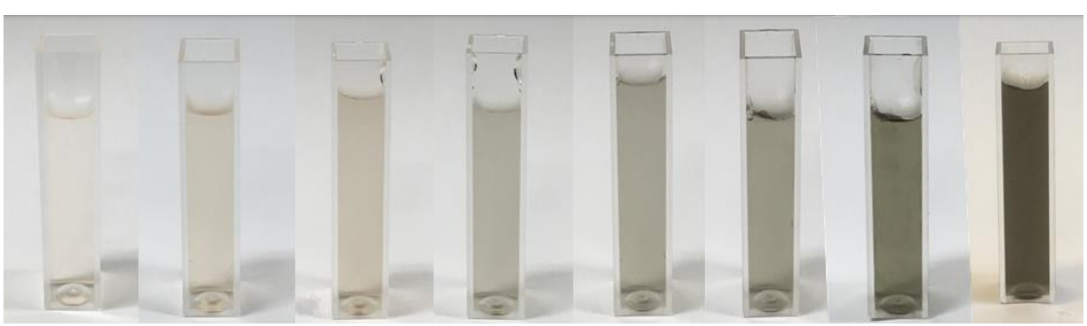

Figure 2.1: PDA color at different time of synthesis, starting from left to right.

2.2.2 cPDA heat treatment

PDA is thermally annealed under inert environment (argon) or reductive environment (N_2 with 5% H_2). Samples to be heat treated were placed in the tube furnace on quartz crucibles. Tube was then purged with gas for more than 5 times to ensure the removal of air. The heating and cooling rate was controlled at 5˚C/min. Figure 2.2 shows the controlled temperature change with respective to time. Temperature was kept for 1 hour when target temperature was reached to ensure completion of expected carbonization. During the heat treatment, a slightly elevated pressure running Ar was used to ensure no air leakage into the tube. Once the temperature cools down to room temperature, samples were then taken out for further processing.

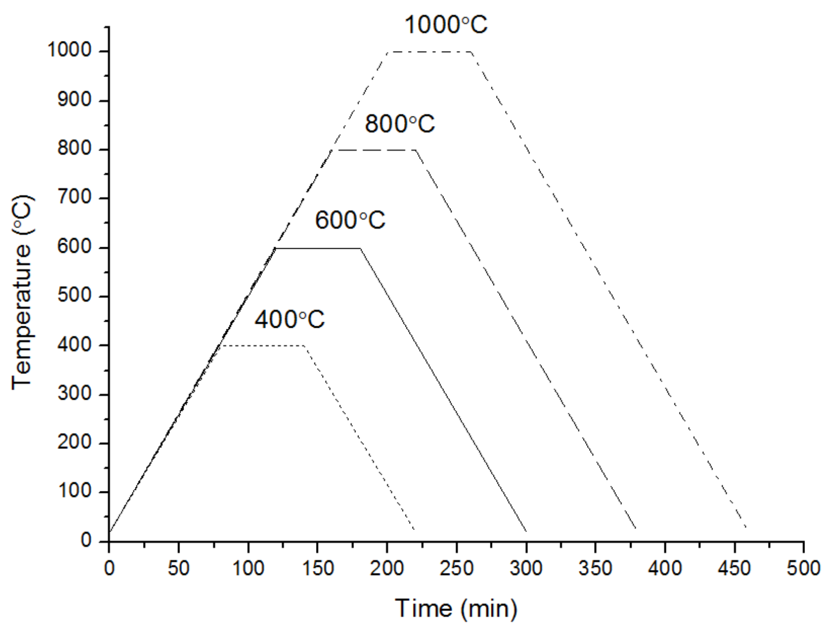

Figure 2.2: cPDA heat treatment temperature profile

2.2.3 Preparation of SiO_2 nanoparticles

SiO_2 nanoparticles (NPs) were made by the modified Stober method [1]. Firstly, 25 mL ethanol (200 proof, Decon Labs Inc., King of Prussia, PA) and 25 mL deionized water were mixed for 10 min using a magnetic stirrer. Then, 2 mL of tetraethyl orthosilicate (TEOS, Aldrich, St. Louis, MO) was added to the solution while keeping the solution stirred. After 20 min of TEOS addition, 4 mL of 28% ammonium hydroxide (NH_4OH, Fisher Scientific Inc., Waltham, MA) was added to promote the growth of SiO_2. Condensation was completed 40 min after the addition of ammonium hydroxide. The final product was then separated by centrifuging, and washed and dried overnight in an oven at 50˚C. A SEM image of the prepared SiO_2 NPs is shown in Figure 2.3.

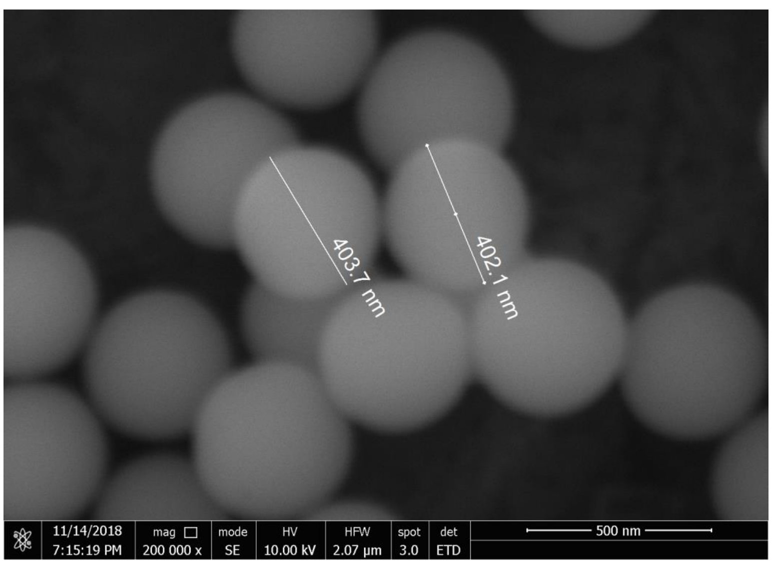

Figure 2.3: SEM image of SiO2 of 400nm diameter used in coating process

2.3 Sample fabrication

2.3.1 CPDA/M-cPDA films for thermoelectric perperty measurements

A processing schematic s shown in Figure 2.4. and a picture of PDA samples in different stages are shown in Figure 2.5. Fused silica substrate was used during the coating process to withhold high temperature annealing of PDA film. For characterization of the structure and performance evolution purpose, annealing temperature was chosen from 100˚C to 1000˚C with 100˚C interval. After heat treatment, four Au electrodes were deposit on the film using ion beam sputter (Magnetron sputter Kurt J. Lesk, Jefferson Hills, PA) with help of a custom-made shadow mask. Copper wires were then connected onto each electrode by sliver conductive paste. Each sample was then set into a custom-made acrylic sample holder (Figure 2.5(d)) and copper wires were secured with taps to ensure durability during manipulations.

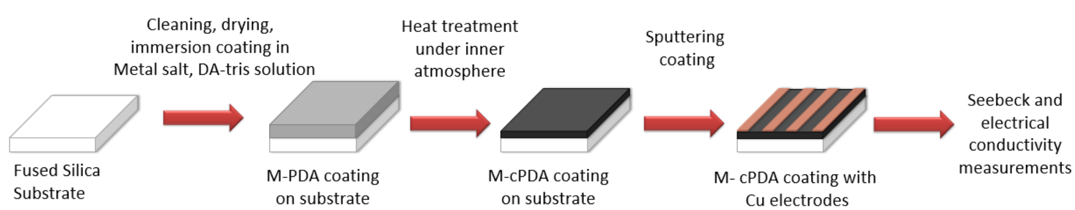

Figure 2.4: Process schematic of cPDA thin film for thermoelectric measurement

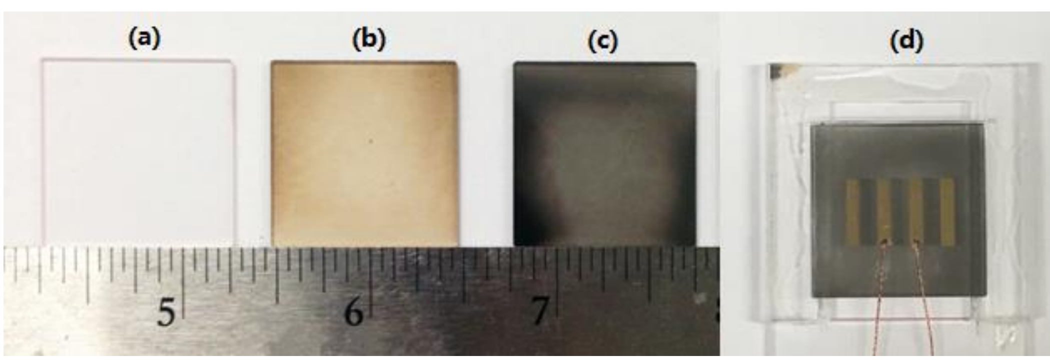

Figure 2.5: Example of PDA at different stages and (d) custom-made sample holder.

2.3.2 Electron-beam induced metal ion reduction

TEM experiments (JEM 1400, JEOL, Tokyo, Japan) were conducted on M-PDA or M-PDA coated SiO_2 NP suspended on copper TEM grids with carbon-formvar® supporting film (400 mesh, Ted Pella Inc., Redding, CA). The acceleration voltage was fixed at 120 kV. The electron beam current was manually adjusted to change the current density. The current density was calculated from the beam current, beam diameter, and magnification, which were recorded during the experiments.

2.3.3 Metal ion doped PDA/cPDA particle for catalytic measurement

Two types of samples were made and tested for catalytic performance: powders and thin films. Powder sample was drop casted on glassy carbon electrode, while coating was directly coated onto conductive substrates.

Fabrication of M-PDA and M-cPDA are discussed in **section 2.2**. To make samples for catalytic characterization, powder was first dispersed in 10 mL of D.I. water, isopropanol alcohol mixed solution (1:1 volume ratio) with 20 μL of 5% Nafion added to increase the bonding to the working electrode. After the mixture was well dispersed in ultrasonication for 15min, it was then deposited onto glassy carbon electrodes (3 mm diameter, CH Instrument, Austin, TX) with pipette. Glassy carbon electrodes with samples were oven-dried overnight at 50˚C.

To fabricate the electrodes with M-PDA coating, the following were taken into consideration: 1) electrically conductive; 2) can withhold high temperature treatment; 3) will not react with acid or base when voltage is applied. Therefore, graphite bars were used as in this study the substrate. In certain casesm #2B pencil leads were used as an alternative material since it is mainly composited of carbon and clay which are both inert to chemical reaction. The surface of the pencil lead is also relatively smooth compare to unpolished graphite rod. Fabrication of M-PDA coating is discussed in **section 2.2**.

2.4 Morphological, chemical, and compositional characterization

2.4.1 Scanning electron microscopy (SEM) and energy dispersive X-ray spectroscopy (EDX)

To characterize the sample morphology and composition, SEM was performed in FEI Quanta450 FEG SEM (FEI Inc. Hillsboro, OR). Specifically, powder sample dispersed on carbon tapes, coatings on Si/SiO_2 substrates, and cPDA coated on fused silica substrates were examined under high-vacuum with 10 kV accelerating voltage; while insulating PDA coated on the fused silica substrates were examined using an accelerating voltage of 10 kV under the low-vacuum mode with partial water vapor.

All energy dispersive x-ray spectroscopy (EDS) analyses were performed in the same chamber using an accelerating voltage of 10 kV and a working distance of approximately 10 mm. Point & ID mode was used for identification of elements; and the mapping mode was used to construct elemental distribution maps.

2.4.2 TEM and electron diffraction

For electron diffraction, an aperture was inserted to select the area of interest. The TEM imaging mode was turned into diffraction mode and image was taken with the CCD camera electronically. Diffraction pattern was then processed using the ImageJ software to measure the diameter of the rings, or the distance between bright dots. The results were compared with powder diffraction file (PDF) for calibration.

2.4.3 AFM

In this study, AFM was used to characterize the thickness of the thin film samples t and their surface morphology, i.e. contour and roughness. The AFM (MMAFMLN-AM, Veeco Metrology, Horsham, PA; Bruker Dimension Icon, Billerica, MA) was operated in the tapping mode. Prior to AFM experiments, thin film samples were intentionally scratched using a stainless-steel razor blade to create a step of film for thickness measurement. Film thicknesses were determined by scanning across the scratches and measurement of the height difference. At least six scans were made on each sample. Film roughness was obtained on 10μm x 10μm areas without scratches.

2.4.4 Thin film and Powder XRD

All XRD instruments involved in this study used Cu as x-ray source to generate Cu Kα x-ray. For thin film samples, XRD (D8 Discover, Bruker, Billerica, MA) was conducted on PDA coated on fused silica. Detector, z height, and rocking curve scan were conducted prior to measurement to ensure alignment of beam and stage for minimum error and maximum accuracy. A 1-cm horizontal slit and a 0.2-mm vertical slit were used to confine the beam. Scanning rate is used at 1s per 0.005 degree for a full spectrum scan, ranging from 5 – 80 degrees 2θ. A Finer scan is done at a scanning rate of 3s per 0.005 degree in selected range depending on the material being characterized.

2.4.4.1 In situ XRD experiment

In-situ XRD (PANalytical X'Pert PRO, Royston, UK) technique was used to measure the phase evolution in M-PDA powder during heating. Powder sample were compacted in stainless steel holder with thermocouple attached. Height scan was conducted prior to testing to ensure no peak shift during scanning. Heating range from 50˚C to 800˚C with 5 to 10˚C step was used. For each sample, scan was conducted in the 2θ range between 40˚ and 50˚, as (111) peak (most intensive) of Cu, and Ni are within this range. Resulted peak commonly shift towards lower 2θ due to thermal expansion. In addition, peak intensity commonly increased with annealing temperature due to growth of nano-crystal.

2.4.5 Neutron scattering

Neutron scattering experiments were conducted at room temperature for 25 min on powdered samples sealed in 2-mm diameter quartz capillaries using the Nanoscale-Ordered Materials Diffractometer (NOMAD) instrument at Oak Ridge National Laboratory. The structural factor, S(Q), was obtained by normalizing diffraction data against a solid vanadium rod and subtracting the background developed for the NOMAD instrument. Pair distribution function (PDF) was obtained by the Fourier transform of S(Q) at the maximum intensity of Q_{max} = 31.4 Å^{-1}. The fitting of PDF was performed at r < 20 Å, using the PDFgui software.

2.4.6 Raman spectroscopy

Raman spectroscopy was performed on thin film samples prepared on Si/SiO_2 substrates using a Horiba LabRAM HR Evolution Raman spectrometer (Horiba, Japan) with a laser excitation wavelength of 532 nm, and 1800 g/mm diffraction grating providing spectral resolution of ~ 2 cm^{-1}. Laser light was focused on ~ 1 μm diameter focal spot with an Olymus MPlan N 100x objective lens. Excitation intensity was maintained below the damage threshold of the samples. At least two scans were performed on each spot. Spectra were collected for at least 3 spots per sample in order to check the homogeneity of the samples. Scans were conducted within the spectral range of

100 cm^{-1} to 3000 cm^{-1}. Background scans were performed on blank Si/SiO_2 substrates before and after scanning the samples.

2.4.7 XPS

X-ray photoelectron spectrum (XPS) analysis of the films was carried out using VG Scientific (Thermo Fisher Scientific Inc., Walthan, MA) 100 mm hemispherical analyzer and a Physical Electronics Mg Kα X-ray source operatied at 300 W. Sample tested were coated on Si substrate and processed as previously described.

2.4.8 BET

Surface area analysis of the powdered samples was conducted using the Brunauer–Emmett–Teller method using a commercial unit (model ASAP 2020 Norcross, Metrometrics, GA 30093).. Approximately 500mg of dried PDA powder was loaded in the test.

2.4.9 ICP-MS

Metal concentrations of single and paired M-PDA powders were determined via acid digestion followed by inductively coupled mass spectrometry (ICP-MS) (Agilent 7900) analysis. Sample digestion was conducted in 15 mL polypropylene vials that were acid rinsed overnight and triple rinsed in deionized water. On average, 1.6 mg of dry powder was diluted to 10 mL in acidified sub-boiled water (2% nitric and 0.5% hydrochloric acid). Both sub-boiled water and acid were used for digestion matrix to minimize background concentrations. Digested M-PDA samples were prepared in duplicate and sonicated for a minimum of 15 minutes to ensure homogenization. Following sonication, suspensions were diluted for ICP-MS analysis and measured in triplicate. Measured metal concentrations were used to calculate the mass of metal per mg of dry powder and corresponding dopamine to metal ratios.

2.5 Mechanical property characterization

Nanoindentation was performed using a commercial unit (Triboindenter TI980, Bruker, Billerica, MA). On different material, indentation tip was selected accordingly. For soft thin film, a conical tip was used while a Berkovich tip was used for harder and thicker samples. For testing mode, a constant force method was used where the peak load was fixed. To avoid creep effect, the loading and unloading time were fixed at 5 sec regardless of the peak load. Holding time was typically selected as 60 sec. For stress-relaxation test, holding time was set to 2 min.

2.6 Thermoelectrical property characterization

2.6.1 Electrical conductivity

Electrical conductivity was calculated based on the film dimensions and the electrical resistance measured using a digital multimeter (Model 2700, Keithley, Cleveland, OH). A two probe configuration was used since the contact resistance between the gold electrodes and the glued copper wire with silver paste was negligible comparing to the resistance of the film. Samples were placed into a custom-made holder to secure them during the test.

2.6.2 Seebeck coefficient

The Seebeck coefficient was measured using a customized set-up. A schematic of this test setup is shown in Figure 2.6. A temperature difference, ΔT (measured by two thermocouples, K type, Omega Engineering, Norwalk, CT), was applied across the sample using a heater/cooler module, which in turn resulted in a thermal voltage, ΔV. The Seebeck coefficient, S, was calculated as the slope of the ΔV - ΔT curve when ΔT varied from -5^{o}C to 5^{o}C. The heat-sink temperature was maintained at ambient temperature.

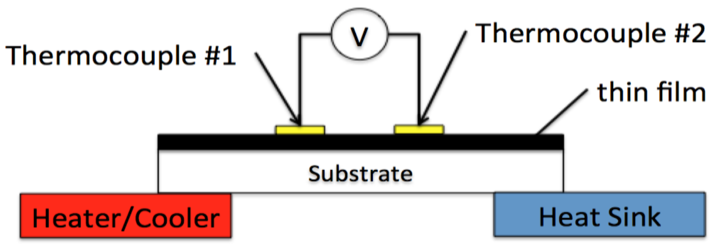

Figure 2.6: Experimental setup for Seebeck coefficient measurement

2.7 Characterization of electrocatalytical properties

An electrochemical workstation (Versa stat 3, Ametek, Berwyn PA) was used for the electrocatalytic measurement. Figure 2.7 shows the layout and materials used in our tests. Linear scan from 0V to -1V with a scan rate of 0.01V/s was used to ensure good accuracy. Working electrode was selected based on sample morphology. For powder sample, 3-mm diameter glassy carbon electrodes were used. And for coating sample, graphite rods were used to carry the catalysis. Inert graphite rod was used as the counter electrode and the Ag/AgCl in saturated KCl was used as reference. The electrolysis was selected based on the experimental design. A solution of 0.5 M sulfuric acid at pH=0 was used in this study.

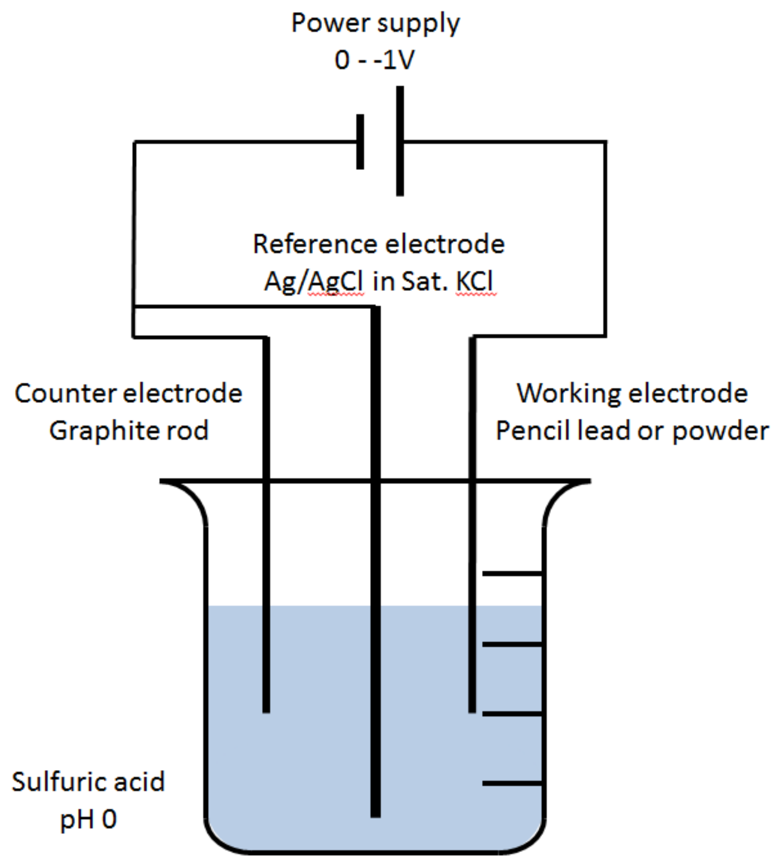

Figure 2.7: Schematic for electrocatalytical measurement

REFERENCE

[1] K. S. Rao, K. El-Hami, T. Kodaki, K. Matsushige, and K. Makino, "A novel method for synthesis of silica nanoparticles," *J Colloid Interface Sci*, vol. 289, no. 1, pp. 125-31, Sep 1 2005.

CHAPTER 3: STRUCTURAL EVOLUTION OF CARBONIZED POLYDOPAMINE (CPDA) AND ITS THERMOELECTRIC PROPERTIES

Chapter 3 is based on the following publication

H. Li,Y. V.Aulin, L. Frazer, E. Borguet, R. Kakodkar, J. Feser, Y. Chen, K. An, D. A. Dikin, and F. Ren, 'Structural evolution of carbonized polydopamine (cPDA) and its thermoelectric properties', *ACS Applied Materials and Interfaces*, **9**, 6655–6660, (2017) DOI: 10.1021/acsami.6b15601.

Structure evolution and thermoelectric properties of carbonized polydopamine thin films

Haoqi Li[1]*,Yaroslav V.Aulin*[2]*, Laszlo Frazer*[2]*, Eric Borguet*[2]*, Rohit Kakodkar*[3]*, Joseph Feser*[3]*, Yan Chen*[4]*, Ke An*[4]*, Dmitriy A. Dikin*[1]*, and Fei Ren*[1,*]

[1]Department of Mechanical Engineering, Temple University, Philadelphia, PA, 19122, USA

[2]Department of Chemistry, Temple University, Philadelphia, PA, 19122, USA

[3]Department of Mechanical Engineering, University of Delaware, Newark, DE, 19716, USA

[4]Chemical and Engineering Materials Division, Oak Ridge National Laboratory, Oak Ridge, 37831, TN, USA

Abstract

Carbonization of nature-inspired polydopamine can yield thin films with high electrical conductivity. Understanding of the structure of carbonized PDA (cPDA) is therefore highly desired. In this study, neutron diffraction, Raman spectroscopy, and other techniques indicate that cPDA samples are mainly amorphous with some short-range ordering and graphite-like structure that emerges with increasing heat treatment temperature. The electrical conductivity and the Seebeck coefficient show different trends with heat treatment temperature, while the thermal conductivity remains insensitive. The largest room-temperature ZT of 2 x 10^{-4} was obtained on samples heat treated at 800^{o}C, which is higher than that of reduced graphene oxide.

KEYWORDS: Polydopamine; Thermoelectric; Neutron total scattering; Raman spectroscopy; Thermal conductivity; Seebeck coefficient

3.1 Introduction

Polydopamine (PDA) is a nature-inspired material obtained through polymerization of biomolecule dopamine (Figure 3.1 (a)), which can be synthesized under mild aqueous conditions simulating marine environments. PDA exhibits strong affinity to a wide range of surfaces [1] due to the existence of multiple functional groups, which can be attached to organic and inorganic materials [2]. Therefore, PDA has been proposed to serve as a universal platform for various surface modifications.

Despite this wide range of applications, the structure of PDA is still under debate. The prevailing opinions believe [3-5] that PDA is not a polymer but stacked oligomers. Meng and Kaxiras [3] proposed that the oligomers form stacked layers or helical structures through C-C bonding. Hong et al. [4] believed that covalent bonding contributed to the formation of oligomers while non-covalent bonding such as hydrogen bonding and π-π interaction were the primary mechanisms for interlayer stacking. Using experimental and simulation techniques, Liebscher et al. [5] showed the oligomer interactions were primarily charge transfer with possible hydrogen bonding. Furthermore, the authors proposed that the oligomers were likely linear, yielding structures similar to that shown in Figure. 3.1 (b). [5] In contrast, Dreyer and coworkers[6] proposed a different model where PDA does not possess covalent bonding but consists of individual monomers held together by non-covalent bonding such as charge transfer, π-π interaction, and hydrogen bonding.

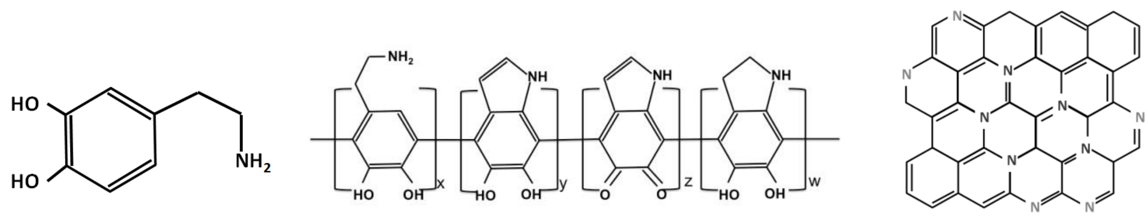

(a) (b) (c)

Figure 3.1: Schematics showing (a) the dopamine molecule, (b) a proposed PDA structure based on covalently bonded linear oligomers [5]. (c) a hypothetical structure of carbonized PDA [9]. Reproduced with permission from reference 5. Copyright 2013 American Chemical Society. Reproduced with permission from reference 9. Copyright 2012 John Wiley and Sons.

PDA can be carbonized by pyrolysis, and carbonized PDA (cPDA) exhibits high electrical conductivity similar to or even greater than reduced graphene oxides. [7,8] For example, Li et al. [7] reported high electrical conductivity in cPDA, up to 1.2 x 10^5 S/m after heat treatment at 1000^{o}C in Ar/H_2. Kong and coworkers [8] also found the electrical conductivity of cPDA film was as high as 2.6 x 10^5 S/m. It is speculated that cPDA might have a structure similar to that shown in Figure. 3.1 (c) [9], which could be considered as nitrogen-doped graphite.

Using transmission electron microscopy, Kong et al. observed layered carbon structures in the cPDA film coated on SnO_2 particles, and proposed that cPDA could be regarded as multi-layer graphene [8]. Additional evidence showing the layered structure of cPDA was obtained in a TEM study performed by Yu and coworkers, [10] where an interlayer d-spacing of 0.34 nm was observed. However, X-ray diffraction on cPDA materials showed inconsistent results. Kong et al. [8] and Ryu et al. [11] both found a peak around $2\theta = 22^o$, which corresponds to a d-spacing of 0.44 nm. In contrast, an earlier study on PDA by Ryu and coworkers[12] showed two XRD peaks at $2\theta = 25.7^o$ and

$2\theta = 12.8^o$, which correspond to d-spacings of 0.347 nm and 0.692 nm, respectively. Raman spectroscopy was also performed to study the structure of cPDA materials. Yu et al. [10] identified two peaks in the Raman spectrum of cPDA after being heat-treated at 800^oC: 1331 cm^{-1} and 1578 cm^{-1}, corresponding to the D and G bands of graphitic materials [13,14]. It is worthwhile to note that the intensity ratio between the D and G bands, I_D/I_G, is greater than unity [10]. Ryu and coworkers [11] also studied the Raman spectroscopy of cPDA pyrolyzed at 1050^oC and found $I_D/I_G = 0.86$, which is lower than that obtained from PDA ($I_D/I_G = 0.94$).

In this work, structural evolution of PDA as a function of the level of carbonization was studied using electron microscopy, Raman spectroscopy, and neutron scattering. In addition, room temperature Seebeck coefficient, electrical conductivity, and thermal conductivity of PDA thin films carbonized at different temperatures were examined.

3.2 Experimental method

In this study, PDA thin films were coated onto fused silica (26013, Ted Pella Inc., Redding, CA) and Si/SiO2 (21620-6, Ted Pella Inc., Redding, CA) substrates. After ultrasonically cleaned in acetone and then deionized water, the substrates were immersed into 50 mM tris buffer (BP1761, Thermo Fisher Scientific Inc., Walthan, MA) containing 13mM dopamine chloride (H8502, Sigma-Aldrich, St. Louis, MO). The pH value of the tris buffer was adjusted to 8.5 using HCl (SA48, Thermo Fisher Scientific Inc., Walthan, MA). Coating was conducted at room temperature without mechanical stirring. After 48 hours, the substrates were removed from the solution, cleaned with deionized water, and dried overnight at 60^oC in an oven.

Substrates with PDA coating were heat treated under runner Ar using a tube furnace (GSL-1500X, MTI, Richmond, CA). In a typical heat treatment run, the sample was heated with a heating rate of 10^{o}C/min, held at peak temperature for an hour, then cooled to room temperature with a nominal cooling rate of 10^{o}C/min.

3.3 Results and discussion

The as-coated PDA films possessed a brownish color, which gradually changed to black as the heat treatment temperature increased. SEM examination showed the PDA films, before and after heat treatment, were continuous across large distance (> 100 micrometer) without surface cracks or porosity (Figure. 3.2 (a)). AFM measurements at multiple locations indicated that the thicknesses of the film are uniform (Figure. S3 in SI) with surface roughness less than 1.2 nm (Table in SI).

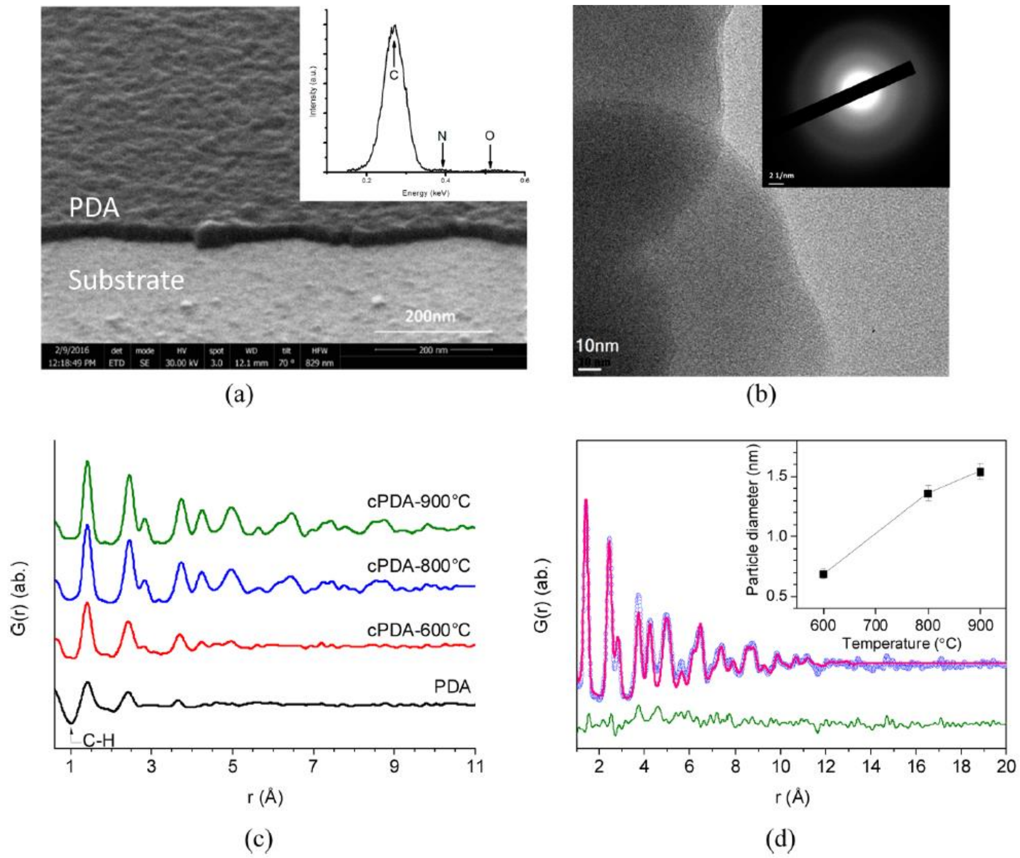

Figure 3.2: (a) SEM image of PDA film, inset is the energy dispersive spectrum. (b) TEM image of carbonized PDA powder, inset is electron diffraction. (c) Neutron pair distribution functions (PDFs) of PDA and carbonized PDA powders at different temperatures and (d) fitting of PDF of cPDA-900^{o}C using the graphite structure. The blue dots, pink line and green line are the observed data, fit data and the difference, respectively. The inset shows the average particle diameters as function of annealing temperature, which were extracted from the PDF fitting.

Neutron total scattering experiments were performed on the PDA powders and the cPDA powders heat-treated at 600^{o}C (cPDA-600), 800^{o}C (cPDA-600), and 900^{o}C (cPDA-600). The neutron pair distribution functions (PDF) that characterize the local structures were measured and fitted with the graphite structure model (Figure 3.2 (c)(d)). The peaks at small r (inter-atomic spacing) region confirm the short-range correlations of the atoms. The local structure is consistent for the annealed cPDA powders of different temperatures, while it is different from that of the PDA powders (Figure 3.2 (c)). The comparison shows the structure evolutions from annealing at high temperatures. A feature of negative peak at r = 1.07 Å is observed in the PDA. It is likely due to C-H, N-H or O-H bonds because hydrogen possesses a negative neutron scattering length and the correlation length agrees with the average bond lengths. This negative peak feature is still observable in cPDA-600 however completely diminished in cPDA-800 and cPDA-900 as a result of fully removal of the hydrogen during carbonization.

The high temperature annealing promotes the local ordering and particle growth. PDA may be considered as a doped amorphous carbon (a-C) that consists of a mixture of sp^3 and sp^2 bonds. When subject to thermal annealing, a-C has the tendency to convert to either graphite (under low pressure) or diamond (under high pressure), which are both thermodynamically stable, solid-state phases of carbon. In our study, thermal annealing was conducted slightly above the atmosphere pressure, therefore the PDA films were converted towards the graphite structure. The graphitization process, including the degree of ordering and the crystalline size, progressed as the annealing temperature increased. As the temperature increased, the $G(r)$ peaks became higher and sharper, indicating the tendency of transforming to a graphite-like structure (Figure 3.2 (c)). The local atomic arrangement in PDA and cPDA annealed at lower temperatures show ordering within a sub-nanometer scale, which results in a quick reduction of the profile intensities in long range. Specifically, for the PDA and cPDA-600 samples, *G(r)* flatten out beyond 0.6 nm, which corresponded to the dimension of the largest structural features in these materials. In contrast, cPDA-800 and cPDA-900 showed peaks at larger *r*, implying the existence of larger ordered features. Therefore, one may conclude that heat treatment at higher temperatures (e.g. 800^{o}C) promote some growth of the ordered sub-nanometer structures.

The local atomic arrangement of cPDA is confirmed to be similar as graphite by the PDF fitting. An example of cPDA-900 is shown in Figure 3.2 (d). Slightly intensity misfit may be due to residual elements like O and N, which tend to reduce the lattice parameters due to their smaller size than C. The calculated lattice parameter a is about 2.447(2) Å for the cPDA samples, which is slightly smaller than that of graphite a = 2.464(2) Å [15]. In contrast, the atomic arrangement perpendicular to the layers may not be well ordered. The interlayer atomic correlation at r ~ 3.36 Å, which is the spacing between layers in graphite, does not exhibit significant intensity in the PDF. The subnano-scaled particle size also limits the periodic extension along this direction. The inset of Figure 3.2 (d) shows the average particle diameter as a function of the annealing temperatures. Although the average particle size monotonically increased from 0.69(4) nm in cPDA-600 to 1.54(7) nm in cPDA-900, the majority of the carbonized cPDA still could not form more than two graphite-like unit cells in a single particle.

In order to explore the graphite-like structures, a series of Raman spectroscopy experiments were conducted on the PDA and cPDA thin films. Raman spectra of all samples show the presence of two distinct bands: D band near 1360 cm^{-1} and G band near

1570 cm^{-1} (Figure 3.3 (a)). As the heat treatment temperature increased, the position of the G band gradually shifted from 1573 cm^{-1} to 1603 cm^{-1} (Figure 3.3 (b)). The intensity ratio between the D and G bands, I_D/I_G, grows with the heat treatment temperature (Figure 3.3 (b)). The simultaneous blue shift of the G-band and the growth of I_D/I_G ratio could be attributed to either i) the amorphization of graphite, or ii) the conversion from amorphous carbon (a-C) to nanocrystalline graphite [13]. We will show that for cPDA, the evidence supports the second hypothesis.

As illustrated by the solid arrows in Figure 3.3 (c) and (d), both the G-band shift and I_D/I_G ratio initially increase, as the graphite breaks into nanocrystalline graphites (NC graphite), and then decrease as the NC graphite becomes amorphous carbon (a-C). Further amorphization to tetragonal carbon (ta-C) will decrease I_D/I_G (Figure 3.3 (d)) but increase the G-band shift (Figure 3.3 (c)). This trend is reversible in the case of converting pure amorphous carbon to graphite. However, if impurity exists, the G band shift and the I_D/I_G ratio may follow different trajectories, as illustrated by the dashed arrows in Figure 3.3 (c) and (d).

As previously discussed, the TEM and diffraction results show PDA and cPDA films were mostly amorphous with some sub-nanometer features that were enlarged as the heat treatment temperature increased. Therefore, the shift of G-band towards higher wavenumbers and the increase of I_D/I_G (Figure 3.3 (b)) are likely due to the heat-treatment induced structural conversion from a-C to NC graphite. Furthermore, since other elements are present, it is not surprising that the trends in Raman shift of G-band and I_D/I_G ratio (Figure 3.3 (b)) deviated from the trajectory indicated by the solid line in Figure. 3.3 (c)(d).

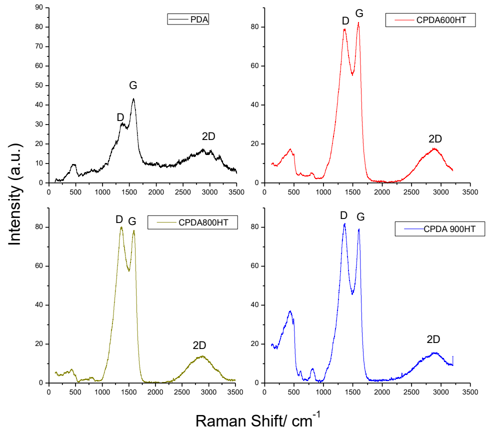

(a)

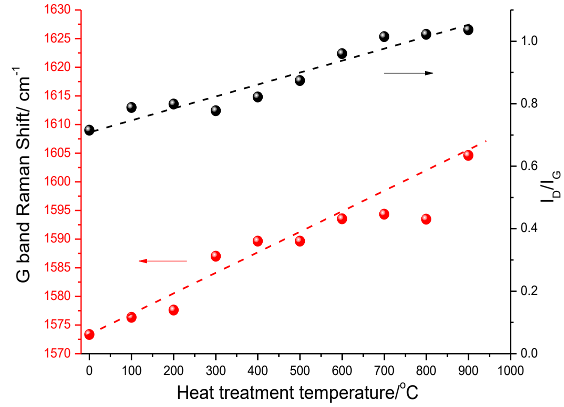

(b)

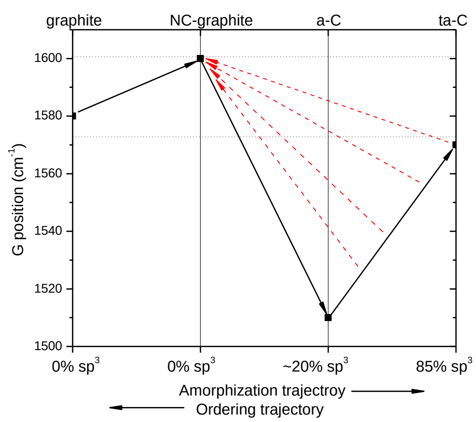

(c)

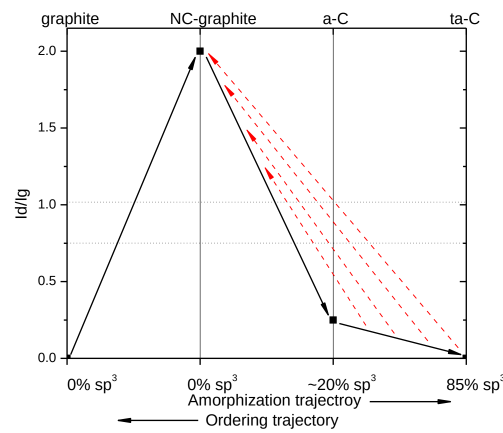

(d)

Figure 3.3: (a) Selected Raman spectra of PDA and cPDA samples with various heat treatment temperatures. (b) G peak position and I_D/I_G as a function of heat treatment temperature. (c) Migration of the G band position with respect to the crystallization degree [13] and (d) change of the I_D/I_G ratio as a function of the crystallization degree [13]. The solid lines in (c) and (d) indicate the paths for pure graphite, while the dash lines indicate the ordering trajectories of graphite with impurities. Reproduced with permission from reference 13. Copyright 2004 The Royal Society.

Electrical conductivity and thermoelectric Seebeck coefficient were measured at ambient conditions (Fig. S1 in SI). PDA and cPDA films heat-treated below 600ºC were electrically insulating and no Seebeck voltage could be measured. For samples heat-treated between 600ºC and 900ºC, a significant increase in electrical conductivity was observed with increasing temperature of treatment (Figure 3.4 (a)). Seebeck coefficients showed negative values (Figure 3.4 (a)), indicating cPDA is an n-type semiconductor. The magnitude of the Seebeck coefficient decreased from around 25 μV/K for cPDA-600 to less than 5 μV/K for cPDA-900. Fig. 4a also shows the trend of the power factor as a function of the heat treatment temperature, which has a peak value of 0.20 μW/m-K^2 for cPDA-800.

Recently, studies of thermoelectric properties of graphene have attracted much attention. Although pristine graphene is a gapless semiconductor, its electrical conductivity shows strong energy dependence near the charge neutrality point, [16] yielding finite Seebeck coefficients. Theoretical calculations indicated that the maximum Seebeck coefficient of pristine graphene is less than 100 μV/K at room temperature, [17] which was confirmed by several experiments [18-20]. Various strategies have been proposed to enhance the thermoelectric properties of graphene such as forming nanostructures and introducing defects [21-24].

Besides graphene, thermoelectric properties of reduced graphene oxide (rGO) have also been studied. Xiao and coworkers [22] showed the Seebeck coefficient of rGO decreased from 17 μV/K to -7 μV/K when the temperature increased from 300 K to 550 K, while the electrical conductivity increased from 2 x 10^3 S/m to 9 x 10^3 S/m. Choi and coworkers [25] examined the Seebeck coefficient and the electrical conductivity of rGO samples at room temperature. As the oxidation level increased, the Seebeck coefficient increased from 11 μV/K to 60 μV/K, while the electrical conductivity decreased from 880 S/m to 0.14 S/m. The largest power factor obtained by Choi et al.[25] was 0.11 μW/m-K^2. Choi and coauthors [25] also mentioned that thermal conductivities of the rGO samples were as low as 0.3 W/m-K. However, the authors did not provide details on thermal conductivity measurements [25].

In the current study, thermal conductivity was measured for PDA and cPDA thin films deposited on Si substrate using the time domain thermoreflectance (TDTR) method [26-29]. The thermal conductivity, shown on the left axis of Figure 3.4 (b), for all samples was around 0.3 W/m-K with little variations. For TDTR on thin films (~ 30nm), it is not possible to separately determine the contributions of the Al-cPDA thermal interface resistance ($R_{Al\text{-}cPDA}$) from the thermal resistance of the film itself ($R_{film} = t/\kappa_{film}$ = 30 nm/0.3 W/m-K = 10^{-7} m^2-K/W). Thus, we report the lower bound of the thermal conductivity, neglecting interfacial resistance. However, Schmidt [30] has previously measured the thermal interface conductance of Al on highly-oriented pyrolytic graphite and found an interface conductance value of ~50 MW/m^2-K near room temperature. Assuming similar values hold for cPDA, i.e. $R_{Al\text{-}cPDA}$ = 1/(50 MW/m^2-K) = 0.2 x 10^{-7} m^2-K/W, the film would represent 80% of the total thermal resistance. Thereby, measured thermal conductivity values are similar to those reported by Choi *et al*. for rGO samples [25]. Due to the large aspect ratio between the laser spot size (~25,000 nm) and the film thickness (~30 nm), the measurements were essentially one-dimensional, having sensitivity only in the through-plane direction. Despite recent advances in measurement of in-plane thermal conductivity using TDTR [28,29], the smallest achievable TDTR spot sizes and the lowest practical modulation frequencies are still not sufficient to directly measure the in-plane thermal conductivity for thin films with thermal conductivities as low as in the cPDA films.

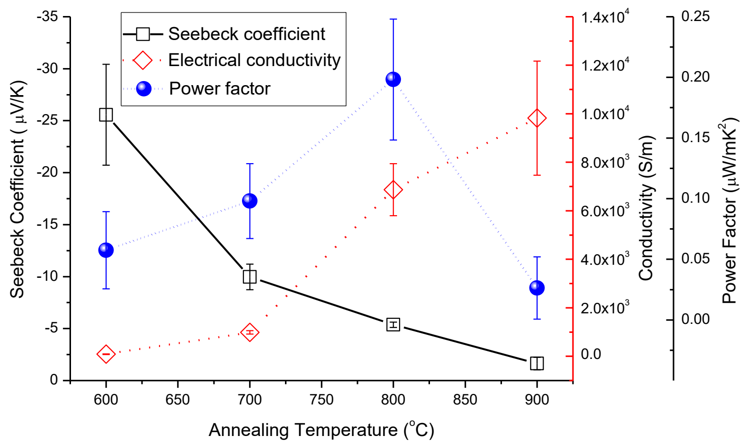

(a)

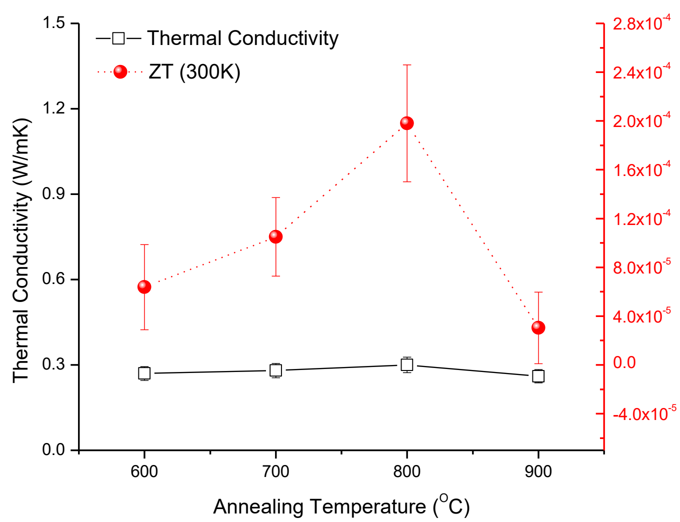

(b)

Figure 3.4: (a) Seebeck coefficient, electrical conductivity, and power factor respective to annealing temperature. (b) thermal conductivity measured by TDTR and Figure of merit respective to annealing temperature.

It is important to note that the electrical conductivity and the Seebeck coefficient were measured in the direction parallel to the substrate. Since the XRD and TEM analyses did not show significant in-plane preferential crystallization/orientation, one may assume that there is no significant anisotropy in the transport properties. The dimensionless Figure of merit (ZT) at room temperature (T = 297 K) can be calculated and shown in Fig. 4b. In this study, the highest ZT of 2 x 10^{-4} was obtained from the cPDA films heat-treated at 800^{o}C, which is higher than that for rGO [25] but is much lower than other state-of-the-art thermoelectric materials. Future studies should explore means to improve the electrical and thermoelectrical properties, which may be obtained by optimizing the processing conditions and through elemental doping. Other properties, including mechanical properties, are also of interest.

3.4 Conclusions

In summary, this study revealed the amorphous nature of PDA and growth of nanostructural graphite during heat treatment. The thermal annealing method can yield large-scale cPDA thin films on many substrates. By controlling the annealing temperature, as demonstrated in this work, various electrical properties could be obtained, which may be utilized toward electronic applications.

REFERENCES

[1] S. M. D. Haeshin Lee, William M. Miller, Phillip B. Messersmith, "Mussel-Inspired Surface Chemistry for Multifunctional Coatings," *Science,* vol. 318, 2007.

[2] M. Krogsgaard, V. Nue, and H. Birkedal, "Mussel-Inspired Materials: Self-Healing through Coordination Chemistry," *Chemistry,* vol. 22, pp. 844-57, Jan 18 2016.

[3] S. Meng and E. Kaxiras, "Theoretical models of eumelanin protomolecules and their optical properties," *Biophys J,* vol. 94, pp. 2095-105, Mar 15 2008.

[4] S. Hong, Y. S. Na, S. Choi, I. T. Song, W. Y. Kim, and H. Lee, "Non-Covalent Self-Assembly and Covalent Polymerization Co-Contribute to Polydopamine Formation," *Advanced Functional Materials,* vol. 22, pp. 4711-4717, 2012.

[5] J. Liebscher, R. Mrowczynski, H. A. Scheidt, C. Filip, N. D. Hadade, R. Turcu*, et al.*, "Structure of polydopamine: a never-ending story?," *Langmuir,* vol. 29, pp. 10539-48, Aug 20 2013.

[6] D. R. Dreyer, D. J. Miller, B. D. Freeman, D. R. Paul, and C. W. Bielawski, "Elucidating the structure of poly(dopamine)," *Langmuir,* vol. 28, pp. 6428-35, Apr 17 2012.

[7] R. Li, K. Parvez, F. Hinkel, X. Feng, and K. Mullen, "Bioinspired wafer-scale production of highly stretchable carbon films for transparent conductive electrodes," *Angew Chem Int Ed Engl,* vol. 52, pp. 5535-8, May 17 2013.

[8] J. Kong, W. A. Yee, L. Yang, Y. Wei, S. L. Phua, H. G. Ong*, et al.*, "Highly electrically conductive layered carbon derived from polydopamine and its functions in SnO2-based lithium ion battery anodes," *Chem Commun (Camb),* vol. 48, pp. 10316-8, Oct 25 2012.

[9] K. Ai, Y. Liu, C. Ruan, L. Lu, and G. M. Lu, "Sp2 C-dominant N-doped carbon sub-micrometer spheres with a tunable size: a versatile platform for highly efficient oxygen-reduction catalysts," *Adv Mater,* vol. 25, pp. 998-1003, Feb 20 2013.

[10] X. Yu, H. Fan, Y. Liu, Z. Shi, and Z. Jin, "Characterization of carbonized polydopamine nanoparticles suggests ordered supramolecular structure of polydopamine," *Langmuir,* vol. 30, pp. 5497-505, May 20 2014.

[11] S. Ryu, J. B. Chou, K. Lee, D. Lee, S. H. Hong, R. Zhao*, et al.*, "Direct Insulation-to-Conduction Transformation of Adhesive Catecholamine for Simultaneous Increases of Electrical Conductivity and Mechanical Strength of CNT Fibers," *Adv Mater,* vol. 27, pp. 3250-5, Jun 3 2015.

[12] J. Ryu, S. H. Ku, M. Lee, and C. B. Park, "Bone-like peptide/hydroxyapatite nanocomposites assembled with multi-level hierarchical structures," *Soft Matter*, vol. 7, 2011.

[13] A. C. Ferrari and J. Robertson, "Raman spectroscopy of amorphous, nanostructured, diamond-like carbon, and nanodiamond," *Philos Trans A Math Phys Eng Sci*, vol. 362, pp. 2477-512, Nov 15 2004.

[14] A. C. Ferrari, "Raman spectroscopy of graphene and graphite: Disorder, electron–phonon coupling, doping and nonadiabatic effects," *Solid State Communications*, vol. 143, pp. 47-57, 2007.

[15] P. Trucano and R. Chen, "Structure of graphite by neutron diffraction," *Nature*, vol. 258, p. 2, 1975.

[16] K. S. Novoselov, A. K. Geim, S. V. Morozov, D. Jiang, M. I. Katsnelson, I. V. Grigorieva, *et al.*, "Two-dimensional gas of massless Dirac fermions in graphene," *Nature*, vol. 438, pp. 197-200, Nov 10 2005.

[17] Y. Ouyang and J. Guo, "A theoretical study on thermoelectric properties of graphene nanoribbons," *Applied Physics Letters*, vol. 94, 2009.

[18] Y. M. Zuev, W. Chang, and P. Kim, "Thermoelectric and magnetothermoelectric transport measurements of graphene," *Phys Rev Lett*, vol. 102, p. 096807, Mar 6 2009.

[19] P. Wei, W. Bao, Y. Pu, C. N. Lau, and J. Shi, "Anomalous thermoelectric transport of Dirac particles in graphene," *Phys Rev Lett*, vol. 102, p. 166808, Apr 24 2009.

[20] J. G. Checkelsky and N. P. Ong, "Thermopower and Nernst effect in graphene in a magnetic field," *Physical Review B*, vol. 80, 2009.

[21] D. Dragoman and M. Dragoman, "Giant thermoelectric effect in graphene," *Applied Physics Letters*, vol. 91, 2007.

[22] N. Xiao, X. Dong, L. Song, D. Liu, Y. Tay, S. Wu, *et al.*, "Enhanced thermopower of graphene films with oxygen plasma treatment," *ACS Nano*, vol. 5, pp. 2749-55, Apr 26 2011.

[23] Y. Xu, Z. Li, and W. Duan, "Thermal and thermoelectric properties of graphene," *Small*, vol. 10, pp. 2182-99, Jun 12 2014.

[24] P. Dollfus, V. Hung Nguyen, and J. Saint-Martin, "Thermoelectric effects in graphene nanostructures," *J Phys Condens Matter*, vol. 27, p. 133204, Apr 10 2015.

[25] J. Choi, N. D. K. Tu, S.-S. Lee, H. Lee, J. S. Kim, and H. Kim, "Controlled oxidation level of reduced graphene oxides and its effect on thermoelectric properties," *Macromolecular Research,* vol. 22, pp. 1104-1108, 2014.

[26] D. G. Cahill, "Analysis of heat flow in layered structures for time-domain thermoreflectance," *Rev Sci Instrum,* vol. 75, p. 4, 2004.

[27] K. Kang, Y. K. Koh, C. Chiritescu, X. Zheng, and D. G. Cahill, "Two-tint pump-probe measurements using a femtosecond laser oscillator and sharp-edged optical filters," *Rev Sci Instrum,* vol. 79, p. 114901, Nov 2008.

[28] J. P. Feser and D. G. Cahill, "Probing anisotropic heat transport using time-domain thermoreflectance with offset laser spots," *Rev Sci Instrum,* vol. 83, p. 104901, Oct 2012.

[29] J. P. Feser, J. Liu, and D. G. Cahill, "Pump-probe measurements of the thermal conductivity tensor for materials lacking in-plane symmetry," *Rev Sci Instrum,* vol. 85, p. 104903, Oct 2014.

[30] A. J. Schmidt, K. C. Collins, A. J. Minnich, and G. Chen, "Thermal conductance and phonon transmissivity of metal–graphite interfaces," *Journal of Applied Physics,* vol. 107, 2010.

CHAPTER 4: STRUCTURE AND THERMOELECTRIC PROPERTIES OF METAL ION DOPED POLYDOPAMINE (PDA)

Chapter 4 is based on the following publication

H.Li, T. Marshall, Y. V. Aulin, A. C. Thenuwara, Y. Zhao, E. Borguet, D. R. Strongin, F. Ren, 'Structrue and Thermoelectric Properties of Metal Ion Doped Polydopamine (PDA)', *Journal of Materials Science*, 8, 6393-6400, (2019) DOI: 10.1007/s10853-019-03337-7.

Structural evolution and electrical properties of metal ion-containing polydopamine

Haoqi Li[1], *Tim Marshall*[2], *Yaroslav V. Aulin*[2], *Akila C. Thenuwara*[2], *Yao Zhao*[1], *Eric Borguet*[2], *Daniel. R. Strongin*[2], *Fei Ren*[1*]

[1]Department of Mechanical Engineering, Temple University, Philadelphia, PA 19122, USA

[2]Department of Chemistry, Temple University, Philadelphia, PA 19122, USA

Abstract

Polydopamine (PDA) is a biopolymer that can be synthesized under mild conditions. Thermal annealing can convert PDA into a conductive phase, the so-called carbonized PDA (cPDA). This work studied the effect of three metal ions, i.e. Cu^{2+}, Mg^{2+}, and Na^{+}, on the synthesis of PDA and its conversion to cPDA. Both Cu^{2+} and Mg^{2+}could interact with PDA, which in turn influenced i) the growth of PDA thin film, ii) morphology change of PDA particles upon thermal annealing, and iii) the electrical properties of heat-treated thin films. In contrast, the presence of Na^{+} ion during the synthesis of PDA did not show any effect. In this study, the morphology of PDA thin films and powder particles were examined using SEM and TEM; their chemical compositions were studied by EDS and ICP-MS; the structure was investigated using electron diffraction and Raman spectroscopy; and the properties were evaluated with respect to the electrical conductivity and thermoelectric Seebeck coefficient. The results from this work provide a potential approach to control the structure and properties of PDA and cPDA materials through metal ion doping.

KEYWORDS: Polydopamine; Metal-polymer coordination; Nanocrystal; Electrical conductivity; Seebeck coefficient

4.1 Introduction

Polydopamine (PDA) is considered a biopolymer inspired by the mussel chemistry [1]. PDA has attracted much attention in recent years due to the ease of its fabrication methods and many interesting properties. PDA can be synthesized through oxidative self-polymerization under mild conditions [1, 2], which can yield nano-scale powders with controllable size [3], or conformal, crack-free thin films on multiple surfaces [4]. The "universal" adhesive behavior of PDA is attributed to the existence of multiple functional groups, e.g. the catechol and amine groups, in the dopamine (DA) molecules. These functional groups allow PDA to interact with other molecules in various ways, such as chelation or hydrogen bonding. Many potential applications of PDA have been proposed, such as surface treatment to modify the hydrophobicity, targeted drug delivery, and capture of heavy metal cations for water treatment [5-8].

PDA can be converted into a carbon-like phase through heat treatment. Carbonized PDA (cPDA) thin films have been found to possess good electrical conductivities as high as 1.2×10^5 S/m [9], which are comparable to reduced graphene oxide (rGO) [1, 10-12]. It is hypothesized that cPDA possessed a structure similar to graphite [13,14]. The promising electrical conductivity of cPDA makes it a potential candidate for nanostructured carbon material. Compared to graphene or rGO, the fabrication process for cPDA does not involve harsh chemicals and therefore is more environmental friendly. Our previous study [2] showed the formation and growth of nano scale graphite-like domains in PDA when thermally annealed. While the structure of PDA was primarily amorphous, graphite-like nanostructure started to form at 600^{o}C, which further grew to approximately 1.5 nm after heat treatment at 900^{o}C [2]. It was also shown that the electrical conductivity continued to increase with increasing annealing temperature while the Seebeck coefficient showed the opposite trend.

Some recent studies focused on the interactions between PDA and metal ions to achieve ion-assisted crosslinking in PDA. Introduction of metal ions can alter the structure of PDA network, and therefore its properties. For example, Im *et al.* [15] studied the chelation of Fe^{3+}, Fe^{2+}, Cu^{2+}, and Al^{3+} by the catechol groups in PDA and demonstrated that the metal ions could not only enhance the attachment of the PDA layer on human hair surface but also increase the overall layer thickness due to increased crosslinking. Kim and coworkers [16] demonstrated immersion of PDA in $FeCl_3$ solution could enhance its stability in strong alkali environment due to the formation of PDA-Fe^{3+} complex. The stability of bonding between organic ligands and metal ions depends on the metal species as well as the oxidation states [17-19]. Monovalent cations such as Na^+ are generally difficult to form coordination bonds and have very low stability constant [18,19]. Divalent alkaline-earth metal ions such as Mg^{2+} bond much easier and have higher stability constants. Cations of transition metals, such as Cu^{2+}, on the other hand, usually form much stronger coordination bonding because the availability of empty outer shell orbitals that can accept lone-pair electrons [20].

In the current study, Cu^{2+}, Mg^{2+}, and Na^+ cations were introduced during the synthesis of PDA. The electrical properties, including DC and AC conductivities and Seebeck coefficient, were studied and explained with respect to the structure. Our data show different metal ions play different roles in affecting the electrical properties of PDA. This result indicates that doping could be used as a strategy to control the structure and properties of PDA materials, which in turn may be utilized to tune the electrical performance of PDA-based devices in the future.

4.2 Experimental Method

A base solution was prepared by diluting tris buffer (2M, Thermo Fisher Scientific Inc., Walthan, MA) to 50 mM with deionized (DI) water and adjusting its pH value to 8.5 using 1N hydrochloride acid (Thermo Fisher Scientific Inc., Walthan, MA). Substrates, either fused silica slides or Si with thermally grown SiO_2 (both from Ted Pella Inc., Redding, CA) were subsequently cleaned with acetone, isopropanol alcohol, and D.I. water in ultrasonication bath. During coating, cleaned substrates were first placed inside the base solution. Dopamine (DA) hydrochloride powder (99%, Alfa Aesar, Haverhill, MA) was then added with a concentration of 2 mg/mL. For each doping experiment, copper chloride ($CuCl_2$), sodium chloride (NaCl), or magnesium chloride ($MgCl_2$), which were purchased from Sigma-Aldrich, St. Louis, MO, was dissolved in the solution with a 1:1 molar ratio between DA molecules and metal ions. The pH of the solution was then readjusted to 8.5 by adding the 2M tris buffer. After coating, samples were removed and washed with DI water, followed by drying with compressed air, and over-night drying in an oven at 50^{o}C. In addition to thin film samples, powders were also collected using filer papers after each coating. Carbonization of PDA samples was conducted in a tube furnace under a flowing argon environment between 600^{o}C and 900^{o}C. Heating and cooling rates were set to 5°C/minute with a holding time of 60 min at the peak temperature. To perform electrical measurements, gold electrodes were sputter coated on the thin films.

Surface morphology of the samples was studied using scanning electron microscopy (SEM, FEI Quanta 450 FEG, FEI Inc. Hillsboro, OR) equipped with energy dispersive x-ray spectroscopy (EDS). Surface roughness and thickness of the film were measured using atomic force microscopy (AFM, Bruker Demission Icon, Bruker, Billerica, MA). Powder samples are studied with transmission electron microscopy (TEM, JEM 1400, JEOL, Tokyo, Japan). Raman spectroscopy was performed using Horiba LabRAM HR Evolution (Horiba, Japan) with a laser excitation wavelength of 532 nm and spot diameter of 0.72 μm. X-ray photoelectron spectrum (XPS) analysis of the films was carried out using VG Scientific (Thermo Fisher Scientific Inc., Walthan, MA) 100 mm hemispherical analyzer and a Physical Electronics Mg Kα X-ray source operating at 300 W. X-ray diffraction (XRD) was carried out by Bruker D8 discover (Bruker, Billerica, MA) with Cu Kα radiation. Electrical conductivity was calculated from the resistance and sample geometry of the thin films, where the thickness of the thin films was measured using atomic force microscope (Demission Icon, Bruker Corp., Billerica, MA) and the resistance was measured using a Keithley 2750 digital multimeter (Keithley, Cleveland, OH). Electrical impedance was measured using an LCR meter (B&K Precision Corp., Yorba Linda, CA) in the range from 20 Hz to 300 kHz. The Seebeck coefficient was measured using a lab-built apparatus [2]. For each heat treatment condition, at least six samples were included in the measurements, based on which the mean values and standard deviations were calculated. Surface area of the powders was measured by Brunauer-Emmett-Teller (BET) method using Micromeritic ASAP 2020 unit (Micromeritics, Norcross, GA). Metal ion concentration was analyzed by inductively coupled plasma mass spectrometry (ICP-MS) method using Agilent 7900 unit (Agilent, Santa Clara, CA).

4.3 Results and discussion

Figure 4.1 shows the SEM images of PDA coating on Si/SiO_2 substrate. All three types of PDA films doped with Cu^{2+} (Cu-PDA), Mg^{2+} (Mg-PDA), and Na^{+} (Na-PDA) during synthesis appeared to be flat, continuous, and crack-free (Figure 4.1), which is similar to the surface morphology of undoped PDA thin films [2]. Some bright spots can be observed on all sample surfaces (Figure 4.1), which are aggregated PDA particles formed during the synthesis and attached to the film surface. EDS analysis results on the coatings were shown in the insets of Figure 4.1. Carbon (C), oxygen (O), and trace amount nitrogen (N) were observed on all Cu-PDA, Mg-PDA, and Na-PDA samples. Copper (Cu) and magnesium (Mg) peaks were detected on the Cu-PDA (inset of Figure 4.1 (a)) and the Mg-PDA (inset of Figure 4.1 (b)) samples, respectively. However, sodium (Na) peak was not detected on the Na-PDA sample (inset of Figure 4.1 (c)). The concentration of metal ions was further measured using ICP-MS (Table S3), which showed the molar ratio between Cu and DA was approximately 1:6.1; the ratio between Mg and DA was approximately 1:4.2, and Na was less than 1/15 of DA. Both EDS and ICP-MS results indicate a significant amount of Mg and Cu ions were introduced into PDA during the synthesis. In contrast, few Na^{+} ions were retained after cleaning and drying. These results also agree well with literature observation on the different tendency to form coordination bonding among monovalent, divalent, and transition metal ions [18-20], as previously discussed in the introduction section.

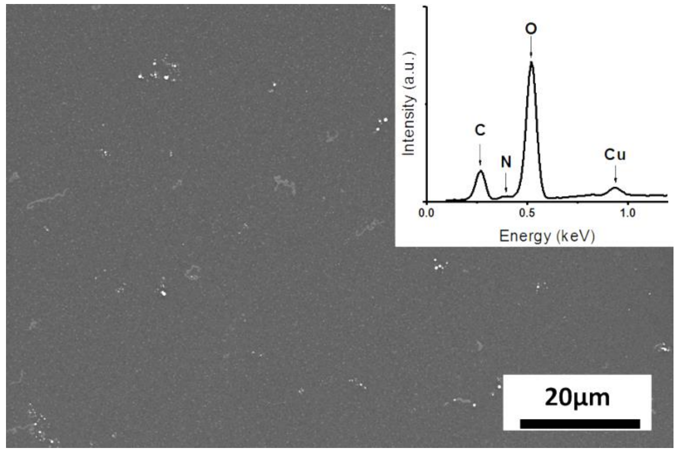

(a)

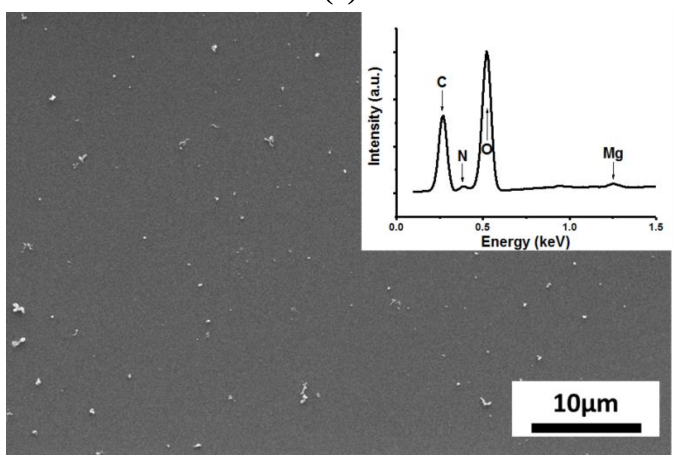

(b)

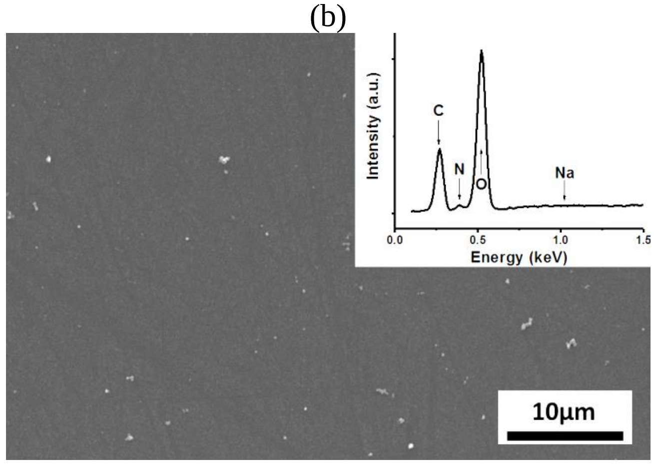

(C)

Figure 4.1: SEM image of (a) Cu-PDA, (b) Mg-PDA, and (c) Na-PDA thin films coated on Si/SiO_2 substrates. Insets show the EDS spectra obtained from areal scans.

AFM measurements revealed all the PDA films were smooth with low surface roughness on the order of nanometers (Table S1). However, the thickness of the thin films was different. For undoped PDA and Na-PDA, the film thickness increased from approximately 4 nm after 1 hr coating to 14 nm after 24 hr coating (Table S2). In contrast, the thickness of Cu-PDA and Mg-PDA films did not show significant increase when the coating time increased from 1 hr (~ 7-8 nm) to 24 hr (~ 7-10 nm) (Table S2). It is unclear why Cu^{2+} and Mg^{2+} ions hindered the growth of PDA thin films in the thickness direction. One possibility is related to the interaction of metal ions with DA monomers or oligomers through coordination bonding. It is commonly believed that the formation of PDA is the result of oligomerization of DA molecules and stacking of the oligomers [5, 21, 22], which relies on the oxidations of the catechol groups to dopaminequinone or semi-quinone that can form coordination bonding with various metal ions [6]. Therefore, Cu^{2+} and Mg^{2+} introduced during the synthesis step may also form coordination bonding with dopaminequinone or semi-quinone [17] and affect the stacking of PDA oligomers.

TEM examination of PDA powders showed the metal ion doped PDA particles had similar morphology to the undoped powders [2], where the powder particle size ranged between 50 and 200 nm in diameter with quasi-spherical or ellipsoidal shapes (SI). After heat treatment, the Na-PDA powder didn't show significant change in morphology (Figure 4.2 (a)). This result was expected since EDS and ICP-MS indicated few Na^{+} ions were retained in the PDA after cleaning and drying (Figure 4.1 (c)). On the other hand, some nanoscale features (dark dots in Figure 4.2 (b)) were observed in the Mg-PDA sample. Most of these nano dots were found on the surface of the PDA particles. Figure 4.2 (c) shows select-area electron diffraction (SAED) pattern obtained from the Mg-PDA sample heat-treated at 800^{o}C, where both diffraction rings corresponding to Mg and MgO are observed.

Similar nano dots, such as those seen in Figure 4.2 (d), were observed in the Cu-PDA samples after heat treatment. SAED analysis showed these dark dots are likely Cu nanocrystals. The two strong diffraction rings in Figure 4.2 (e) correspond to the {111} and the {220} planes of Cu. It is interesting to note that the Cu nanocrystals found in samples treated with higher temperatures tended to show larger size (see examples indicated by circles in Figure 4.2 (f)). Meanwhile, brighter areas (as indicated by arrows in Figure 4.2 (f)) were observed in these samples. These brighter areas did not show any diffraction features and are likely pores. XPS analysis results on the thin film samples are shown in Figure 4.3. For Cu-PDA, the presence of the Cu^{2+} satellite peaks indicate the divalent oxidation state of copper (dash line in Figure 4.3 (a)). After heat treatment at 800^{o}C, the strong Cu^{2+}satellite peak disappeared, the amplitude of the weak Cu^{2+} satellite peak reduced, and the 2p peaks shifted towards lower binding energy, which indicate the reduction of Cu^{2+} ions. This result implies the dark inclusions observed in the TEM images of the Cu-PDA particles after heat treatment (Figure 4.2 (d) and (f)) were likely metallic Cu. Similar reduction trend was also observed in the Mg-PDA sample. As shown in Figure 4.3 (b), binding energy of the Mg_{2p} peak shifted from ~ 52 eV to ~ 50 eV, implying partial reduction of Mg^{2+} to Mg [23,24]. In contrast, XPS scan did not detect peaks associated with Na or its ions with significant magnitude, which agreed with the EDS result (Figure 4.1 (c)).

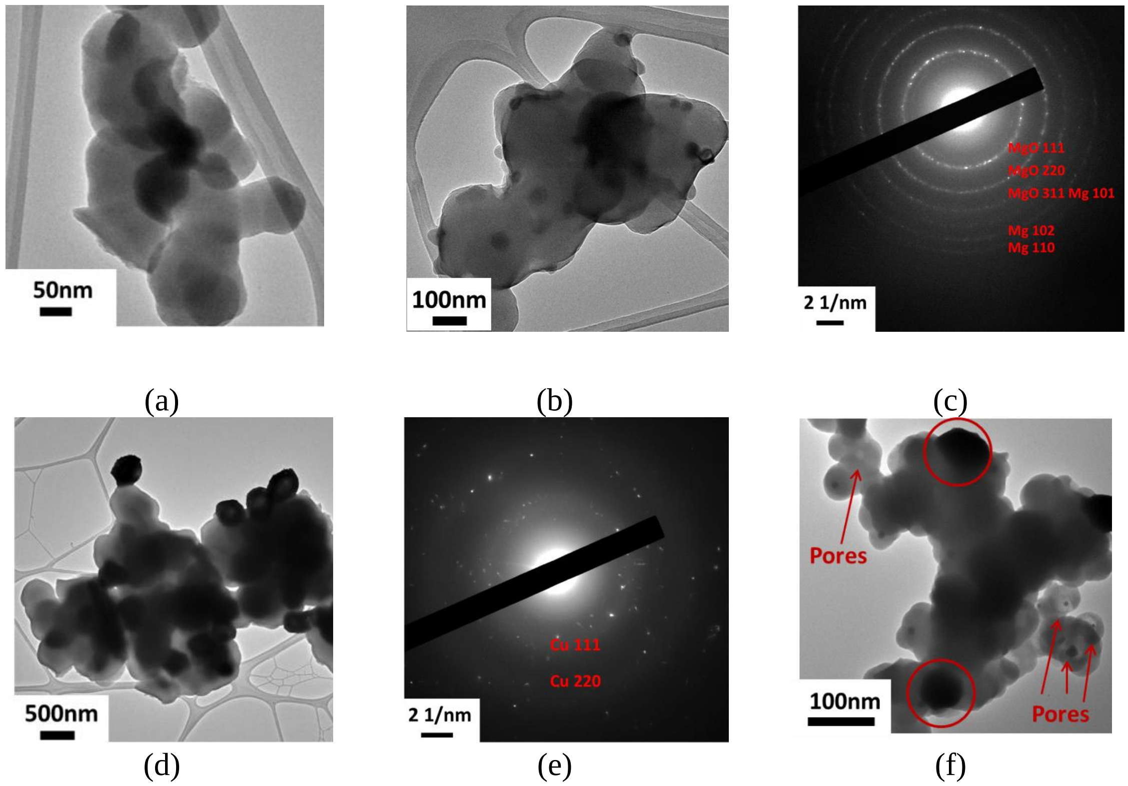

Figure 4.2: TEM images and selected area electron diffraction (SAED) of cPDA powder samples. (a) TEM image of Na-PDA powder after heat treatment at 800°C. (b)&(c) TEM image and SAED of Mg-PDA powder after heat treatment at 800°C. (d) & (e) TEM image and SAED of CU-PDA powder after heat treatment at 700°C. (f) TEM image of Cu-PDA powder after heat treatment at 1000°C.

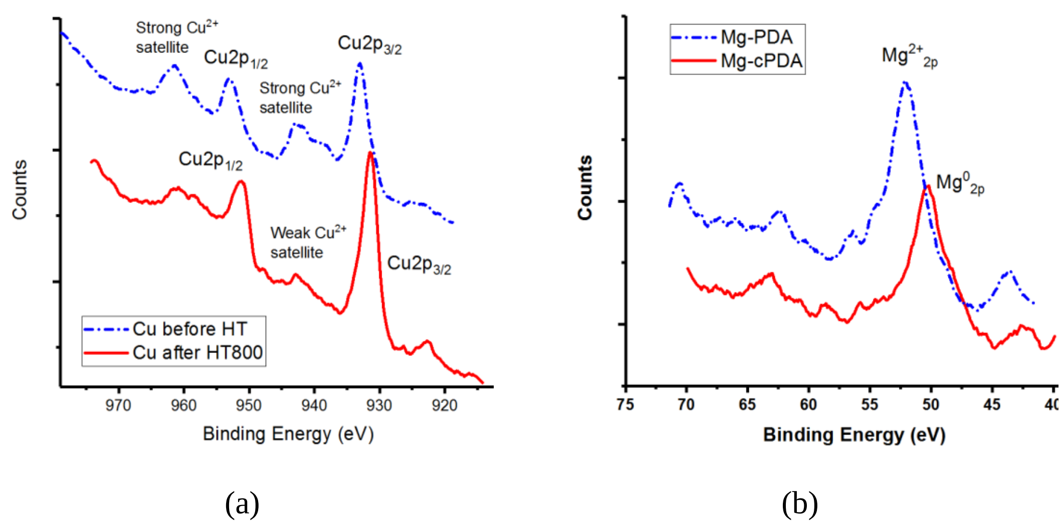

Figure 4.3: Comparison of XPS spectra of (a) Cu^{2+} doped PDA (b) Mg^{2+} doped PDA before and after heat treatment at 800˚C.

To explore the structure of the PDA phase, Raman spectroscopy measurements were conducted on samples heat treated between 600°C and 900°C. The D band (~1350 cm^{-1}) and the G band (~1580 cm^{-1}) were observed on all samples included in this study. The position of the G band blue-shifted as the heat treatment temperature increased (Figure 4a), meanwhile, the intensity ratios between the D bands and G bands (I_D/I_G) of all three samples also increased with increasing heat treatment temperature (Figure 4.4 (b)). These results are similar to those reported for undoped PDA [2] and indicate the formation and growth of nanoscale graphite domains [25,26].

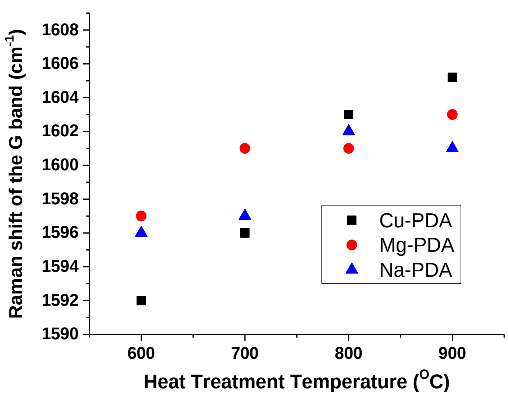

(a)

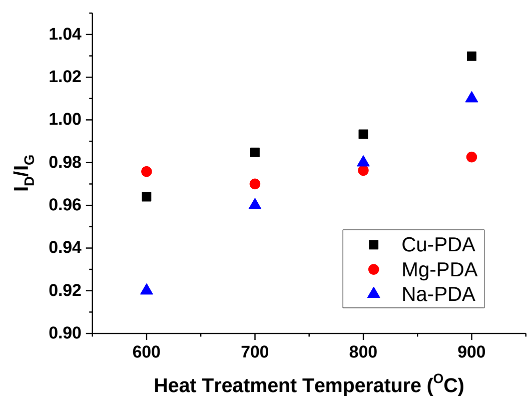

(b)

Figure 4.4: Effect of annealing temperature on (a) the position of the G band, and (b) intensity ratio between the D band and the G band. The increasing trends in the two sets of data indicate the conversion from amorphous carbon to nanocrystalline graphite [2, 25, and 26] in all metal ion doped samples.

To evaluate the effect of the electrical properties of the PDA thin films, electrical conductivity and Seebeck coefficient were measured at room temperature (Table 4.1). As heat treatment temperature increases, both the Na-PDA and Mg-PDA samples showed monotonic increase in electrical conductivity and monotonic decrease in Seebeck coefficient, which were similar to the undoped PDA sample (Table 4.1). As shown in our previous work [2], this behavior is expected as the carbonization degree of PDA increases with increasing annealing temperature. As above mentioned, Na^+ was not effectively retained in PDA and therefore did not affect the film formation and the carbonization process. In the case of Mg-PDA, although Mg^{2+} existed in the PDA sample after synthesis, precipitated Mg and MgO nanoparticles might have a small effect on the structure of the PDA phase since they tended to migrate to the surface (Figure 4.2 (b)).

On the other hand, Cu-PDA sample showed some different behavior: the electrical conductivity first increased after annealing at 700^{o}C and then dramatically decreased when the annealing temperature was beyond 800^{o}C (Table 4.1). As a result, the Cu-PDA sample possessed the highest electrical conductivity among all samples thermally annealed at 700^{o}C, which may be due to the contribution from Cu nanocrystals in the cPDA matrix (Figure 4.2 (d)). However, the Cu-PDA samples showed the lowest electrical conductivities after annealing at 800^{o}C and 900^{o}C (Table 4.1). This may be related to the generation of pores in the cPDA matrix as a result of growth of Cu nanoparticles at higher temperatures (Figure 4.2 (f)). Meanwhile, the Seebeck coefficient of Cu-PDA samples also exhibited a general trend of decreasing as the annealing temperature increased (Table 4.1), similar to those observed in undoped and other metal ion doped PDA samples.

Electrical impedance was also measured between 20 Hz and 300 kHz on samples heat treated at 600^{o}C and 800^{o}C. As shown in (see Figure S5), the impedance exhibited a sharp drop in 600˚C samples as the frequency increase starting around 5000 Hz and decreased by more than 50% at 300 kHz. In contrast the impedance of 800˚C samples showed much less decrease as frequency increased, which indicates the non-ohmic contribution to the overall electrical impedance is negligible. The different frequency responses between the 600°C samples and 800°C samples are related to the effect of heat treatment on the structural evolution of PDA [2] and metal-doped PDA materials.

Table 4.1: Room temperature electrical conductivity (σ) and Seebeck coefficient (S) of PDA thin films.

Annealing Temperature (˚C)		600	700	800	900
σ (S/m)	Undoped PDA	88 ± 15	9.9 ± 0.7 x 10^2	6.9 ± 1.1 x 10^3	3.8 ± 0.4 x 10^4
	Cu-PDA	160 ± 30	7.8 ± 1.4 x 10^3	6.1 ± 0.2 x 10^2	1.8 ± 1.3 x 10^2
	Mg-PDA	7.9 ± 1.6	4.5 ± 1.9 x 10^2	8.2 ± 1.6 x 10^3	3.7 ± 0.5 x 10^4
	Na-PDA	5.7 ± 3.9	5.7 ± 0.9 x10^2	4.1 ± 0.2 x 10^3	3.2 ± 0.2 x 10^4
S (μV/K)	Undoped PDA	26 ± 5	9.7 ± 1.2	5.4 ± 0.4	1.6 ± 0.6
	Cu-PDA	21 ± 0.85	7.0 ± 2.0	9.3 ± 3.3	4.7 ± 2.0
	Mg-PDA	3.2 ± 0.3	1.3 ± 0.4	3.7 ± 1.0	1.2 ± 0.2
	Na-PDA	3.0 ± 0.3	10 ± 2.3	5.0 ± 0.9	1.7 ± 0.8

4.4 Conclusions

Polydopamine (PDA) materials were synthesized in the presence of Cu^{2+}, Mg^{2+}, and Na^{+} ions. Thickness of PDA thin films was reduced when Cu^{2+} and Mg^{2+} were present. After thermal annealing, Cu nanoparticles formed within the PDA matrix, whose growth resulted in larger particle size and porosity in the PDA phase. Upon heating, Mg nanoparticles were observed mainly on the surface of PDA particles with some oxidation. Raman spectroscopy results indicated that the PDA phase was converted from amorphous towards nanocrystalline graphite despite the presence of the metal species. The Cu-PDA sample showed different electrical properties (electrical conductivity and thermoelectric Seebeck coefficient), likely due to the existence of Cu nanoparticles and pores in the

PDA matrix. In contrast, Mg-PDA sample exhibited little variation from the undoped PDA.

REFERENCE

[1] S. M. D. Haeshin Lee, William M. Miller, Phillip B. Messersmith, "Mussel-Inspired Surface Chemistry for Multifunctional Coatings," *Science,* vol. 318, 2007.

[2] H. Li *et al.*, "Structure Evolution and Thermoelectric Properties of Carbonized Polydopamine Thin Films," *ACS Appl Mater Interfaces,* vol. 9, no. 8, pp. 6655-6660, Mar 1 2017.

[3] X. Jiang, Y. Wang, and M. Li, "Selecting water-alcohol mixed solvent for synthesis of polydopamine nano-spheres using solubility parameter," *Sci Rep,* vol. 4, p. 6070, Aug 14 2014.

[4] Y. Chen, Y. Zhao, and Z. Liang, "Solution processed organic thermoelectrics: towards flexible thermoelectric modules," *Energy & Environmental Science,* vol. 8, no. 2, pp. 401-422, 2015.

[5] D. R. Dreyer, D. J. Miller, B. D. Freeman, D. R. Paul, and C. W. Bielawski, "Perspectives on poly(dopamine)," *Chemical Science,* vol. 4, no. 10, 2013.

[6] Y. Liu, K. Ai, and L. Lu, "Polydopamine and its derivative materials: synthesis and promising applications in energy, environmental, and biomedical fields," *Chem Rev,* vol. 114, no. 9, pp. 5057-115, May 14 2014.

[7] R. v. d. W. Martin E. Lynge, Almar Postma, Brigitte Stadler, "Polydopamine - a nature-inspired polymer coating for biomedical science," *Nanoscale,* vol. 3, 2011.

[8] C. E. Brubaker and P. B. Messersmith, "The present and future of biologically inspired adhesive interfaces and materials," *Langmuir,* vol. 28, no. 4, pp. 2200-5, Jan 31 2012.

[9] R. Li, K. Parvez, F. Hinkel, X. Feng, and K. Mullen, "Bioinspired wafer-scale production of highly stretchable carbon films for transparent conductive electrodes," *Angew Chem Int Ed Engl,* vol. 52, no. 21, pp. 5535-8, May 17 2013.

[10] Z. Jia *et al.*, "Electrical and mechanical properties of poly(dopamine)-modified copper/reduced graphene oxide composites," *Journal of Materials Science,* vol. 52, no. 19, pp. 11620-11629, 2017.

[11] Z. Jia *et al.*, "Preparation and electrical properties of sintered copper powder compacts modified by polydopamine-derived carbon nanofilms," *Journal of Materials Science,* vol. 53, no. 9, pp. 6562-6573, 2018.

[12] Y. Zhao, H. Wang, B. Qian, H. Li, and F. Ren, "Copper-polydopamine composite derived from bioinspired polymer coating," *Journal of Alloys and Compounds,* vol. 742, pp. 191-198, 2018.

[13] J. Kong *et al.*, "Highly electrically conductive layered carbon derived from polydopamine and its functions in SnO2-based lithium ion battery anodes," *Chem Commun (Camb),* vol. 48, no. 83, pp. 10316-8, Oct 25 2012.

[14] K. Ai, Y. Liu, C. Ruan, L. Lu, and G. M. Lu, "Sp2 C-dominant N-doped carbon sub-micrometer spheres with a tunable size: a versatile platform for highly efficient oxygen-reduction catalysts," *Adv Mater,* vol. 25, no. 7, pp. 998-1003, Feb 20 2013.

[15] K. M. Im, T.-W. Kim, and J.-R. Jeon, "Metal-Chelation-Assisted Deposition of Polydopamine on Human Hair: A Ready-to-Use Eumelanin-Based Hair Dyeing Methodology," *ACS Biomaterials Science & Engineering,* vol. 3, no. 4, pp. 628-636, 2017.

[16] S. Kim, T. Gim, and S. M. Kang, "Stability-enhanced polydopamine coatings on solid substrates by iron(III) coordination," *Progress in Organic Coatings,* vol. 77, no. 8, pp. 1336-1339, 2014.

[17] M. M. Harding, M. W. Nowicki, and M. D. Walkinshaw, "Metals in protein structures: a review of their principal features," *Crystallography Reviews,* vol. 16, no. 4, pp. 247-302, 2010.

[18] S. J. Flora and V. Pachauri, "Chelation in metal intoxication," *Int J Environ Res Public Health,* vol. 7, no. 7, pp. 2745-88, Jul 2010.

[19] C. B. Black, H.-W. Huang, and J. A. Cowan, "Biological coordination chemistry of magnesium, sodium, and potassium ions. Protein and nucleotide binding sites," *Coord. Chem. Rev.,* vol. 135/136, p. 38, 1994.

[20] D. G. Brewer, P. T. T. Wong, and M. C. Sears, "the nature of the coordination bond in metal complexes of substituted pyridine derivatives. III. 4- metylpyridine complexes of some divalent transition metal ions," *Canadian J. Chem,* vol. 46, 1968.

[21] S. Hong, Y. S. Na, S. Choi, I. T. Song, W. Y. Kim, and H. Lee, "Non-Covalent Self-Assembly and Covalent Polymerization Co-Contribute to Polydopamine Formation," *Advanced Functional Materials,* vol. 22, no. 22, pp. 4711-4717, 2012.

[22] N. F. Della Vecchia, R. Avolio, M. Alfè, M. E. Errico, A. Napolitano, and M. d'Ischia, "Building-Block Diversity in Polydopamine Underpins a Multifunctional Eumelanin-Type Platform Tunable Through a Quinone Control Point," *Advanced Functional Materials,* vol. 23, no. 10, pp. 1331-1340, 2013.

[23] B. V. Crist, *Handbook of Monochromatic XPS spectra: The Elements of Native Oxides*. Wiley, 2000, p. 548.

[24] H.-H. Huang, W.-C. Shih, and C.-H. Lai, "Nonpolar resistive switching in the Pt/MgO/Pt nonvolatile memory device," *Applied Physics Letters*, vol. 96, no. 19, 2010.

[25] A. C. Ferrari and J. Robertson, "Raman spectroscopy of amorphous, nanostructured, diamond-like carbon, and nanodiamond," *Philos Trans A Math Phys Eng Sci*, vol. 362, no. 1824, pp. 2477-512, Nov 15 2004.

[26] A. C. Ferrari, "Raman spectroscopy of graphene and graphite: Disorder, electron–phonon coupling, doping and nonadiabatic effects," *Solid State Communications*, vol. 143, no. 1-2, pp. 47-57, 2007.

CHAPTER 5: ELECTRON-BEAM INDUCED IN-SITU GROWTH OF SELF-SUPPORTED METAL NANOPARTICLES IN ION-CONTAINING POLYDOPAMINE

Chapter 5 is based on the following publication

H. Li, Y. Zhao, Z. Zhang, Gangadhar, Andaluri, and F. Ren, 'Electron-beam induced *in situ* growth of self-supported metal nanoparticles from ion-containing polydopamine', *Materials Letters*, 251, 277-281, (2019), DOI: 10.1016/j.matlet.2019.05.087.

Electron-beam induced *in situ* growth of self-supported metal nanoparticles in ion-containing polydopamine

Haoqi Li[a], Yao Zhao[a], Zhuolei Zhang[a], Gangadhar Andaluri[b], and Fei Ren[a]

[a]Department of Mechanical Engineering, Temple University, Philadelphia, PA 19122, USA

[b]Department of Civil & Environmental Engineering, Temple University, Philadelphia, PA 19122, USA

Abstract

Polydopamine (PDA) is a biopolymer inspired by the mussel chemistry. Due to its capability to bind various metal ions, PDA has been explored in several potential applications including absorbents for heavy metal contaminants and templates for nanoparticle growth. In this study, we prepared metal ion-containing PDA by introducing chloride salts of Cu, Ni, and Co during the PDA synthesis. The PDA powders were then examined using transmission electron microscopy. We discovered that nanoparticles (NPs) formed under intense electron beam irradiation. For Cu-containing PDA, both equiaxed NPs and rod-like nano crystals were observed. On the other hand, Ni and Co NPs were mainly equiaxed with smaller average diameters. The formation of metal NPs is likely a result of electron beam induced reduction. We also demonstrated that electron beam could induce growth of Cu NPs on the surface of PDA-coated SiO_2 particles. This result suggested that PDA coating could be used as a platform to grow metal NPs on ceramics and potentially other substrates.

KEYWORDS: Polydopamine; Metal ion; Transmission electron microscopy; Electron beam irradiation; Metal nanoparticle

5.1 Introduction

Polydopamine (PDA), a biopolymer inspired by the mussel chemistry, has attracted much interest in the past decade when Lee and coworkers [1,2] reported a universal adhesive behavior of PDA on various substrates. It was shown that PDA could be synthesized through a self-assembly process and form nanometer scale coating on many material surfaces [1]. However, with much debate existing in the research community, there is no consensus on the exact structure of PDA. One popular hypothesis regards PDA as a stacked oligomer rather than a polymer. Using density functional theory, Kaxiras *et al.* [3] found that dopamine monomers primarily form ring tetramers via covalent bonds. Individual oligomers then stack to form larger particles through non-covalent bonding such as π-π interaction and hydrogen bonding [4]. Some studies found graphite-like structures in heat-treated PDA, which indirectly support the stacking model of PDA. For example, Yu *et al.* [5] found the inter-atomic spacing of carbonized PDA (cPDA) is similar to 0.34 nm. Our previous work [6] also discovered growth of nanocrystalline graphite phase in PDA after thermal annealing using neutron scattering and Raman spectroscopy.

As discussed in many studies, one interesting property of PDA is its universal adhesion to various substrates [1,7-10], which can be utilized in applications such as surface modification and targeted drug delivery [7]. This unique adhesive property of PDA can be attributed to its catechol-containing monomer, dopamine (DA). The oxidized catechol function groups can not only form in-plane covalent bonds and cross-plane π-π bonds with other nearby catechols, but also bind to oxides through hydrogen bonding and to metals through coordination bonding [11]. The ability of PDA to bind metals has been utilized to capture heavy metal ions for water treatment applications [12]. In addition, coordination bonding with metal ions has also been utilized to promote the growth of PDA. For example, Im *et al*. [13] found Fe^{3+} could enhance the polymerization of PDA by creating extra crosslinking between PDA chains.

Furthermore, the combination of the adhesive behavior and the metal binding property of PDA can be utilized to graft metal and metal oxides on substrates such as carbon fibers and graphene sheets [14,15]. A handful of studies have reported making metal-PDA composites from PDA materials containing Fe^{3+}, Ag^{+}, Au^{3+}, Co^{2+}, Cu^{2+}, Ni^{2+}, W^{6+}, and *etc*. [13,16-19]. Heat treatment was usually used in these processes to convert metal ions to metals or metal oxides. In some cases, hollowed structures of metal-PDA composites could be fabricated by removing the substrates (e.g. through chemical etching) [17,18,20]. In other cases, PDA could be removed (e.g., by plasma treatment), leaving metal NPs attached on the substrates [16].

In this study, we reported a new discovery that electron beam irradiation could also result in formation and growth of metal NPs in metal ion-containing PDA. This new phenomenon was observed when subjecting metal ion-containing PDA powders to intense electron beam during transmission electron microscopy (TEM) experiments. Three divalent metal ions (Cu^{2+}, Ni^{2+}, and Co^{2+}) were included in this study due to their good coordination bonding behavior [21] and their potential applications as electrocatalysts [22-24]. We further demonstrated *in situ* growth of Cu nanoparticles on SiO_2, which is an example of ceramic catalyst support [25]. Our finding suggested that PDA could be used as a template for nanoparticle growth on ceramic substrates, which offers an alternative route for synthesis of metal-based catalysts.

5.2 Experimental method

5.2.1 Preparation of PDA powder

Method to prepare metal-ion containing PDA powders is described as follows. Tris buffer (Fisher Scientific Inc., Waltham, MA) was diluted from 2 M to 50 mM using deionized water. The pH value of the buffer was adjusted to 8.5 using 1N hydrochloride acid (Fisher Scientific Inc., Waltham, MA). In a typical synthesis experiment, 124 mg of dopamine hydrochloride powder (Alfa Aesar, Haverhill, MA) was added to 50 mL tris buffer, after which metal chloride powders ($CuCl_2$, $NiCl_2$, or $CoCl_2$, Alfa Aesar, Haverhill, MA) was added. The molar ratio between dopamine molecules and metal ions was fixed at 1:1. The mixture was stirred using magnetic stirrer for 24 hours in air. Powders were then collected by filtration, washed with deionized water, and oven-dried overnight at 50^{o}C. PDA powder without metal ions was also prepared using this procedure.

5.2.2 Preparation of PDA coated SiO_2 nanoparticles

SiO_2 nanoparticles (NPs) were made by the modified Stober method [26]. Firstly, 25 mL ethanol (200 proof, Decon Labs Inc., King of Prussia, PA) and 25 mL deionized water were mixed for 10 min using a magnetic stirrer. Then, 2 mL of tetraethyl orthosilicate (TEOS, Aldrich, St. Louis, MO) was added to the solution while keeping the solution stirred. After 20 min of TEOS addition, 4 mL of 28% ammonium hydroxide (NH_4OH, Fisher Scientific Inc., Waltham, MA) was added to promote the growth of SiO_2. Condensation was completed 40 min after the addition of ammonium hydroxide. The final product was then separated by centrifuging, and washed and dried overnight in an oven at 50˚C.

To coat SiO_2 NPs with metal-ion containing PDA, dried SiO_2 NPs were added in the tris buffer containing metal chloride and dopamine chloride. After 24 hours incubation, the mixture was centrifuged, and the SiO_2 NPs were separated. The collected powder was then washed and dried overnight in an oven at 50˚C for further characterization.

5.2.3 Transmission electron microscopy experiment

TEM experiments (JEM 1400, JEOL, Tokyo, Japan) were conducted on powder samples suspended on copper TEM grids with carbon-formvar supporting film (Ted Pella Inc., Redding, CA). The acceleration voltage was fixed at 120 kV. To change the current density, the electron beam current was manually adjusted. The current density was calculated from the beam current, beam diameter, and magnification, which were recorded during the experiments.

5.3 Results and discussion

All as-synthesized PDA powders, with or without metal ions, showed similar morphology: the powder particles were spheroidal and aggregated into larger clusters (Figures 5.1 (a), (b), S1). Selected-area electron diffraction (SAED) revealed these powders were amorphous (Figure 5.1 (c)), which agreed with our previous finding [6]. The morphology of the pristine PDA did not show significant change when the intensity of the electron beam was increased. On the other hand, the PDA powders containing Cu^{2+} (Cu-PDA), Ni^{2+} (Ni-PDA), and Co^{2+} (Co-PDA) behaved differently under intense electron beam irradiation.

When the electron beam density increased to approximately 20 mA mm^{-2}, the Cu-PDA powders started to shrink, and small dark particles appeared inside the powder particles. Most of these dark particles were spheroidal (Figure 5.1 (d)) while some exhibited hexagonal or triangular shapes (Figure 5.1 (e)). These nanoparticles (NPs) were as large as 200 nm (Figures 5.1 (d), (e)). SAED analysis indicated these dark particles were metallic Cu. For example, Figure 5.1 (f) shows diffraction rings corresponding to the (111), (200), (220), and (311) planes of Cu crystal. Slow increase of the TEM beam current would lead to formation and growth of Cu rods (Figures 5.1 (g) and (h)). The diameter of these rods was approximately 50 nm, and their length varied between ~ 100 nm and 1000 nm (Figures 5.1 (g), (h)). SAED showed these rods were Cu single crystals (Figure 5.1 (i)). For the Cu rod corresponding to Figure 5.1 (i) the crystal grew along the [110] direction. It is interesting to point out that the Cu NPs and nano rods initially formed inside and then grew out of the PDA particles. A video clip showing the growth of Cu NPs and nano rods is available in SI. If the TEM current was rapidly increased after the formation of Cu NPs, instead of growing into rods, some Cu NPs would break and leave shattered pieces on the TEM support film (Figure S2). This shattering phenomenon of Cu particles was also observed by other researchers [27]. When high power electron beam hits a Cu particle, internal electric field could build up and generate opposing forces within the particle that can eventually tear it up [28].

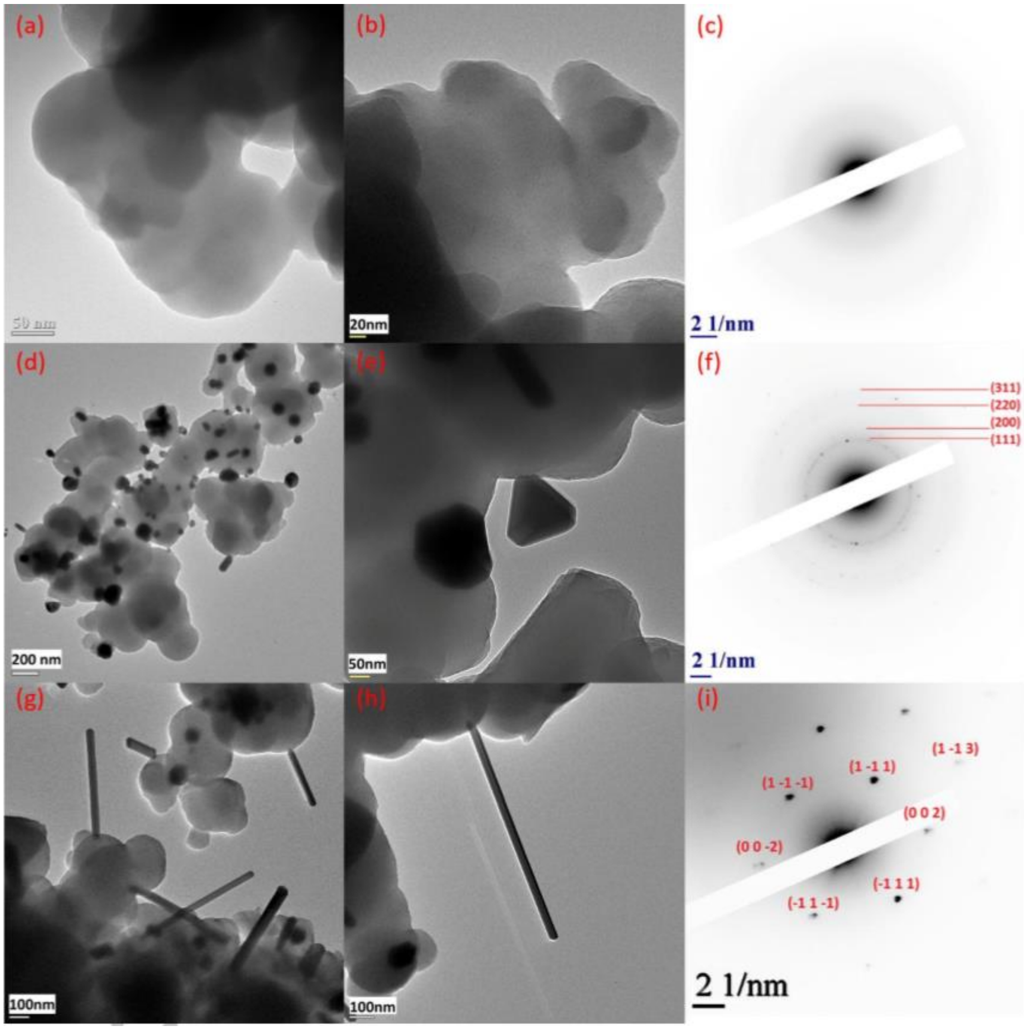

Figure 5.1: (a) TEM image of undoped PDA particles; (b) TEM image of Cu-PDA before electron beam treatment and (c) its diffraction pattern; (d)&(e) TEM images of Cu-PDA after electron beam treatment showing growth of nanoparticles; (f) selected area electron diffraction pattern showing diffraction rings corresponding to Cu; (g)&(h) TEM images showing Cu nano rods; (i) selected area electron diffraction pattern obtained from a Cu nanorod.

In contrast to Cu-PDA, Ni-PDA and Co-PDA samples went through different morphology change under electron irradiation. Nanoparticles were first observed when the electron beam density was increased to approximately 35 mA mm^{-2} for the Ni-PDA sample and 100 mA mm^{-2} for the Co-PDA sample, respectively. These nanoparticles were smaller than the Cu NPs, typically less than 20 nm for Ni NPs (Figure 5.2 (a)), and less than 50 nm for Co NPs (Figure 5.2 (b)). SAED confirmed these nanoparticles were metallic Ni (Figure 5.2 (c)) or Co (Figure 5.2 (d)). When the electron beam was further increased, no formation of nano rods was observed in either Ni-PDA or Co-PDA powders. Instead, the Ni or Co NPs became liquid like and flew within and between PDA particles (a video showing the flowing phenomenon of Ni NPs can be found in SI). Some "fluidized" NPs merged to form larger particles (Figure 5.2 (e)) that were later discovered to be single crystals by SAED (Figure 5.2 (f)). The flowing phenomenon implied that the PDA particles were porous and permeable. Using the Brunauer-Emmett-Teller (BET) method, we found the average pore size of PDA was approximately 20 nm and the specific surface area was 10 m^2/g. It is possible that these connected pore space would also serve as channels for ion transportation which was necessary for the growth of metal NPs.

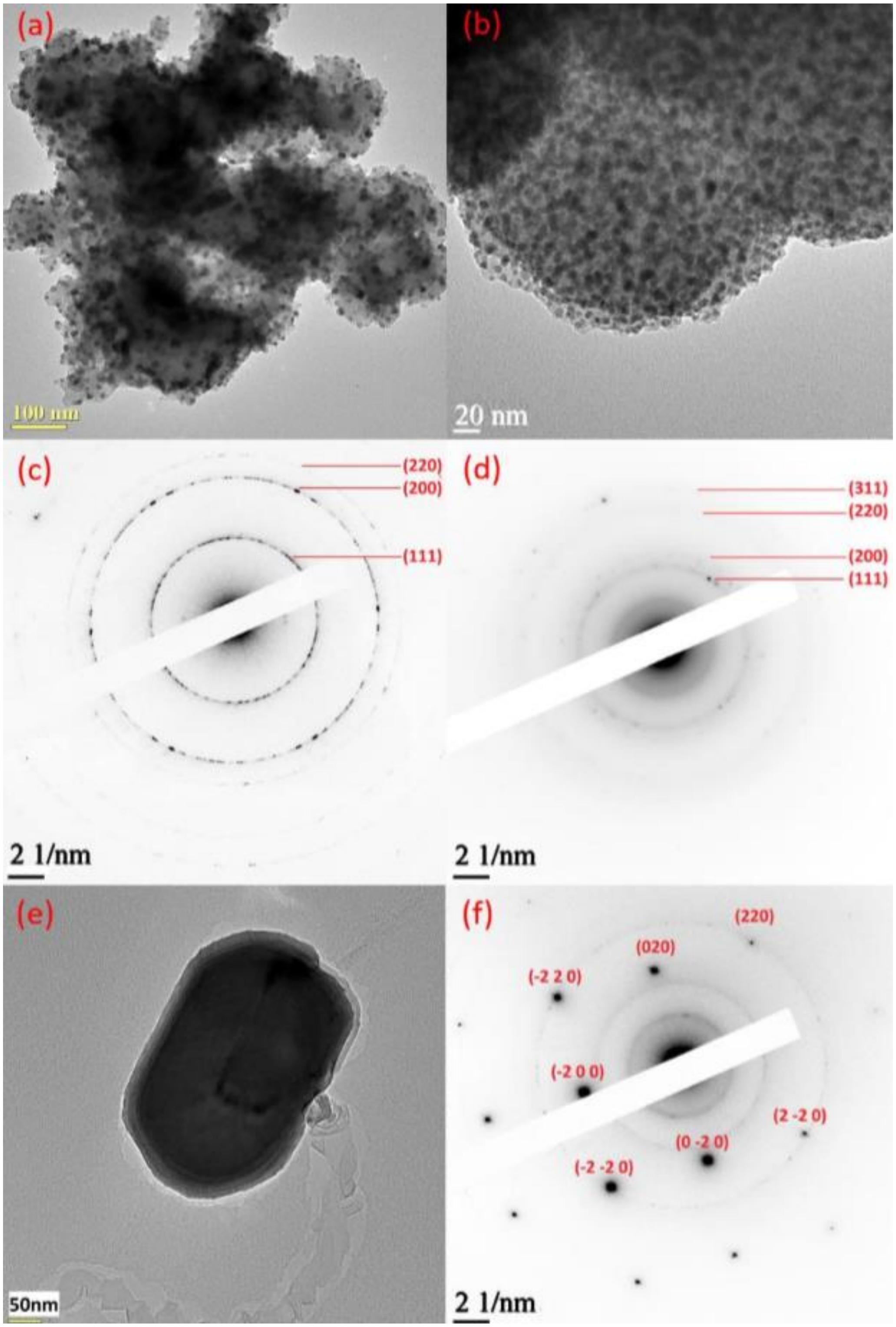

Figure 5.2: TEM images of (a) Ni-PDA and (b) Co-PDA after electron beam irradiation, selected area electron diffraction patterns of (c) Ni-PDA and (d) Co-PDA, (e) a single crystal Ni nanoparticle and (f) its electron diffraction pattern.

Synthesis of inorganic NPs from metal cations contained in porous structures has been widely studied. For instances, dendrimers were used as templates to synthesize NPs of Au, Ag, Cu, Pt, Ni, Pd, CdS, and CdSe [29]. With repeating branches, dendrimers could provide a large number of active sites to bind metal cations, and the porous structures of dendrimers also allowed the cations to flow. On the other hand, electron irradiation induced NP growth was also observed in other materials [27,30-32]. For example, Shi *et al*. was able to grow Ag NPs from AgCl using electron beam irradiation, which broke the ionic bonding between Ag^+ and Cl^- ions and provided free electrons to reduce Ag^+ [30]. Yen *et al*. [27] also observed growth of Cu nano wire from polymer-encapsulated CuCl. Another example was the growth of Ag nanowires from Ag^+ ion-containing zeolite [31]. In this case, nucleation of Ag NPs was initially induced by electron reduction. Electron charging on Ag NPs further attracted Ag^+ ions and fueled the growth of nanowires [31]. The effect of electrochemical reduction effect of free electrons was also reported in plasma induced NP formation [33].

The nanoparticle formation phenomenon observed in this study may be explained by the electron induced reduction effect. After capturing free electrons from the electron beam, Cu^{2+}, Ni^{2+}, and Co^{2+} ions contained in PDA were first reduced to form metal nuclei. Nearby positively charged cations were then attracted by and migrated towards the electron-charged metal NPs, fueling the growth of the NPs. Meanwhile, electron-matter interaction can also result in other effects such as heating [34]. As previously mentioned, various studies have showed NPs could be obtained by thermal annealing of ion-containing PDA [17,19,20]. However, contribution of electron beam induced heating to the formation and growth of metal NPs observed in this study remains unclear and requires future investigation.

Metal and semiconducting NPs can be utilized in many existing and potential applications such as catalysts in fuel cells, electrochemical cells, and catalytic converters, where catalytic NPs are often attached to certain supports or substrates [25]. The universal adhesive behavior of PDA may be used to assist binding NPs with the support materials. Figure 5.3 (a) shows TEM images of SiO_2 particles without and with Cu-PDA coating. When electron current density was increased, some small dark dots were observed on the surface of Cu-PDA coated SiO_2 particles (Figure 5.3 (b)). Continuous electron irradiation led the small dots to further grow to larger particles and nano rods (Figure 5.3 (c)), which were determined to be Cu by SAED (Figure 5.3(d)). This observation demonstrates that PDA could serve as a binder between metal nanoparticles and ceramic substrates, which opens up a new route towards fabrication of substrate-supported nanoparticle materials.

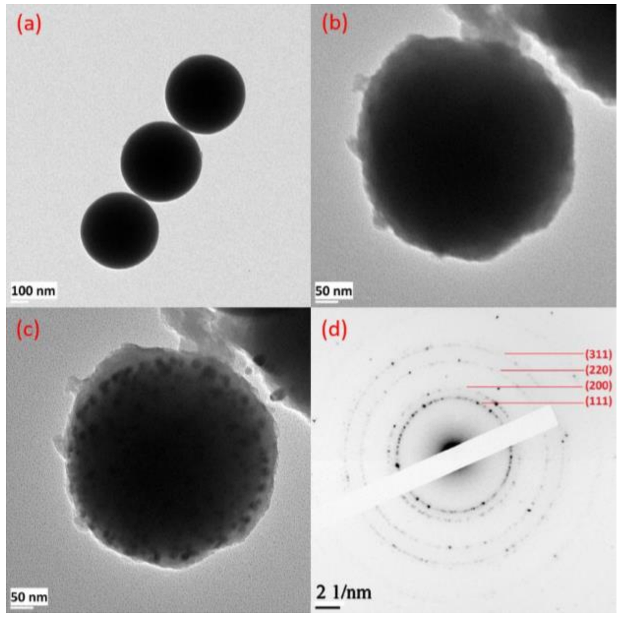

Figure 5.3: TEM image of (a) SiO2 particles without PDA coating, (b)&(c) SiO2 particles with PDA coating and electron beam irradiation, and (d) selected area electron diffraction pattern.

5.4 Conclusions

Electron beam irradiation induced *in situ* growth of metal NPs was observed on metal-ion containing polydopamine materials. Cu NPs, approximately 50 to 200 nm in diameter, and Cu nano rods, as long as 1 μm, could be obtained using this approach. On the other hand, Ni and Co NPs were much smaller in size (as small as 5 nm) and exhibited flowing behavior. The metallic nature of these NPs and nano rods were confirmed from the electron diffraction patterns. Cu NPs and nano rods could also grow on Cu-PDA coated SiO_2 particles using this electron beam irradiation method. Our findings suggest PDA can be used as a template to assist *in situ* NP growth on ceramic substrates through an electron beam induced reduction process.

REFERENCE

[1] S. M. D. Haeshin Lee, William M. Miller, Phillip B. Messersmith, "Mussel-Inspired Surface Chemistry for Multifunctional Coatings," *Science*, vol. 318, p. 5, 2007.

[2] J. H. Ryu, P. B. Messersmith, and H. Lee, "Polydopamine Surface Chemistry: A Decade of Discovery," *ACS Appl Mater Interfaces,* vol. 10, no. 9, pp. 7523-7540, Mar 7 2018.

[3] E. Kaxiras, A. Tsolakidis, G. Zonios, and S. Meng, "Structural model of eumelanin," *Phys Rev Lett,* vol. 97, no. 21, p. 218102, Nov 24 2006.

[4] S. Hong, Y. S. Na, S. Choi, I. T. Song, W. Y. Kim, and H. Lee, "Non-Covalent Self-Assembly and Covalent Polymerization Co-Contribute to Polydopamine Formation," *Advanced Functional Materials,* vol. 22, no. 22, pp. 4711-4717, 2012.

[5] X. Yu, H. Fan, Y. Liu, Z. Shi, and Z. Jin, "Characterization of carbonized polydopamine nanoparticles suggests ordered supramolecular structure of polydopamine," *Langmuir,* vol. 30, no. 19, pp. 5497-505, May 20 2014.

[6] H. Li *et al.*, "Structure Evolution and Thermoelectric Properties of Carbonized Polydopamine Thin Films," *ACS Appl Mater Interfaces,* vol. 9, no. 8, pp. 6655-6660, Mar 1 2017.

[7] D. R. Dreyer, D. J. Miller, B. D. Freeman, D. R. Paul, and C. W. Bielawski, "Perspectives on poly(dopamine)," *Chemical Science,* vol. 4, no. 10, 2013.

[8] Z. Jia *et al.*, "The Electrical conductivities and Tribological properties of Vacuum Hot-Pressed Cu/Reduced Graphene Oxide Composite," *Journal of Materials Engineering and Performance,* vol. 26, no. 9, pp. 4434-4441, 2017.

[9] Z. Jia *et al.*, "Preparation and electrical properties of sintered copper powder compacts modified by polydopamine-derived carbon nanofilms," *Journal of Materials Science,* vol. 53, no. 9, pp. 6562-6573, 2018.

[10] Y. Zhao, H. Wang, B. Qian, H. Li, and F. Ren, "Copper-polydopamine composite derived from bioinspired polymer coating," *Journal of Alloys and Compounds,* vol. 742, pp. 191-198, 2018.

[11] Y. Li, J. Wen, M. Qin, Y. Cao, H. Ma, and W. Wang, "Single-Molecule Mechanics of Catechol-Iron Coordination Bonds," *ACS Biomaterials Science & Engineering,* vol. 3, no. 6, pp. 979-989, 2017.

[12] D. T. Sun *et al.*, "Rapid, Selective Heavy Metal Removal from Water by a Metal-Organic Framework/Polydopamine Composite," *ACS Cent Sci,* vol. 4, no. 3, pp. 349-356, Mar 28 2018.

[13] K. M. Im, T.-W. Kim, and J.-R. Jeon, "Metal-Chelation-Assisted Deposition of Polydopamine on Human Hair: A Ready-to-Use Eumelanin-Based Hair Dyeing Methodology," *ACS Biomaterials Science & Engineering,* vol. 3, no. 4, pp. 628-636, 2017.

[14] Y. Niu, X. Huang, L. Zhao, W. Hu, and C. M. Li, "One-Pot Synthesis of Co/CoFe2O4 Nanoparticles Supported on N-Doped Graphene for Efficient Bifunctional Oxygen Electrocatalysis," *ACS Sustainable Chemistry & Engineering,* vol. 6, no. 3, pp. 3556-3564, 2018.

[15] J. Huang, Y. Xu, Y. Xiao, H. Zhu, J. Wei, and Y. Chen, "Mussel-Inspired, Biomimetics-Assisted Self-Assembly of Co3O4 on carbon fibers for flexible supercapacitors," *ChemElectroChem,* vol. 4, no. 9, pp. 2269-2277, 2017.

[16] T.-L. Chang, X. Yu, and J. F. Liang, "Polydopamine-enabled surface coating with nano-metals," *Surface and Coatings Technology,* vol. 337, pp. 389-395, 2018.

[17] X. Guo *et al.*, "Fabrication of Co@SiO2@C/Ni submicrorattles as highly efficient catalysts for 4-nitrophenol reduction," *Dalton Trans,* vol. 46, no. 35, pp. 11598-11607, Sep 12 2017.

[18] Y. Liang *et al.*, "Metal-polydopamine frameworks and their transformation to hollow metal/N-doped carbon particles," *Nanoscale,* vol. 9, no. 16, pp. 5323-5328, Apr 20 2017.

[19] C. Liu *et al.*, "Noble-metal-free tungsten oxide/carbon (WOx/C) hybrid manowires for highly efficient hydrogen evolution," *Nanotechnology,* vol. 28, no. 44, p. 445403, Nov 3 2017.

[20] H. Song, Z. Wang, J. Yang, X. Jia, and Z. Zhang, "Facile synthesis of copper/polydopamine functionalized graphene oxide nanocomposites with enhanced tribological performance," *Chemical Engineering Journal,* vol. 324, pp. 51-62, 2017.

[21] M. Krogsgaard, V. Nue, and H. Birkedal, "Mussel-Inspired Materials: Self-Healing through Coordination Chemistry," *Chemistry,* vol. 22, no. 3, pp. 844-57, Jan 18 2016.

[22] X. Liu, H. Zheng, Z. Sun, A. Han, and P. Du, "Earth-Abundant Copper-Based Bifunctional Electrocatalyst for Both Catalytic Hydrogen Production and Water Oxidation," *ACS Catalysis,* vol. 5, no. 3, pp. 1530-1538, 2015.

[23] V. Vij *et al.*, "Nickel-Based Electrocatalysts for Energy-Related Applications: Oxygen Reduction, Oxygen Evolution, and Hydrogen Evolution Reactions," *ACS Catalysis*, vol. 7, no. 10, pp. 7196-7225, 2017.

[24] H. Zhong *et al.*, "Electrocatalytic Cobalt Nanoparticles Interacting with Nitrogen-Doped Carbon Nanotube in Situ Generated from a Metal-Organic Framework for the Oxygen Reduction Reaction," *ACS Appl Mater Interfaces,* vol. 9, no. 3, pp. 2541-2549, Jan 25 2017.

[25] Thomas Leonhard, Peter Florchinger, Alf Degen, Wolfgang Held, Soren Hinze, and E. Pott, "High-performance Ceramic Substrate for Catalytic Converters," *MTZ,* vol. 5, 2003.

[26] K. S. Rao, K. El-Hami, T. Kodaki, K. Matsushige, and K. Makino, "A novel method for synthesis of silica nanoparticles," *J Colloid Interface Sci,* vol. 289, no. 1, pp. 125-31, Sep 1 2005.

[27] Ming-Yu Yen, Ching-Wen Chiu, Fu-Rong Chen, Ji-Jung Kai, Chi-Young Lee, and H.-T. Chiu, "Convergent Electron Beam Induced Growth of Copper Nanostructures: Evidence of the Importance of a Soft Template," *Langmuir,* vol. 20, no. 2, 2004.

[28] N. Jiang, "Beam damage by the induced electric field in transmission electron microscopy," *Micron,* vol. 83, pp. 79-92, Apr 2016.

[29] Richard M. Crooks, Mingqi Zhao, Li Sun, Victor Chechik, and L. K. Yeung, "Dendrimer Encapsulated Metal Nanoparticles: Synthesis, Characterization, and Applications to Catalysis," *Accounts of Chemical Research,* vol. 34, 2001.

[30] G. Shi, S. Bao, W. Lai, Z. Rao, X. Zhang, and Z. Wang, "Electron beam induced growth of silver nanoparticles," *Scanning*, vol. 35, no. 2, pp. 69-74, Mar-Apr 2013.

[31] Michael J. Edmondson *et al.*, "Electron-Beam induced Growth of Bare Silver Nanowire from Zeolite Crystallites," *Adv. Mater.*, vol. 13, no. 21, 2001.

[32] P. A. Anderson *et al.*, "Production of Ultrafine Single-Crystal Copper Wires through Electron Beam Irradiation of Cu-containing Zeolite X," *J. Inorg. Gen. Chem*, vol. 631, no. 2-3, pp. 443-447, 2005.

[33] Ji-Jun Zou, Yue-ping Zhang, and C.-J. Liu, "Reduction of Supported Noble-Metal Ions Using Glow Discharge Plasma," *Langmuir,* vol. 22, 2006.

[34] R. F. Egerton, P. Li, and M. Malac, "Radiation damage in the TEM and SEM," *Micron,* vol. 35, no. 6, pp. 399-409, 2004.

CHAPTER 6: MECHANICAL PROPERTIES OF POLYDOPAMINE (PDA) THIN FILMS

Chapter 6 is based on the following publication

H. Li, J. Xi, Y. Zhao, F. Ren, ‘Mechanical properties of polydopamine (PDA) thin films’, *MRS Advance*, published online Jan. 2019, DOI:10.1557/adv.2019.52

Mechanical properties of polydopamine (PDA) thin films

Haoqi Li, Jiaxin Xi, Yao Zhao, Fei Ren

Department of Mechanical Engineering, College of Engineering, Temple University, Philadelphia, PA 19122, U.S.A.

Abstract

Polydopamine (PDA) is a biopolymer, which can form uniform thin films on almost all solid substrates as well as at the liquid/air interface. Carbonized polydopamine possesses graphite-like structure and exhibits high electrical conductivity, which makes it a potential carbon-based thin film conductor. However, studies on mechanical behavior of PDA and its derived materials are very limited. In this study, PDA samples were synthesized through self-assembly of dopamine in aqueous solution. Elastic modulus of thin films was measured using the nanoindentation technique. It is shown that the Young's modulus of PDA thin film increased with increasing heat treatment temperature (up to 600˚C). Doping with Cu ions also increased the Young's modulus of PDA. Furthermore, all PDA thin films, with and without Cu, exhibited creep behavior.

6.1 Introduction

Polydopamine (PDA) is a biopolymer inspired by mussel chemistry [1]. It has attracted much attention owing to its interesting properties and ease of synthesis. An auto-oxidation process under mild conditions in dopamine solution [2] can yield nanoscale PDA powder with controllable size [3], smooth, crack-free, and thin coatings on solid substrates, or free-standing films at the solution/air interface [4]. Multiple function groups give PDA the ability to interact with other molecules and metal ions through secondary bonding or coordination bonding [5]. PDA is proposed to be used in surface modification with tailored hydrophobicity, target drug delivery, and capture of heavy metal ions for water treatment [6-9]. In addition, thin PDA films can also be converted to a graphite-like phase via heat treatment under protective atmosphere. Carbonized PDA (cPDA) is found to have an electrical conductivity [10] as high as 1.2 x 10^5 S/m which is comparable to reduced graphene oxide (rGO) [1, 11]. Such founding may open up the possibilities for cPDA to be used in various electronic applications, such as sensors, flexible electrodes, and protective shielding coatings.

However, the mechanical behavior of PDA and cPDA thin films, which is essential for design and fabrication of devices based on this material, is not well understood. Lin et al [12] has built in-silico models to simulate the mechanical properties of PDA with different crosslinking schemes. The results from simulation showed the Young’s modulus of covalently linked PDA range from 4.1 GPa to 4.4 GPa. This result also matched the lower bound of their experimental results obtained from nanoindentation, which ranged from 4.3 GPa to 10.5 GPa. Lin also mentioned the heterogeneous nature of the PDA coating thickness and concluded this as the reason of large variation of the experimental results. It is important to point out that Lin and coworkers found the Young's modulus increased as the indentation penetration increased, which is an indication of substrate (silicon) effect. The lowest Young's modulus of 4.3 GPa corresponded to the smallest penetration of 150 nm. However, the authors did not provide detailed information about the thickness of the PDA thin films [12, 13]. Another study performed by Klosterman and coworkers tested PDA thin films using the buckling method. Results showed a Young's modulus of 2.0 GPa, which was lower than the in-silico model prediction (2.3 GPa). The authors argued that the simulation model only considered the internal forces within PDA granules, whereas inter-granular interaction would affect the experimental result. Therefore, inter-granular force is weaker than internal bonding [14].

While there exists some variation in the measurement data of PDA thin films [12, 14] the mechanical property of carbonized PDA has not been investigated. Furthermore, effect of other processing conditions, such as doping with metal ions, is unknown. The addition of metal ion dopant into polymer matrix incubates dative bonds with proper donor-acceptor combinations. With coordination bonds, the structure of the resultant often differs from its pristine form, so as the mechanical properties. Holten-Andersen et al. studied how the addition of metal ions or metal nanoparticles would affect hydrogels' mechanical properties by replacing intermolecular linkage from covalent bonding to coordination link [15]. In addition, the number of bonds formed between polymer and metal nanoparticles will also alter the property [16]. The mechanical property of hydrogel can also be tuned since the bonding is often chemically reversible [16].

This work aims to expend our knowledge on the mechanical behavior of PDA and its derived materials by studying the Young's modulus of PDA and Cu ion doped PDA as a function of heat treatment temperature. Nanoindentation was conducted on freestanding films, whose thickness was several times larger than the indentation penetration to minimize the substrate effect. Our results show both heat treatment and Cu doping led to increased Young's modulus.

6.2 Experimental details

Synthesis was conducted using a previously reported process [1, 2]. In brief, 2 mg/mL of dopamine hydrochloride powder (99%, Alfa Aeser, Haverhill, MA) was added into 50 mM tris buffer (pH = 8.5, Thermo Fisher Scientific Inc., Walthan, MA). For doping experiment, molar ratio of 1:1 was used between dopamine and $CuCl_2$ (Sigma-Aldrich, St. Louis, MO). The pH of the solution was adjusted back to 8.5 using 2M tirs buffer to ensure the alkaline environment for DA polymerization. Cleaned fused silica substrates were immersed in the solution. After 24 h, the substrates were removed, cleaned, and dried. Freestanding films floating on the solution surface were collected onto silicon substrates, and oven-dried. The dried films were heat treated in a tube furnace with running nitrogen at 300˚C and 600˚C. The nominal heating and cooling rate was fixed at 5˚C/min, a 60-min hold was performed at the peak temperature.

Nanoindentation was performed using a commercial unit (Triboindenter TI980, Bruker, Billerica, MA) with a conical tip under load control mode. The peak load was fixed at 25 μN. The loading, unloading segments were 2 sec, and the holding segment was 5 sec. Thickness of the thin films was measured using atom force microscopy (AFM, Bruker Demission Icon, Bruker, Billerica, MA). Surface morphology of the thin films was examined using scanning electron microscopy (SEM, FEI Quanta 450 FEG, FEI Inc.

Hillsboro, OR) with a 10 kV acceleration voltage. TEM experiments (JEM 1400, JEOL, Tokyo, Japan) were conducted on powder samples suspended on copper TEM grids with carbon-formvar supporting film (Ted Pella Inc., Redding, CA). The acceleration voltage was fixed at 120 kV. Thermal stability of PDA and Cu-PDA powders was studied using differential scanning calorimetry (DSC 2500, TA Instrument, Inc, New Castle, DE) with a nominal heating and cooling rate of 10˚C/min.

6.3 Results and discussions

PDA coating on fused silica appeared to be brownish, which darkened with a blackish color after heat treatment at 600˚C (Figure 6.1 (a)). This colour change is an indication of carbonization, which is accompanied by a mass loss and an increase in electrical conductivity [2]. Figure 6.1 (b) shows an SEM image of a freestanding film collected on silicon substrate and oven dried in air. In contrast to crack-free PDA coatings on substrates [2], multiple cracks can be seen in the freestanding film. These cracks may be caused by the shrinkage of the PDA film during the drying process. After heat treatment, the roughness of freestanding film seemed to be reduced (Figure 6.1 (c)) as the thickness decreased from ~ 570 nm prior to heat treatment to approximately 50 nm after heat-treated at 600˚C. In Figure 6.1 (c), dark regions of cPDA were separated by cracks, which appeared bright due to electron charging. Our previous study showed the surface roughness within the uncracked regions was on the order of a few nanometers, which was not significantly affected by the heat treatment temperature [2].

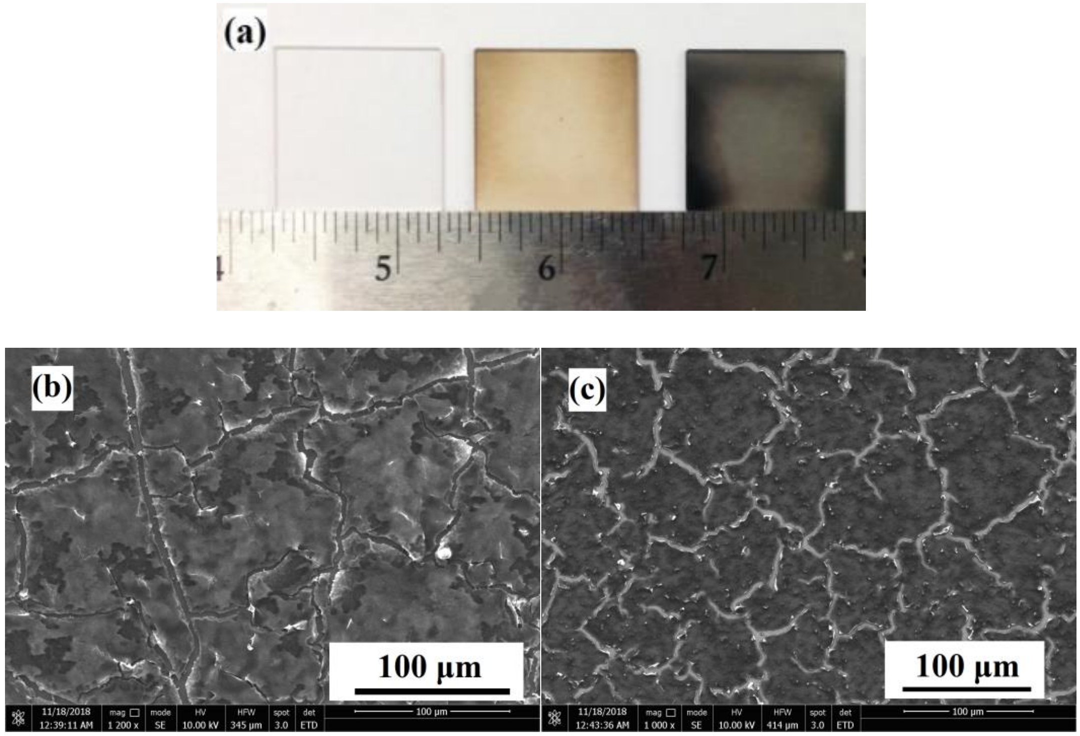

Figure 6.1: Images of PDA thin films. (a) Optical images of fused silica substrate (left), PDA coating on silica (middle), and carbonized PDA on silica substrate (right). (b) SEM image of PDA freestanding film collected on silicon substrate. (c) SEM image of PDA freestanding film after heat treatment at 300˚C.

Figure 6.2 (a) shows a representative SEM image of Cu-ion doped PDA freestanding film. Cracks were still present. However, the Cu-PDA film seemed to be smoother without residual PDA particles (inset of Figure 6.2 (a)). After heat treatment, nanoscale particles developed in the Cu-PDA thin film, accompanied by some surface roughening (Figure 6.2 (b)&(c)). The surface roughening is related to the formation of Cu nanoparticles, which were approximately 0.9µm after heat treatment at 300^{o}C (Figure 6.2 (b)) and merge into bigger cluster as large as 3µm after heat treatment at 600^{o}C (Figure 6.2 (c)). Figure 6.2 (d) shows a TEM image of Cu-PDA powder after heat treatment. The dark circular dots were Cu nanoparticles, which were confirmed from electron diffraction analysis (Figure 6.2 (e)). Therefore, it is believed that Cu ions initially doped into the PDA underwent a precipitation process to form metallic nanoparticles. The stability of

Cu-PDA was also examined using differential scanning calorimetry (DSC), which showed an exothermic peak between 300˚C and 400˚C (Figure 6.3). This exothermic peak is likely related to the formation of Cu nanoparticles. In contrast, no such exothermic reaction was observed in pure PDA (Figure 6.3).

To measure the mechanical properties, nanoindentation was performed on freestanding films. The film thickness varied from 50 nm and 570 nm (Table 6.1). At least 10 tests were conducted on each sample in the crack-free regions. The peak indentation depth varied between different materials. For PDA films without heat treatment, the indentation penetration was approximately 40 nm, which decreased to 10 nm in samples heat treated at 600˚C. Similar trend was observed on Cu-PDA films. For all samples, the indentation penetration was less than 1/5 of the total film thickness. Therefore, the substrate effect in this study is not significant.

The three curves included in Figure 6.4 (a) showed very different behavior, indicating the effect of heat treatment, thus the carbonization process, on the mechanical behavior of PDA thin films. Under the same peak indentation load, the maximum indentation penetration decreased with increasing heat treatment temperature, implying increased stiffness. From the unloading portion of the curve, Young's modulus was calculated [17]. As shown in Figure 6.4 (b), prior to heat treatment, PDA film had an average Young's modulus of 2.3 GPa, which is similar to the value reported by Klosterman et al [14]. After heat treatment, the Young's modulus increased to 7.2 GPa, which further increased to 14.7 GPa after heat treatment at 600˚C.

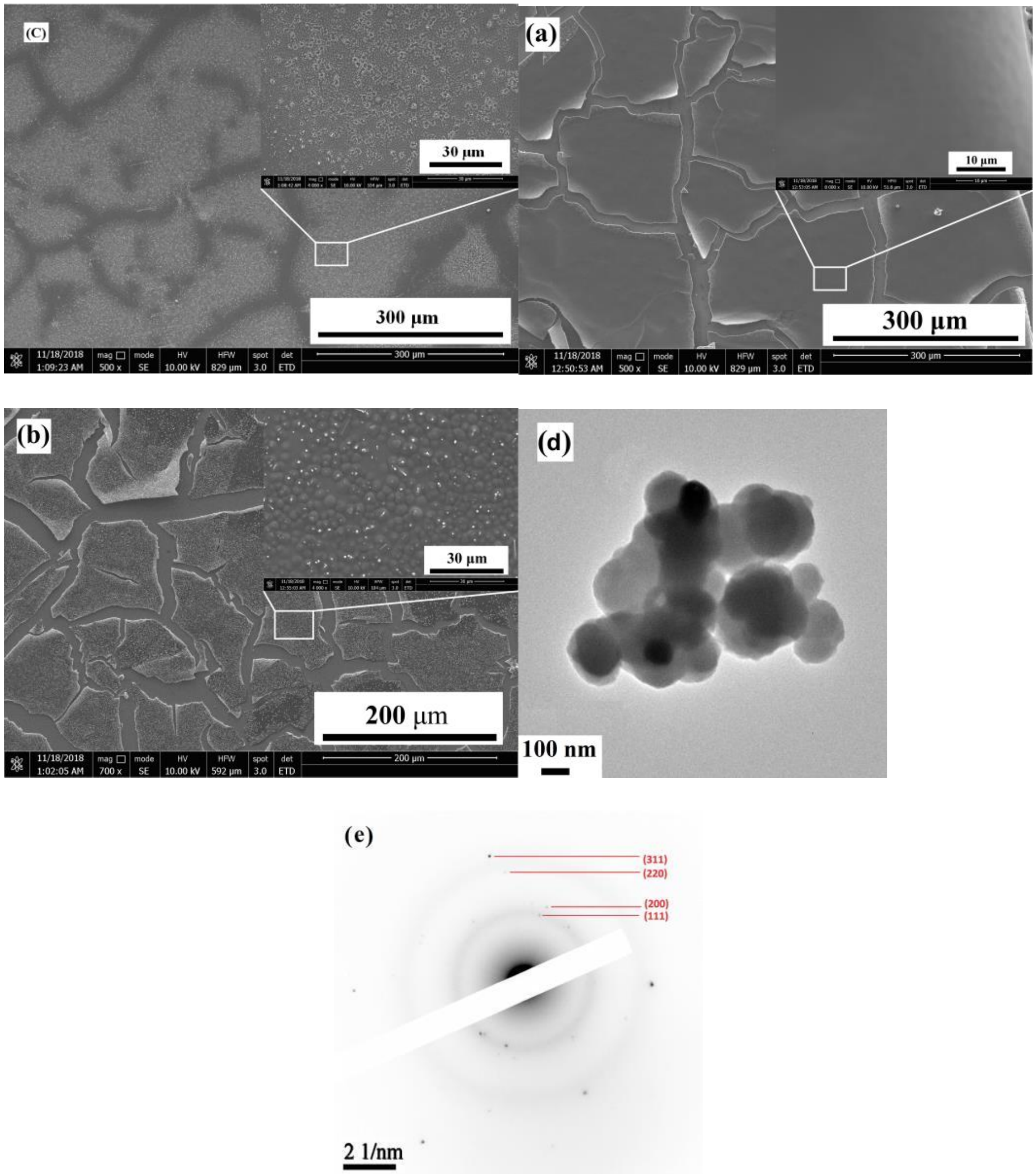

Figure 6.2: SEM images of freestanding Cu-PDA thin film collected on silicon substrate (a) before and (b) after heat treatment at 300˚C. (c) after heat treatment at 600˚C. (d)TEM image of Cu-PDA powder heat treated at 300˚C; and (e) selected area electron diffraction pattern of heat-treated Cu-PDA powder

Doping with Cu ion increased the Young's modulus of PDA. Without heat treatment, Cu-PDA film showed a Young's modulus of 10.2 GPa, which is more than three times higher than the pristine PDA film. It is possible that the Cu ions in the PDA promoted inter-granular interaction by introducing cross-linking bonds between PDA oligomers, which in turn enhanced the average bonding strength in PDA. Heat treatment also increased the Young's modulus of the Cu-PDA thin film. After heat treatment at 600˚C, the Cu-cPDA film exhibited a Young's modulus of 19.2 GPa (Figure 6.4 (b)). This increase may be related to i) carbonization of the PDA phase, and ii) formation of Cu nanoparticles (Figure 6.2 (b)).

All samples exhibited some degree of creep (see plateaus in Figure 6.4 (a)). This behavior is better illustrated in Figure 6.4 (c), where when holding at the peak load (~ 2 to 5 sec), the indentation penetration depth continued to increase. The creep behavior observed during nanoindentation, indicating viscoelasticity in PDA materials, can be well described using a generalized Kelvin model [18]. As illustrated in scheme 3.4.1, a Kelvin model consists of a spring element serially connected with several Kelvin units, which include a dashpot and a spring connected in parallel. In this work, the creep data, i.e. time-dependent indentation, can be well characterized by the simplest Kelvin model,

$$u = u_0 + u_1\left(1 - e^{-t/t_1}\right) \tag{1}$$

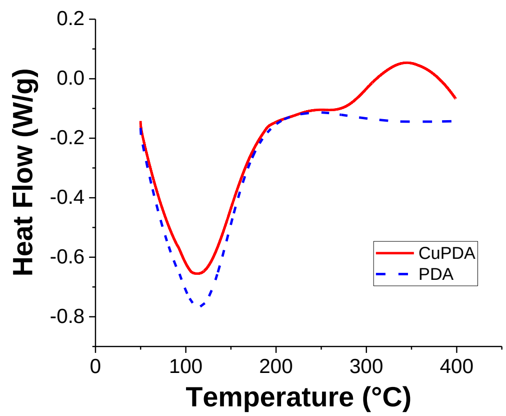

Figure 6.3: Heat flow during the heating of pristine and Cu doped PDA powders determined by differential scanning calorimetry.

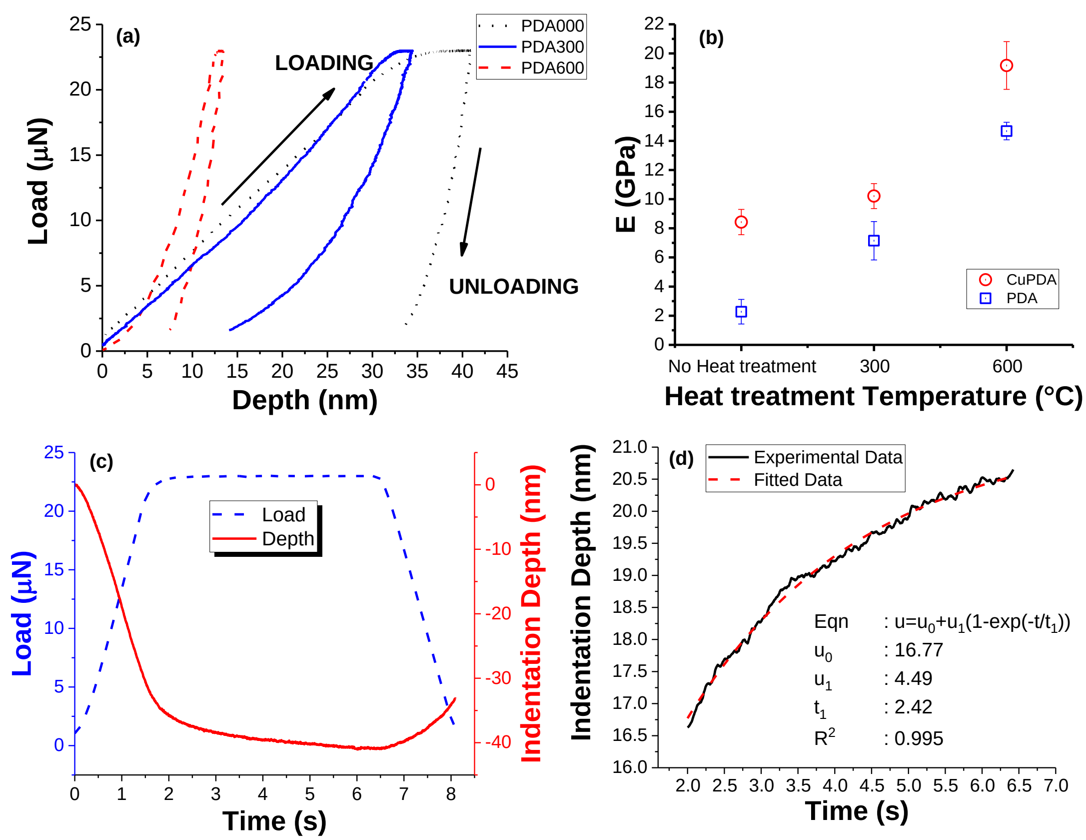

Figure 6.4: (a) Typical loading and unloading curve for PDA films with different treatment temperatures; (b) Young's modulus of pristine and Cu doped PDA film as a function of heat treatment temperature; (c) Typical time-dependent load and penetration curves during nanoindentation tests; (d) a selected curve showing time-dependent indentation depth during the hold period at peak load, and its fitting to the Generalized Kelvin model.

where u is the indentation depth; t is the holding time; u_0, u_1, and t_1 are fitting parameters, which may be considered as the magnitude of instantaneous deformation, magnitude of time-dependent deformation, and relaxation time, respectively. An example of curve fitting to equation (1) is shown in Figure 6.4 (d). Fitting results of experimental data to the Kelvin model is listed in Table 6.1. The increase in heat treatment temperature, as well as the addition of Cu, seems to decrease the constant u_0 and u_1, which is consistent with the trend observed in Young's modulus (Figure 6.4 (b)). Since u_0 represents the time-independent deformation and u_1 represents the time-dependent deformation, an increase in Young's modulus will result in decrease in both u_0 and u_1. For Cu-PDA samples, decreases in both u_1 and t_1 were observed with increasing temperature, implying the viscoelastic behavior was reduced in samples received heat treatment. However, the undoped PDA samples do not show a consistent trend in t_1, which deserves further investigation.

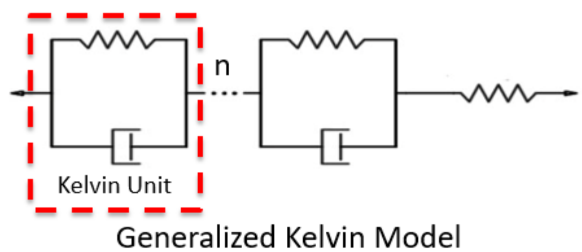

Scheme 6.1: Generalized Kelvin Model

Table 6.1: Average film thickness measured by AFM and fitting parameters to the general Kelvin creep model.

Sample	PDA	PDA300C	PDA600C	Cu-PDA	Cu-PDA300C	Cu-PDA600C
Thickness (nm)	570±26	276±48	65±9	512±23	393±37	55±9
u_0 (nm)	29.49±5.69	14.52±1.95	14.00±4.22	16.73±0.62	11.54±0.56	7.34±0.50
u_1 (nm)	4.54±0.42	1.18±0.24	0.81±0.13	3.74±0.56	0.89±0.26	0.43±0.03
t_1 (s)	2.02±0.35	4.92±0.46	2.60±1.67	2.43±0.25	2.18±0.41	0.50±0.11

6.4 Conclusions

In this work, mechanical properties of PDA and Cu ion doped PDA thin films were measured by nanoindentation technique. The Young's modulus of pristine PDA film without heat treatment was 2.3 ± 0.84 GPa. With heat treatment at 600˚C, this value increased to 14.7 ± 1.3 GPa. The addition of Cu ions in the PDA film increased the Young's modulus to 8.4 ± 0.9 GPa, which was further enhanced to 19.2 ± 1.6 GPa after heat treatment at 600˚C. Creep behavior was observed in both pure PDA and Cu-PDA, which can be described by a three-element generalized Kelvin model.

REFERENCES

[1] S. M. D. Haeshin Lee, William M. Miller, Phillip B. Messersmith, "Mussel-Inspired Surface Chemistry for Multifunctional Coatings," *Science,* vol. 318, 2007.

[2] H. Li *et al.*, "Structure Evolution and Thermoelectric Properties of Carbonized Polydopamine Thin Films," *ACS Appl Mater Interfaces,* vol. 9, no. 8, pp. 6655-6660, Mar 1 2017.

[3] X. Jiang, Y. Wang, and M. Li, "Selecting water-alcohol mixed solvent for synthesis of polydopamine nano-spheres using solubility parameter," *Sci Rep,* vol. 4, p. 6070, Aug 14 2014.

[4] J. H. Ryu, P. B. Messersmith, and H. Lee, "Polydopamine Surface Chemistry: A Decade of Discovery," *ACS Appl Mater Interfaces,* vol. 10, no. 9, pp. 7523-7540, Mar 7 2018.

[5] H. Li *et al.*, "Structural evolution and electrical properties of metal ion-containing polydopamine," *Journal of Materials Science,* vol. 54, no. 8, pp. 6393-6400, 2019.

[6] D. R. Dreyer, D. J. Miller, B. D. Freeman, D. R. Paul, and C. W. Bielawski, "Perspectives on poly(dopamine)," *Chemical Science,* vol. 4, no. 10, 2013.

[7] Y. Liu, K. Ai, and L. Lu, "Polydopamine and its derivative materials: synthesis and promising applications in energy, environmental, and biomedical fields," *Chem Rev,* vol. 114, no. 9, pp. 5057-115, May 14 2014.

[8] R. v. d. W. Martin E. Lynge, Almar Postma, Brigitte Stadler, "Polydopamine - a nature-inspired polymer coating for biomedical science," *Nanoscale,* vol. 3, 2011.

[9] C. E. Brubaker and P. B. Messersmith, "The present and future of biologically inspired adhesive interfaces and materials," *Langmuir,* vol. 28, no. 4, pp. 2200-5, Jan 31 2012.

[10] R. Li, K. Parvez, F. Hinkel, X. Feng, and K. Mullen, "Bioinspired wafer-scale production of highly stretchable carbon films for transparent conductive electrodes," *Angew Chem Int Ed Engl,* vol. 52, no. 21, pp. 5535-8, May 17 2013.

[11] Z. Jia *et al.*, "The Electrical conductivities and Tribological properties of Vacuum Hot-Pressed Cu/Reduced Graphene Oxide Composite," *Journal of Materials Engineering and Performance,* vol. 26, no. 9, pp. 4434-4441, 2017.

[12] S. Lin, C. T. Chen, I. Bdikin, V. Ball, J. Gracio, and M. J. Buehler, "Tuning heterogeneous poly(dopamine) structures and mechanics: in silico covalent cross-linking and thin film nanoindentation," *Soft Matter,* vol. 10, no. 3, pp. 457-64, Jan 21 2014.

[13] V. Ball *et al.*, "Deposition Mechanism and Properties of Thin Polydopamine Films for High Added Value Applications in Surface Science at the Nanoscale," *BioNanoScience*, vol. 2, no. 1, pp. 16-34, 2011.

[14] L. Klosterman, Z. Ahmad, V. Viswanathan, and C. J. Bettinger, "Synthesis and Measurement of Cohesive Mechanics in Polydopamine Nanomembranes," *Advanced Materials Interfaces,* vol. 4, no. 10, 2017.

[15] M. J. H. Niels Holten-Andersen, Henrik Birkedal, Bruce P. Lee, Phillip B. Messersmith, Ka Yee C. Lee, J. Herbert Waite, "pH-induced metal-ligand cross-links inspired by mussel yield self-healing polymer networks with near-covalent elastic moduli," *Proceedings of the National Academy of Sciences of the United States of Ameria,* vol. 108, no. 7, 2011.

[16] Q. Li, D. G. Barrett, P. B. Messersmith, and N. Holten-Andersen, "Controlling Hydrogel Mechanics via Bio-Inspired Polymer-Nanoparticle Bond Dynamics," *ACS Nano*, vol. 10, no. 1, pp. 1317-24, Jan 26 2016.

[17] W. Oliver and G. Pharr, "An improved technique for determining hardness and elastic modulus using load and displacement sensing indentation experiments," *J. Mater. Res.*, vol. 7, no. 6, 1992.

[18] Q. V. Le, F. Meftah, Q. C. He, and Y. Le Pape, "Creep and relaxation functions of a heterogeneous viscoelastic porous medium using the Mori-Tanaka homogenization scheme and a discrete microscopic retardation spectrum," *Mechanics of Time-Dependent Materials,* vol. 11, no. 3-4, pp. 309-331, 2008.

CHAPTER 7: POLYDOPAMINE (PDA) INDUCED SURFACE FUNCTIONALIZATION AND SYNTHESIS OF SELF-SUPPORTED NANO-CATALYSIS FOR HYDROGEN EVOLUTION REACTION (HER)

Chapter 7 is based on the following submitted manuscript

H. Li, J. Xi, A. Donaghue, J. Keum, K. An, Y. Zhao, E. McKenzie, and F. Ren, 'Polydopamine (PDA) induced surface functionalization and synthesis of self-supported nano-catalysis for hydrogen evolution reaction (HER)'

Polydopamine(PDA) induced surface functionalization and synthesis of self-supported nano-catalysis for hydrogen evolution reaction (HER)

Haoqi Li[1], Jiaxin Xi[1], Adrienne Donaghue[2], Jong Keum[3], Ke An[3], Yao Zhao[1], Erica McKenzie[2], Fei Ren[1]

[1]Department of Mechanical Engineering, Temple University, Philadelphia, PA 19122, USA

[2]Department of Civil & Environmental Engineering, Temple University, Philadelphia, PA 19122, USA

[3]Chemical and Engineering Materials Division, Oak Ridge National Laboratory, Oak Ridge, TN 37830, USA

Abstract

Polydopamine (PDA) is an emerging nature-inspired biopolymer material that possesses many interesting properties such as self-assemble and universal adhesive. It can also form coordination bonding with various metal ions, which can be later reduced to form metal nanoparticles after thermal annealing in protective environment. This interesting feature of the PDA has been utilized to synthesize several types of metal particles including Pt, Ni, Cu, and Ni-Cu alloy. The morphology and chemistry of these nanoparticles were examined using electron microscopic techniques, while their potential applications as catalysts in hydrogen evolution reaction for water splitting application was evaluated using an electronchemecial workstation. Our result has shown that the PDA-Pt composite possessed comparable performance to the Pt/C material. The catalytic performance of the PDA materials containing Cu, Ni, and Cu-Ni varied as a function of heat treatment temperature. This work demonstrated the feasibility of using PDA as a potential carbonaceous support for nanoparticulate metal catalysts, where processing simplicity and manufacturing scalability are appreciated.

KEYWORDS: Polydopamine, Metal nanoparticles, Hydrogen evolution reaction, catalysis

7.1 Introduction

With over a decade of research and exploration, polydopamine (PDA) has been found to possess multiple interesting properties such as capabilities of universal coating and self-assembly in alkaline solutions [1]. Thanks to its catechol function groups, PDA can also form coordination bonding with metal ions, especially with transition metal ions [2]. A handful of studies have reported making metal-PDA (M-PDA) composites from PDA materials containing Fe^{3+}, Ag^{+}, Au^{3+}, Pd^{2+}, Co^{2+}, Cu^{2+}, Ni^{2+}, W^{6+}, and etc. [3-8]. Direct reduction of noble metals such as Ag, Au, and Pd have been demonstrated without the addition of other reductants [5, 9-10]. Although non-precious metal ions cannot be reduced by PDA alone, other methods had been applied. Heat treatment was usually used in these processes to convert metal ions to metals or metal oxides. On the other hand, electron beam reduction had also demonstrated as a potential method in in-situ metal ion reduction [11].

Carbonization of PDA in inert atmosphere can convert insulating PDA into conductive cPDA [12]. It has exhibited a high electrical conductivity similar to or even higher than reduced graphene oxides, as high as 2.6×10^5 S/m. Li and coworkers [13] have successfully fabricated wafer-scale cPDA and transferred onto a soft substrate, making flexible electronic circuits and sensor, demonstrating the great potential of cPDA. In addition, our previous research [14] has also found that annealing the metal-doped PDA would not only convert PDA into conductive cPDA, but also converted metal-ions into nanoparticles (NPs). One potential application of such supported metal NPs is catalyst for chemical reactions, such as water splitting.

Electrochemical water splitting has attracted much attention for hydrogen production owing to its abilities to produce high purity hydrogen, which has the potential to serve as renewable energy storage media with zero carbon emission when consumed. The best performing single-phase element catalyst for hydrogen evolution reaction (HER) is Pt, which is not economically attractive for commercialization. Researchers have been focused on improving the overall efficiency of catalysis while cutting down the cost by various methods, including reducing the size or dimension of the material [15], attaching catalysis to porous substrates, and alloying Pt with non-precious metal [16], or replacing Pt with non-precious metal alloys [17]. While many studies have focused on the performance characterization of catalysts such as their over-potential and degradation, little change has been made to the commonly used fabrication method, which employs Nafion as a conductive binder to bind metal NPs onto conductive substrates.

In our present work, we utilized PDA's universal adhesive property and the ability to form coordination bonds with metal cations to synthesize self-supported metal NPs catalysis for HER. Pt NPs were directly reduced onto the conductive substrate with uniform distribution. Its HER performance was compared against commercially available Pt/C powder mounted on glassy carbon electrodes. Results showed our novel processing method simplified the process without sacrificing the performance. The new processing method was further extended to synthesize Cu, Ni, and Cu-Ni alloy NPs in thin films and powders of M-PDA. Their morphology and structure were studied and their HER performance was also measured and discussed.

7.2 Experimental Methods

7.2.1 Synthesis of metal NPs on PDA thin film and powder

Cu, Ni, and bi-elemental alloy attached to PDA were synthesized in two steps. First, 1:1 molar ratio of metal chlorides (Sigma-Aldrich, St. Louis, MO) and dopamine hydrochloride (99%, Alfa Aesar, Haverhill, MA) were added into 50 mL of 50 mM TRIS buffer (pH adjusted to 8.5 Thermo Fisher Scientific Inc., Waltham, MA). Substrates to be coated were submerged into the solution. Typical synthesis process would last for 24h. Powder samples were collected by centrifuge. Both coated substrates and powder were rinsed three times and then dried in an air oven at 50°C for overnight. In the second step, dried coatings and powders were heat treated under N_2 environment at 600°C, 800°C, 1000°C for 1hr in a tube furnace,

To make Pt samples, PDA coating on graphite rod (99.9995%, Alfa Aesar, Haverhill, MA) was first synthesized and washed. Powder $PtCl_4$ (>99.9%, Sigma-Aldrich, St. Louis, MO) is dissolved in D.I. water as Pt supply. Coated graphite rod was then immersed in 50mM $PtCl_4$ solution for 3h. The PDA coating would directly reduce the Pt^{4+} ions into Pt NPs, which remained on the PDA coating. The product was then heat treated at 800°C using the same procedure as previously described..

7.2.2 Structural characterization

Scanning electron microscopy (SEM, 10kV, FEI Quanta450 FEG SEM, FEI Inc. Hillsboro, OR) was used to characterize the surface of coated graphite rod, while transmission electron microscopy (TEM, 120kV, JEM-1400, JOEL, Tokyo, Japan) was used to characterize the nano particles on the annealed M-cPDA powder. In-situ X-ray diffraction (XRD, X'Pert Pro, Malvern PANalytical Ltd., Malvern, United Kingdom) was employed to conduct diffraction scan while heating up the powder samples. The temperature ranged from 50 ˚C to 850 ˚C with 5 ˚C steps, and the XRD scan was conducted in the 2θ range between 40˚ and 50˚, which contained the (111) peaks of Cu and Ni. To characterize the carbon phase in the metal NPs decorated, cPDA thin film, Raman spectroscopy was used with a 532 nm green laser for excitation. Inductively coupled mass spectrometry (ICP-MS, Agilent 7900, Agilent Technologies, Santa Clara, CA) was used to quantify the metal content in the powder samples.

7.2.3 Catalytic performance

Coated graphite rod samples were directly connected to the testing circuit and tested without further treatment after thermal annealing. However, only 15 mm of the rod was immersed under electrolyte to ensure consistent testing surface area. For comparison, Powder samples were deposited on 3-mm diameter glassy carbon electrodes. Ten milligrans of powder sample was mixed with 20 μL of Nafion binder, 5 mL water, and 5 mL alcohol with ultra-sonication. The mixed suspension was then drop-cast onto the electrodes using a pipette and dried in the oven. Commercially available Pt/C powder (40%, FuelCellStore, College Station, TX) was also tested in this study. M-cPDA powder fabricated by the previously mentioned method was used as a comparison to coated M-cPDA samples.

To evaluate the electrochemical behavior, current-voltage scans were conducted using an electrochemical work station (Versastat 3, Ametek, Berwyn, PA) between 0 and -1V with a scan rate of 0.005V/s. Tests were conducted in sulfuric acid solution with a pH value of 0. Graphite rods and Ag/AgCl electrodes were used as the counter and the reference electrodes, respectively.

7.3 Results and discussions

As shown in Figure 7.1 (a), $PtCl_4$ was successfully reduced to Pt NPs by the PDA thin film without heat treatment or addition of other reductants. Pt NPs decorated on the PDA film were uniform with an average diameter of around 20 nm. The HER performance of Pt-PDA against Ag/AgCl reference electrode is shown in Figure 7.1 (b). Both Pt-PDA with and without thermal annealing showed lower overpotential at 10 mA/cm^2 comparing to the electrode fabricated using commercial Pt/C powder, The overpotential of thermally annealed Pt-PDA sample (245 mV) was slightly higher than that without thermal treatment (236 mV). Although thermal annealing could reduce the electrical resistance of the PDA film, it caused cracks in the PDA films due to thermal shrinkage. Although Pt-PDA had lower overpotential at the current density of 10 mA/cm^2 current density, the Pt/C sample outperformed the Pt-PDA sample at higher current densities.

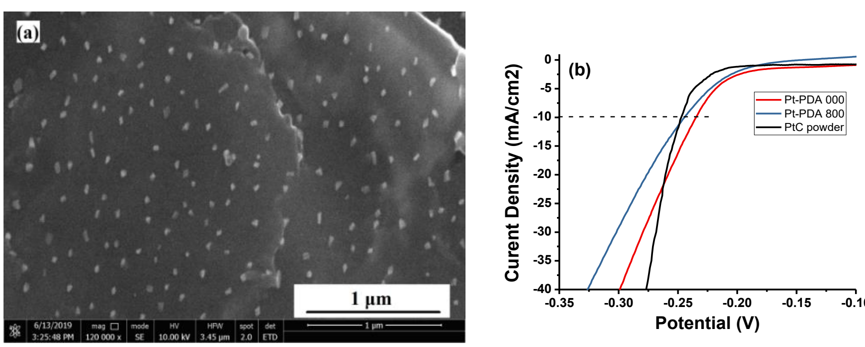

Figure 7.1: (a) SEM image of Pt-PDA coated on graphite rod; (b) catalytic performance of various samples (Pt-PDA, thermally annealed Pt-PDA, and commercial Pt/C) in pH=0 sulfuric acid solution against Ag/AgCl electrode.

On the other hand, for Cu, Ni, and Cu-Ni PDA samples, metal NPs were observed in powder samples, which were heat treated at 600 ˚C and above. As shown in Figure 7.2, as annealing temperature increases, metal NPs appeared and merged into larger particles. This phenomenon was also observed in M-PDA samples from our previous study [11]. After heat treatment at 600 ˚C, the average size of Cu NPs was approximately 50 nm, which increased to as large as 500 nm after heat treatment at 1000 ˚C. In addition to equiaxed particles, nanorods were also observed in the Cu-PDA samples. In contrast, the size of Ni NPs was about 5 nm after heat treatment at 600 ˚Cm which grew to approximately 100 nm after heat treatment at 1000 ˚C. The CuNi-PDA samples showed the coexistence of both larger and smaller particles, which could be Cu and Ni NPs, respectively. Heat treatment at a higher temperature seemed to affect the stability of the metal NPs, such that the total number of NPs and their overall volume were reduced.

For M-PDA coated on graphite rods, Cu and Ni NPs were also observed. At 600°C, Cu and Ni NPs were evenly distributed across the surface and it is similar to samples heat-treated at 800°C (Figure 7.2 (j), (k)). However, when heat treated at 1000°C, Cu NPs merged into larger particles, which was similar to that observed on powder samples (Figure 7.2 (c)). Different from powder samples, bigger particles as large as 1 μm were observed on coated Ni-PDA film samples at 800 ˚C as shown in Figure 7.2 (k).

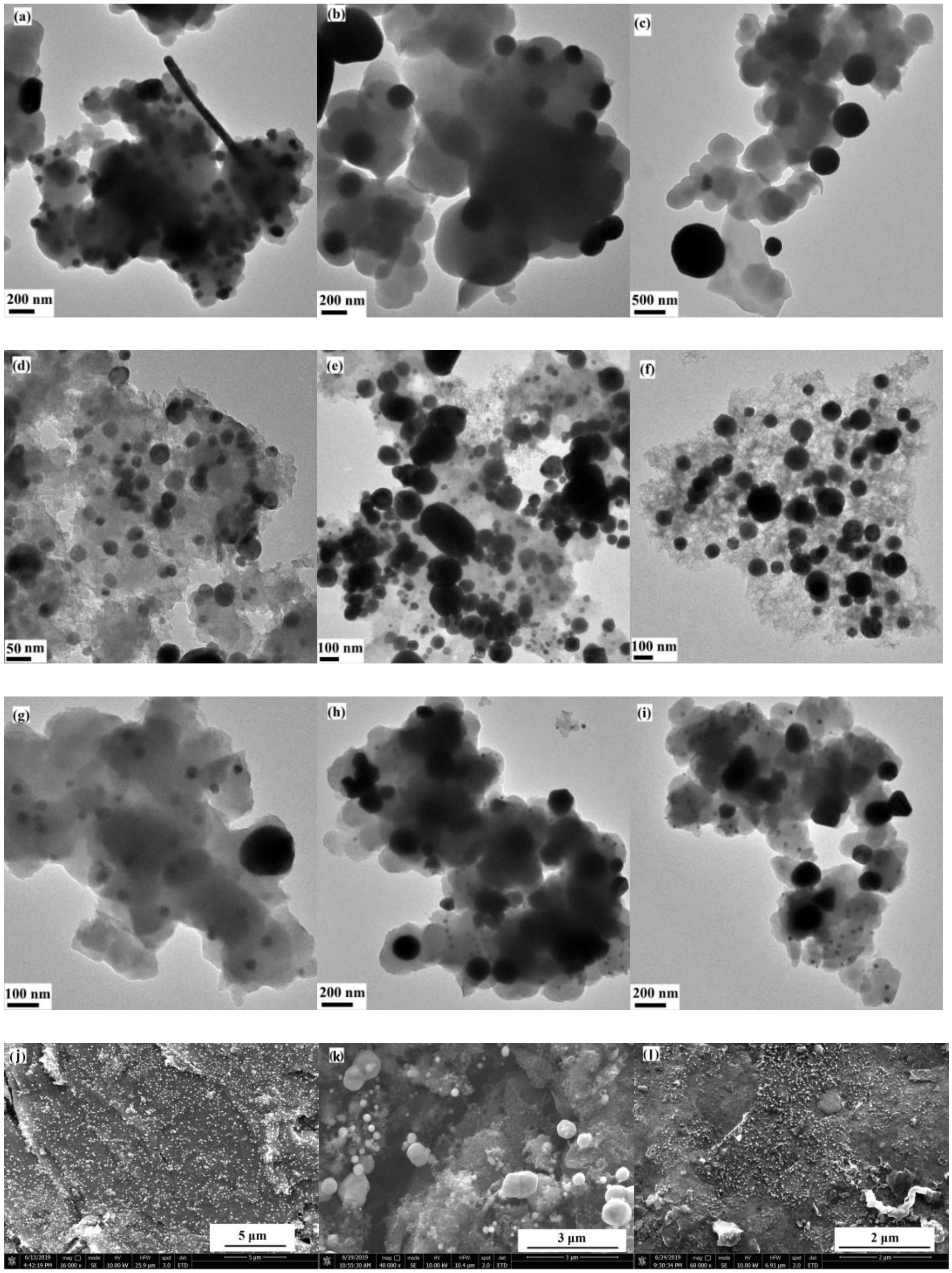

Figure 7.2: TEM images of Cu-PDA thermally annealed at (a) 600ºC, (b) 800 ºC, (c) 1000˚C; Ni-PDA thermally annealed at (d) 600 ºC, (e) 800 ºC, (f) 1000˚C; and CuNi-PDA thermally annealed at (g) 600 ºC, (h) 800 ºC, (i)1000 ˚C. SEM images of M-PDA samples containing (j) Cu, (k) Ni, and (l) Cu-Ni NPs.

ICP-MS revealed the content of metal ions within the M-PDA system, the results are shown in Table 7.1. With single element doping, the molar ratio of Cu to PDA was 1:6.11, while the ratio between Ni and PDA was 1:2.78. This is likely due to that Cu has a higher coordination number comparing to Ni [14, 18]. In addition, the final molar ratio of metal ion to PDA is usually less than the theoretical coordination number owing to the spatial arrangement of the polymer. However, when Ni^{2+} and Cu^{2+} ions were added together, the Cu^{2+} dominates the bonding site in PDA. Comparing to Cu-PDA without Ni^{2+}, the addition of Ni^{2+} promoted the chelation of Cu^{2+} with PDA and the molar ratio of PDA to Cu^{2+} increased to 2.79. This is possible owing to the higher activity of Ni, and higher stability of Cu in bio-complex coordination [19], which resulted in the replacement of Ni by Cu.

Table 7.1: ICP-MS Results of Metal to PDA Molar Ratio in M-PDA

Sample	Cu-PDA	Ni-PDA	CuNi-PDA	
Metal type	Cu	Ni	Cu	Ni
PDA to Metal Ratio	6.11	2.78	2.79	53.65

In-situ XRD was used to study the phase evolution in meta-PDA composites (Figure 7.3). For Cu-PDA, the (111) peak at $2\theta = 43^\circ$ first appeared at 350˚C. And for Ni-PDA, the (111) peak at $2\theta = 44^\circ$ first appeared at 380˚C. For the CuNi-PDA sample, a peak first appeared at 350˚C as Cu started to be reduced. Followed by precipitation of Ni, Cu and Ni started to form an alloy and a peak at $2\theta = 43.5^\circ$ emerged. As the temperature increased, and more Ni being reduced, the Cu peak at 43˚ merged into the peak at 43.5˚ and eventually fully converted into one peak [20]. This experiment showed that coordinatively bonded Cu and Ni ions in PDA could form alloys after thermal annealing.

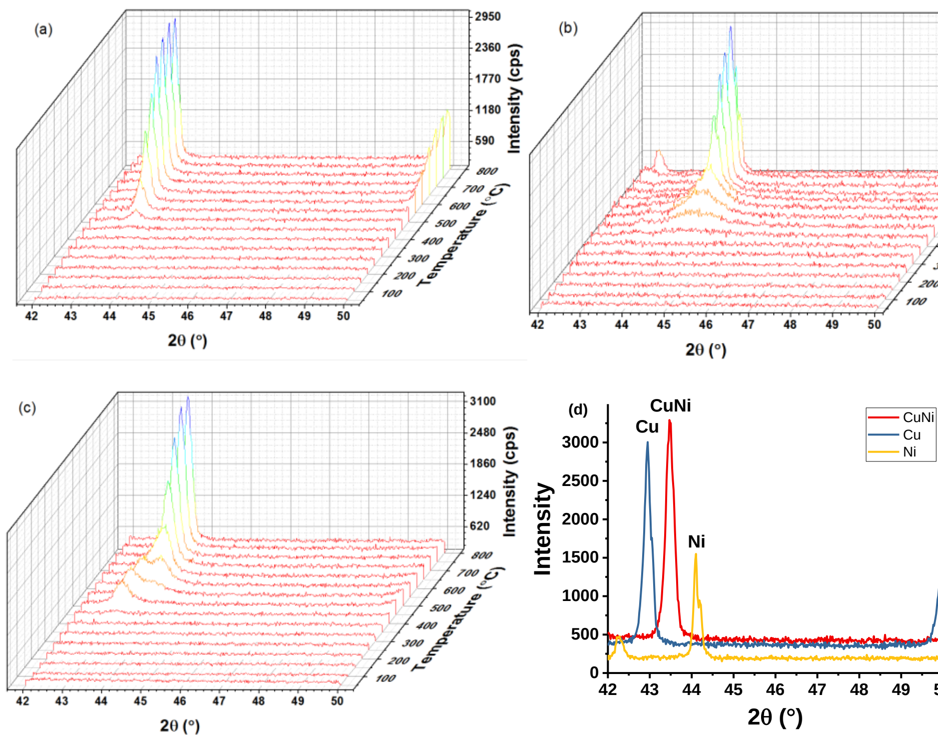

Figure 7.3: In-situ XRD waterfall plot for (a) Cu-PDA, (b) Ni-PDA, and (c) CuNi-PDA. (d) XRD peak of Cu, Ni, and CuNi-PDA annealed at 800 ˚C.

Figure 7.4 shows the I-V curves of the metal-PDA samples against Ag/AgCl reference electrode. For all samples, those thermally annealed at 600°C had similar overpotential comparing to samples annealed 800°C, while significant increase in overpotential was observed in 1000°C samples. This could be due to the growth of metal NPs leading to reduced surface area. Cu-PDA on graphite annealed at 600°C, 800°C, and 1000°C had an overpotential of 555 mV, 592 mV, and 599 mV at a current density of 10 mA/cm^2. On the other hand, Ni-PDA showed a better performance of 423 mV, 400 mV, and 581 mV. Based on the result of SEM and XRD, Cu-Ni alloy was formed during the annealing process and these NPs yields the best performance among all three samples with overpotentials of 421 mV, 415 mV, 541 mV. Although the conductivity of carbonized PDA increases with annealing temperature, which should result in a reduced overpotential, the growth of NP and thus the reduction of surface area at higher temperature would lead to an increase in the overpotential. In addition to the growth of the NPs, the cracking in the PDA film induced by thermal shrinkage could also reduce its electrical conductivity and thus increase the overpotential.

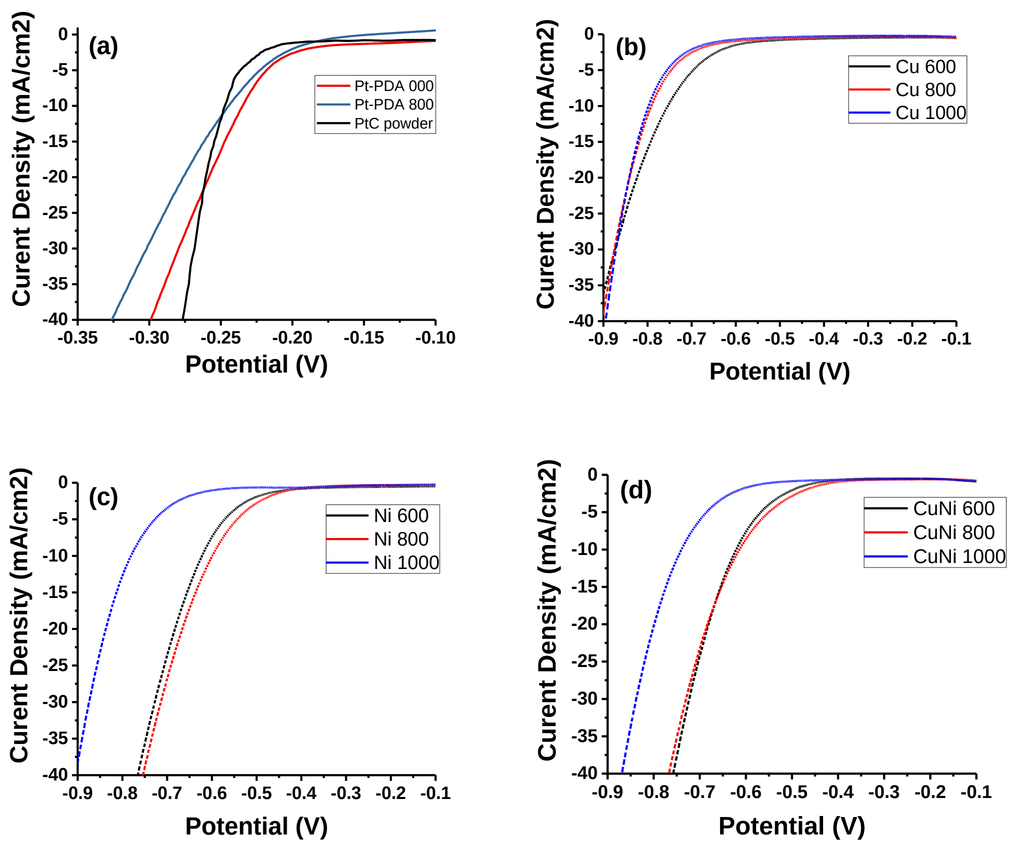

Figure 7.4: catalytic performance of (a) Pt-PDA, (b) Cu-PDA, (c) Ni-PDA, (d) CuNi-PDA, coated graphite rod annealed at different temperature in pH 0 sulfuric acid against Ag/AgCl electrode.

7.4 Conclusions

In this work, Pt has been successfully reduced and evenly decorated on the PDA substrate, which showed comparable catalytic performance to commercially available Pt/C. In addition, Cu and Ni metal ions had also been successfully reduced into metal NPs or nano-alloys by thermal annealing in inert atmosphere. The fabrication technique developed in this work is simple, which is based on a one-pot synthesis. Results from this work demonstrated the potentials of PDA assisted synthesis of self-supportive NPs as catalyst for water splitting application. With better control of the size, shape, and distribution of the metal nanoparticles, NPs decorated on conductive PDA thin film could also be used in many other applications beyond HER catalysis. .

REFERENCES

[1] S. M. D. Haeshin Lee, William M. Miller, Phillip B. Messersmith, "Mussel-Inspired Surface Chemistry for Multifunctional Coatings," *Science,* vol. 318, 2007.

[2] V. Ball, "Polydopamine films and particles with catalytic activity," *Catalysis Today,* vol. 301, pp. 196-203, 2018.

[3] K. M. Im, T.-W. Kim, and J.-R. Jeon, "Metal-Chelation-Assisted Deposition of Polydopamine on Human Hair: A Ready-to-Use Eumelanin-Based Hair Dyeing Methodology," *ACS Biomaterials Science & Engineering,* vol. 3, no. 4, pp. 628-636, 2017.

[4] T.-L. Chang, X. Yu, and J. F. Liang, "Polydopamine-enabled surface coating with nano-metals," *Surface and Coatings Technology,* vol. 337, pp. 389-395, 2018.

[5] W. Tamakloe, D. A. Agyeman, M. Park, J. Yang, and Y.-M. Kang, "Polydopamine-induced surface functionalization of carbon nanofibers for Pd deposition enabling enhanced catalytic activity for the oxygen reduction and evolution reactions," *Journal of Materials Chemistry A,* vol. 7, no. 13, pp. 7396-7405, 2019.

[6] X. Guo *et al.*, "Fabrication of Co@SiO2@C/Ni submicrorattles as highly efficient catalysts for 4-nitrophenol reduction," *Dalton Trans,* vol. 46, no. 35, pp. 11598-11607, Sep 12 2017.

[7] Y. Liang *et al.*, "Metal-polydopamine frameworks and their transformation to hollow metal/N-doped carbon particles," *Nanoscale,* vol. 9, no. 16, pp. 5323-5328, Apr 20 2017.

[8] C. Liu *et al.*, "Noble-metal-free tungsten oxide/carbon (WOx/C) hybrid manowires for highly efficient hydrogen evolution," *Nanotechnology,* vol. 28, no. 44, p. 445403, Nov 3 2017.

[9] H. Y. Son, J. H. Ryu, H. Lee, and Y. S. Nam, "Silver-Polydopamine Hybrid Coatings of Electrospun Poly(vinyl alcohol) Nanofibers," *Macromolecular Materials and Engineering,* vol. 298, no. 5, pp. 547-554, 2013.

[10] S. Du *et al.*, "New insights into the formation mechanism of gold nanoparticles using dopamine as a reducing agent," *J Colloid Interface Sci,* vol. 523, pp. 27-34, Aug 1 2018.

[11] H. Li, Y. Zhao, Z. Zhang, G. Andaluri, and F. Ren, "Electron-beam induced in situ growth of self-supported metal nanoparticles in ion-containing polydopamine," *Materials Letters,* vol. 252, pp. 277-281, 2019.

[12] H. Li *et al.*, "Structure Evolution and Thermoelectric Properties of Carbonized Polydopamine Thin Films," *ACS Appl Mater Interfaces,* vol. 9, no. 8, pp. 6655-6660, Mar 1 2017.

[13] R. Li, K. Parvez, F. Hinkel, X. Feng, and K. Mullen, "Bioinspired wafer-scale production of highly stretchable carbon films for transparent conductive electrodes," *Angew Chem Int Ed Engl,* vol. 52, no. 21, pp. 5535-8, May 17 2013.

[14] H. Li *et al.*, "Structural evolution and electrical properties of metal ion-containing polydopamine," *Journal of Materials Science,* vol. 54, no. 8, pp. 6393-6400, 2019.

[15] J. Li and G. Zheng, "One-Dimensional Earth-Abundant Nanomaterials for Water-Splitting Electrocatalysts," *Adv Sci (Weinh),* vol. 4, no. 3, p. 1600380, Mar 2017.

[16] Z. Du, Y. Wang, J. Li, and J. Liu, "Facile fabrication of Pt–Ni alloy nanoparticles supported on reduced graphene oxide as excellent electrocatalysts for hydrogen evolution reaction in alkaline environment," *Journal of Nanoparticle Research,* vol. 21, no. 1, 2019.

[17] J. Greeley, T. F. Jaramillo, J. Bonde, I. B. Chorkendorff, and J. K. Norskov, "Computational high-throughput screening of electrocatalytic materials for hydrogen evolution," *Nat Mater,* vol. 5, no. 11, pp. 909-13, Nov 2006.

[18] L. Yang *et al.*, "Transition-metal-ion-mediated polymerization of dopamine: mussel-inspired approach for the facile synthesis of robust transition-metal nanoparticle-graphene hybrids," *Chemistry,* vol. 20, no. 25, pp. 7776-83, Jun 16 2014.

[19] D. G. Brewer, P. T. T. Wong, and M. C. Sears, "the nature of the coordination bond in metal complexes of substituted pyridine derivatives. III. 4- metylpyridine complexes of some divalent transition metal ions," *Canadian J. Chem,* vol. 46, 1968.

[20] Yong Zhang *et al.*, "Microstructures and properties of high-entropy alloys," *Prog. Mater. Sci.*, vol. 61, p. 93, 2014.

CHAPTER 8: CONCLUSIONS AND FUTURE WORK

In this study, structural, compositional, mechanical, electrical and thermal transport properties of PDA, cPDA, and M-PDA were characterized in details. A new method of fabricating self-supported metal nanoparticle (NP) with assistance of PDA has also been developed. The catalytic performance of self-supported metal NPs and alloys was also evaluated.

Electrical conductivity and Seebeck coefficient of PDA (**Chapter 3**) and M-PDA (**Chapter 4**) were measured as a function of heat treatment temperature on thin film materials. The highest electrical conductivity obtained in this study was 9.8×10^3 S/m from thin film samples thermally annealed at 800 °C, which correlated to the optimum thermoelectric power factor of 4×10^{-4} μW/m-K^2 (**Chapter 3** and **Chapter 4**). Although this value was lower compared to state-of-the-art thermoelectric materials, this study provided valuable insights into the electrical and thermal transport behavior of the PDA and cPDA thin film materials

Raman spectroscopy and neutron diffraction experiments revealed the growth of graphitical crystalline domains in PDA during heat treatment. Addition of metallic elements, such as Cu, would not prevent the carbonization of PDA into carbonized PDA (cPDA)..With higher heat treatment temperature, more carbon would be converted to the sp^2 state, forming the hexagonal structure. Furthermore, further heat treatment would separate Cu from the Cu-PDA system during the annealing to Cu NPs within the cPDA matrix. This phase separation was found to lower the conductivity and overall thermoelectric power factor of M-PDA material (**Chapter 3**).

Inspired by the precipitation of metal nanoparticle during thermal annealing of M-PDA, we utilized high energy electron in TEM to reduce metal cations into metal NPs in the M-PDA system (**Chapter 5**), including Co, Ni, and Cu doped PDA. Additionally, Cu NPs had been successfully synthesized on the surface of SiO_2 particles by electron beam irradiation. This finding opens up the potential of making self-supported metal catalysis on various substrates. The catalytic behavior of self-supported metal NPs in HER reactions was further studied (**Chapter 7**). Single element and bi-element Cu, and Ni are synthesized by annealing the M-PDA film or powders in an inert environment. Investigation of bi-elemental composition by ICP-MS showed Cu dominated the active sites and SEM images showed it grew into larger NPs comparing to Ni. The in-situ XRD also revealed the nucleation and growth temperature of each element, providing valuable insights for processing of these materials. Besides, direct reduction of Pt ions on PDA film was also tested. The HER performance was tested by measuring the overpotential of each sample coating at10 mA/cm^2. Ni-PDA showed a better catalysis activity comparing to Cu-PDA while similar to CuNi-PDA.

The mechanical properties of PDA thin film materials were tested by nano-indentation (**Chapter 6**). Young's modulus increased with respective to heat treatment temperature and the introduction of Cu dopant. It possible that heat treatment promoted the growth of carbon from amorphous to nanocrystalline; while the addition of dopant enhanced the crosslinking of PDA. As expected, phase separation on the Cu-cPDA was observed. Pristine PDA had a Young's modulus of 2.3 GPa, which increased to 14.7 GPa when heat treated at 600°C, as a result of carbonization. On the other hand, the Cu-PDA started with 8.4 GPa and increased to 19.2 GPa. In addition, as synthesized PDA showed creep behavior which can be described by modified Kelvin model.

The current work covered a wide range of PDA research. However, there remains many unknowns to be explored. For example, the catalysis performance of the M-cPDA for hydrogen evolution reaction could be improved if a better understanding of the reduction mechanism were acquired. In addition, it is worthwhile to study other properties of PDA-metal NPs such as the tribological properties and anti-bacterial behavior of Ag decorated PDA coating; optical properties of metal-ion doped PDA light; and chemical, photochemical reduction of PDA, etc.

With simple, one-pot fabrication and universal coating properties, PDA could potentially be used as an easy-to-process protective coating. Since PDA has similar structure to eumelanin, it possesses strong UV absorption property. The polymerization process of DA is an oxidization reaction; therefore, it could also be used as a reduction agent to protect substrate surface from oxidation. In addition, as mentioned before, cPDA has similar structure to N-doped graphene. Hence, cPDA could potentially be used in flexible electronics, wearable devices, sensors, and etc. On the other hand, the ability of PDA to form coordination bonding with metal cations can also been used to fabricate N-doped metal-polymer composite or even N doped metal-carbon composite. The final products may be utilized in catalytic applications.

BIBLIOGRAPHY

[1] C. A. Marsden, "Dopamine: the rewarding years," *Br J Pharmacol*, vol. 147 Suppl 1, pp. S136-44, Jan 2006.

[2] K. C. Berridge, T. E. Robinson, and J. W. Aldridge, "Dissecting components of reward: 'liking', 'wanting', and learning," *Curr Opin Pharmacol,* vol. 9, no. 1, pp. 65-73, Feb 2009.

[3] H. Lee, S. M. Dellatore, W. M. Miller, and P. B. Messersmith, "Mussel-Inspired Surface Chemistry for Multifunctional Coatings " *science*, vol. 318, p. 5, 2007.

[4] K. S. Schanze, H. Lee, and P. B. Messersmith, "Ten Years of Polydopamine: Current Status and Future Directions," *ACS Appl Mater Interfaces,* vol. 10, no. 9, pp. 7521-7522, Mar 7 2018.

[5] M. E. Lynge, R. van der Westen, A. Postma, and B. Stadler, "Polydopamine - a nature-inspired polymer coating for biomedical science," *Nanoscale,* vol. 3, p. 13, 2011.

[6] b. l. G. A.J. Hamilton, "Melanins in fungal pathogens," *Journal of Medical Microbiology,* vol. 51, 2002.

[7] N. Kollias, "the spectroscopy of human melanin pigmentation," *Melanin: its role in human photoprotection,* 1995.

[8] J. H. Ryu, P. B. Messersmith, and H. Lee, "Polydopamine Surface Chemistry: A Decade of Discovery," *ACS Appl Mater Interfaces,* vol. 10, no. 9, pp. 7523-7540, Mar 7 2018.

[9] J. Kong *et al.*, "Highly electrically conductive layered carbon derived from polydopamine and its functions in SnO2-based lithium ion battery anodes," *Chem Commun (Camb),* vol. 48, no. 83, pp. 10316-8, Oct 25 2012.

[10] X. Yu, H. Fan, L. Wang, and Z. Jin, "Formation of polydopamine nanofibers with the aid of folic acid," *Angew Chem Int Ed Engl,* vol. 53, no. 46, pp. 12600-4, Nov 10 2014.

[11] Z. Wang *et al.*, "Tunable, Metal-Loaded Polydopamine Nanoparticles Analyzed by Magnetometry," *Chemistry of Materials,* vol. 29, no. 19, pp. 8195-8201, 2017.

[12] T.-L. Chang, X. Yu, and J. F. Liang, "Polydopamine-enabled surface coating with nano-metals," *Surface and Coatings Technology,* vol. 337, pp. 389-395, 2018.

[13] Z. Wang *et al.,* "High Relaxivity Gadolinium-Polydopamine Nanoparticles," *Small*, vol. 13, no. 43, Nov 2017.

[14] D. Zhou *et al.*, "Fe/N/C hollow nanospheres by Fe(iii)-dopamine complexation-assisted one-pot doping as nonprecious-metal electrocatalysts for oxygen reduction," *Nanoscale,* vol. 7, no. 4, pp. 1501-9, Jan 28 2015.

[15] Y. Zhao, C. Wang, J. Liu, and F. Wang, "PDA-assisted formation of ordered intermetallic CoPt3 catalysts with enhanced oxygen reduction activity and stability," *Nanoscale,* vol. 10, no. 19, pp. 9038-9043, May 17 2018.

[16] D. Champier, "Thermoelectric generators: A review of applications," *Energy Conversion and Management,* vol. 140, pp. 167-181, 2017.

[17] C. E. Brubaker and P. B. Messersmith, "The present and future of biologically inspired adhesive interfaces and materials," *Langmuir,* vol. 28, no. 4, pp. 2200-5, Jan 31 2012.

[18] Y. Liu, K. Ai, and L. Lu, "Polydopamine and its derivative materials: synthesis and promising applications in energy, environmental, and biomedical fields," *Chem Rev,* vol. 114, no. 9, pp. 5057-115, May 14 2014.

[19] D. R. Dreyer, D. J. Miller, B. D. Freeman, D. R. Paul, and C. W. Bielawski, "Perspectives on poly(dopamine)," *Chemical Science,* vol. 4, no. 10, 2013.

[20] N. Farnad, K. Farhadi, and N. H. Voelcker, "Polydopamine Nanoparticles as a New and Highly Selective Biosorbent for the Removal of Copper (II) Ions from Aqueous Solutions," *Water, Air, & Soil Pollution,* vol. 223, no. 6, pp. 3535-3544, 2012.

[21] R. Cai *et al.*, "One-Step Synthesis of Silver Nanoparticles on Polydopamine-Coated Sericin/Polyvinyl Alcohol Composite Films for Potential Antimicrobial Applications," *Molecules,* vol. 22, no. 5, Apr 30 2017.

[22] S. Ryu *et al.*, "Direct Insulation-to-Conduction Transformation of Adhesive Catecholamine for Simultaneous Increases of Electrical Conductivity and Mechanical Strength of CNT Fibers," *Adv Mater,* vol. 27, no. 21, pp. 3250-5, Jun 3 2015.

[23] R. Zou *et al.*, "Carbonized polydopamine nanoparticle reinforced graphene films with superior thermal conductivity," *Carbon,* vol. 149, pp. 173-180, 2019.

[24] O. Bubnova and X. Crispin, "Towards polymer-based organic thermoelectric generators," *Energy & Environmental Science,* vol. 5, no. 11, 2012.

[25] Y. Xuan *et al.*, "Thermoelectric properties of conducting polymers: The case of poly(3-hexylthiophene)," *Physical Review B,* vol. 82, no. 11, 2010.

[26] Q. H. Bed Poudel, Yi Ma, Yucheng Lan, Austin Minnich, Bo Yu, Xiao Yan, Dezhi Wang, Andrew Muto, Daryoosh Vashaee, Xiaoyuan Chen, Junming Liu, Mildred S. Dresselhaus, Gang Chen, Zhifeng Ren, "High thermoelectric performance of nanostructured bismuth antimony telluride bulk alloys," *Science,* vol. 320, 2008.

[27] E. S. Venkatasubramanian Rama, Thomas Colpitts, Brooks O'Quinn, "Thin-film thermoelectric devices with high room-temperature Figures of merit," *Nature,* vol. 413, 2001.

[28] H. J. Goldsmid, "The Electrical Conductivity and Thermoelectric Power of Bismuth Telluride," *Proceedings of the Physical Society,* vol. 71, no. 4, 1958.

[29] B. Russ, A. Glaudell, J. J. Urban, M. L. Chabinyc, and R. A. Segalman, "Organic thermoelectric materials for energy harvesting and temperature control," *Nature Reviews Materials,* vol. 1, no. 10, 2016.

[30] S. Trasatti, "Work function, electronegativity, and electrochemical behaviour of metals: III. Electrolytic hydrogen evolution in acid solutions," *J. Electroanal. Chem. Interfacial Electrochem.,* vol. 39, no. 1, p. 22, 1972.

[31] P. Quaino, F. Juarez, E. Santos, and W. Schmickler, "Volcano plots in hydrogen electrocatalysis - uses and abuses," *Beilstein J Nanotechnol,* vol. 5, pp. 846-54, 2014.

[32] D. He *et al.*, "Amorphous nickel boride membrane on a platinum-nickel alloy surface for enhanced oxygen reduction reaction," *Nat Commun,* vol. 7, p. 12362, Aug 9 2016.

[33] B. Zhang, C. Xiao, S. Xie, J. Liang, X. Chen, and Y. Tang, "Iron–Nickel Nitride Nanostructures in Situ Grown on Surface-Redox-Etching Nickel Foam: Efficient and Ultrasustainable Electrocatalysts for Overall Water Splitting," *Chemistry of Materials,* vol. 28, no. 19, pp. 6934-6941, 2016.

[34] P. W. Menezes *et al.*, "Uncovering the Nature of Active Species of Nickel Phosphide Catalysts in High-Performance Electrochemical Overall Water Splitting," *ACS Catalysis,* vol. 7, no. 1, pp. 103-109, 2016.

[35] M. P. Browne *et al.*, "The goldilocks electrolyte: examining the performance of iron/nickel oxide thin films as catalysts for electrochemical water splitting in various aqueous NaOH solutions," *Journal of Materials Chemistry A,* vol. 4, no. 29, pp. 11397-11407, 2016.

[36] V. Vij *et al.*, "Nickel-Based Electrocatalysts for Energy-Related Applications: Oxygen Reduction, Oxygen Evolution, and Hydrogen Evolution Reactions," *ACS Catalysis,* vol. 7, no. 10, pp. 7196-7225, 2017.

[37] J. Duan, S. Chen, and C. Zhao, "Ultrathin metal-organic framework array for efficient electrocatalytic water splitting," *Nat Commun,* vol. 8, p. 15341, Jun 5 2017.

[38] M. Gong *et al.*, "Nanoscale nickel oxide/nickel heterostructures for active hydrogen evolution electrocatalysis," *Nat Commun,* vol. 5, p. 4695, Aug 22 2014.

[39] K. S. Rao, K. El-Hami, T. Kodaki, K. Matsushige, and K. Makino, "A novel method for synthesis of silica nanoparticles," *J Colloid Interface Sci,* vol. 289, no. 1, pp. 125-31, Sep 1 2005.

[40] M. Krogsgaard, V. Nue, and H. Birkedal, "Mussel-Inspired Materials: Self-Healing through Coordination Chemistry," *Chemistry,* vol. 22, no. 3, pp. 844-57, Jan 18 2016.

[41] S. Meng and E. Kaxiras, "Theoretical models of eumelanin protomolecules and their optical properties," *Biophys J,* vol. 94, no. 6, pp. 2095-105, Mar 15 2008.

[42] S. Hong, Y. S. Na, S. Choi, I. T. Song, W. Y. Kim, and H. Lee, "Non-Covalent Self-Assembly and Covalent Polymerization Co-Contribute to Polydopamine Formation," *Advanced Functional Materials,* vol. 22, no. 22, pp. 4711-4717, 2012.

[43] J. Liebscher *et al.*, "Structure of polydopamine: a never-ending story?," *Langmuir,* vol. 29, no. 33, pp. 10539-48, Aug 20 2013.

[44] D. R. Dreyer, D. J. Miller, B. D. Freeman, D. R. Paul, and C. W. Bielawski, "Elucidating the structure of poly(dopamine)," *Langmuir,* vol. 28, no. 15, pp. 6428-35, Apr 17 2012.

[45] Y. Hong, Z. Tang, and Z. Zhang, "Enhanced electrochemical properties of LiMnPO4/C composites by tailoring polydopamine-derived carbon coating," *Electrochimica Acta,* vol. 176, pp. 369-377, 2015.

[46] R. Li, K. Parvez, F. Hinkel, X. Feng, and K. Mullen, "Bioinspired wafer-scale production of highly stretchable carbon films for transparent conductive electrodes," *Angew Chem Int Ed Engl,* vol. 52, no. 21, pp. 5535-8, May 17 2013.

[47] K. Ai, Y. Liu, C. Ruan, L. Lu, and G. M. Lu, "Sp2 C-dominant N-doped carbon sub-micrometer spheres with a tunable size: a versatile platform for highly efficient oxygen-reduction catalysts," *Adv Mater,* vol. 25, no. 7, pp. 998-1003, Feb 20 2013.

[48] X. Yu, H. Fan, Y. Liu, Z. Shi, and Z. Jin, "Characterization of carbonized polydopamine nanoparticles suggests ordered supramolecular structure of polydopamine," *Langmuir,* vol. 30, no. 19, pp. 5497-505, May 20 2014.

[49] J. Ryu, S. H. Ku, M. Lee, and C. B. Park, "Bone-like peptide/hydroxyapatite nanocomposites assembled with multi-level hierarchical structures," *Soft Matter,* vol. 7, no. 16, 2011.

[50] A. C. Ferrari and J. Robertson, "Raman spectroscopy of amorphous, nanostructured, diamond-like carbon, and nanodiamond," *Philos Trans A Math Phys Eng Sci*, vol. 362, no. 1824, pp. 2477-512, Nov 15 2004.

[51] A. C. Ferrari, "Raman spectroscopy of graphene and graphite: Disorder, electron–phonon coupling, doping and nonadiabatic effects," *Solid State Communications,* vol. 143, no. 1-2, pp. 47-57, 2007.

[52] P. Trucano and R. Chen, "Structure of graphite by neutron diffraction," *Nature,* vol. 258, p. 2, 1975.

[53] K. S. Novoselov *et al.*, "Two-dimensional gas of massless Dirac fermions in graphene," *Nature,* vol. 438, no. 7065, pp. 197-200, Nov 10 2005.

[54] Y. Ouyang and J. Guo, "A theoretical study on thermoelectric properties of graphene nanoribbons," *Applied Physics Letters,* vol. 94, no. 26, 2009.

[55] Y. M. Zuev, W. Chang, and P. Kim, "Thermoelectric and magnetothermoelectric transport measurements of graphene," *Phys Rev Lett,* vol. 102, no. 9, p. 096807, Mar 6 2009.

[56] P. Wei, W. Bao, Y. Pu, C. N. Lau, and J. Shi, "Anomalous thermoelectric transport of Dirac particles in graphene," *Phys Rev Lett,* vol. 102, no. 16, p. 166808, Apr 24 2009.

[57] J. G. Checkelsky and N. P. Ong, "Thermopower and Nernst effect in graphene in a magnetic field," *Physical Review B,* vol. 80, no. 8, 2009.

[58] D. Dragoman and M. Dragoman, "Giant thermoelectric effect in graphene," *Applied Physics Letters,* vol. 91, no. 20, 2007.

[59] N. Xiao *et al.*, "Enhanced thermopower of graphene films with oxygen plasma treatment," *ACS Nano,* vol. 5, no. 4, pp. 2749-55, Apr 26 2011.

[60] Y. Xu, Z. Li, and W. Duan, "Thermal and thermoelectric properties of graphene," *Small,* vol. 10, no. 11, pp. 2182-99, Jun 12 2014.

[61] P. Dollfus, V. Hung Nguyen, and J. Saint-Martin, "Thermoelectric effects in graphene nanostructures," *J Phys Condens Matter,* vol. 27, no. 13, p. 133204, Apr 10 2015.

[62] J. Choi, N. D. K. Tu, S.-S. Lee, H. Lee, J. S. Kim, and H. Kim, "Controlled oxidation level of reduced graphene oxides and its effect on thermoelectric properties," *Macromolecular Research,* vol. 22, no. 10, pp. 1104-1108, 2014.

[63] D. G. Cahill, "Analysis of heat flow in layered structures for time-domain thermoreflectance," *Rev Sci Instrum,* vol. 75, no. 12, p. 4, 2004.

[64] K. Kang, Y. K. Koh, C. Chiritescu, X. Zheng, and D. G. Cahill, "Two-tint pump-probe measurements using a femtosecond laser oscillator and sharp-edged optical filters," *Rev Sci Instrum,* vol. 79, no. 11, p. 114901, Nov 2008.

[65] J. P. Feser and D. G. Cahill, "Probing anisotropic heat transport using time-domain thermoreflectance with offset laser spots," *Rev Sci Instrum,* vol. 83, no. 10, p. 104901, Oct 2012.

[66] J. P. Feser, J. Liu, and D. G. Cahill, "Pump-probe measurements of the thermal conductivity tensor for materials lacking in-plane symmetry," *Rev Sci Instrum,* vol. 85, no. 10, p. 104903, Oct 2014.

[67] A. J. Schmidt, K. C. Collins, A. J. Minnich, and G. Chen, "Thermal conductance and phonon transmissivity of metal–graphite interfaces," *Journal of Applied Physics,* vol. 107, no. 10, 2010.

[68] H. Li *et al.*, "Structure Evolution and Thermoelectric Properties of Carbonized Polydopamine Thin Films," *ACS Appl Mater Interfaces,* vol. 9, no. 8, pp. 6655-6660, Mar 1 2017.

[69] X. Jiang, Y. Wang, and M. Li, "Selecting water-alcohol mixed solvent for synthesis of polydopamine nano-spheres using solubility parameter," *Sci Rep,* vol. 4, p. 6070, Aug 14 2014.

[70] Y. Chen, Y. Zhao, and Z. Liang, "Solution processed organic thermoelectrics: towards flexible thermoelectric modules," *Energy & Environmental Science,* vol. 8, no. 2, pp. 401-422, 2015.

[71] Z. Jia *et al.*, "Electrical and mechanical properties of poly(dopamine)-modified copper/reduced graphene oxide composites," *Journal of Materials Science,* vol. 52, no. 19, pp. 11620-11629, 2017.

[72] Z. Jia *et al.*, "Preparation and electrical properties of sintered copper powder compacts modified by polydopamine-derived carbon nanofilms," *Journal of Materials Science,* vol. 53, no. 9, pp. 6562-6573, 2018.

[73] Y. Zhao, H. Wang, B. Qian, H. Li, and F. Ren, "Copper-polydopamine composite derived from bioinspired polymer coating," *Journal of Alloys and Compounds,* vol. 742, pp. 191-198, 2018.

[74] K. M. Im, T.-W. Kim, and J.-R. Jeon, "Metal-Chelation-Assisted Deposition of Polydopamine on Human Hair: A Ready-to-Use Eumelanin-Based Hair Dyeing Methodology," *ACS Biomaterials Science & Engineering,* vol. 3, no. 4, pp. 628-636, 2017.

[75] S. Kim, T. Gim, and S. M. Kang, "Stability-enhanced polydopamine coatings on solid substrates by iron(III) coordination," *Progress in Organic Coatings,* vol. 77, no. 8, pp. 1336-1339, 2014.

[76] M. M. Harding, M. W. Nowicki, and M. D. Walkinshaw, "Metals in protein structures: a review of their principal features," *Crystallography Reviews,* vol. 16, no. 4, pp. 247-302, 2010.

[77] S. J. Flora and V. Pachauri, "Chelation in metal intoxication," *Int J Environ Res Public Health,* vol. 7, no. 7, pp. 2745-88, Jul 2010.

[78] C. B. Black, H.-W. Huang, and J. A. Cowan, "Biological coordination chemistry of magnesium, sodium, and potassium ions. Protein and nucleotide binding sites," *Coord. Chem. Rev.,* vol. 135/136, p. 38, 1994.

[79] D. G. Brewer, P. T. T. Wong, and M. C. Sears, "the nature of the coordination bond in metal complexes of substituted pyridine derivatives. III. 4- metylpyridine complexes of some divalent transition metal ions," *Canadian J. Chem,* vol. 46, 1968.

[80] N. F. Della Vecchia, R. Avolio, M. Alfè, M. E. Errico, A. Napolitano, and M. d'Ischia, "Building-Block Diversity in Polydopamine Underpins a Multifunctional Eumelanin-Type Platform Tunable Through a Quinone Control Point," *Advanced Functional Materials,* vol. 23, no. 10, pp. 1331-1340, 2013.

[81] B. V. Crist, *Handbook of Monochromatic XPS spectra: The Elements of Native Oxides*. Wiley, 2000, p. 548.

[82] H.-H. Huang, W.-C. Shih, and C.-H. Lai, "Nonpolar resistive switching in the Pt/MgO/Pt nonvolatile memory device," *Applied Physics Letters,* vol. 96, no. 19, 2010.

[83] Z. Jia *et al.*, "The Electrical conductivities and Tribological properties of Vacuum Hot-Pressed Cu/Reduced Graphene Oxide Composite," *Journal of Materials Engineering and Performance,* vol. 26, no. 9, pp. 4434-4441, 2017.

[84] Y. Li, J. Wen, M. Qin, Y. Cao, H. Ma, and W. Wang, "Single-Molecule Mechanics of Catechol-Iron Coordination Bonds," *ACS Biomaterials Science & Engineering,* vol. 3, no. 6, pp. 979-989, 2017.

[85] D. T. Sun *et al.*, "Rapid, Selective Heavy Metal Removal from Water by a Metal-Organic Framework/Polydopamine Composite," *ACS Cent Sci*, vol. 4, no. 3, pp. 349-356, Mar 28 2018.

[86] Y. Niu, X. Huang, L. Zhao, W. Hu, and C. M. Li, "One-Pot Synthesis of Co/CoFe2O4 Nanoparticles Supported on N-Doped Graphene for Efficient Bifunctional Oxygen Electrocatalysis," *ACS Sustainable Chemistry & Engineering*, vol. 6, no. 3, pp. 3556-3564, 2018.

[87] J. Huang, Y. Xu, Y. Xiao, H. Zhu, J. Wei, and Y. Chen, "Mussel-Inspired, Biomimetics-Assisted Self-Assembly of Co3O4 on carbon fibers for flexible supercapacitors," *ChemElectroChem*, vol. 4, no. 9, pp. 2269-2277, 2017.

[88] X. Guo *et al.*, "Fabrication of Co@SiO2@C/Ni submicrorattles as highly efficient catalysts for 4-nitrophenol reduction," *Dalton Trans*, vol. 46, no. 35, pp. 11598-11607, Sep 12 2017.

[89] Y. Liang *et al.*, "Metal-polydopamine frameworks and their transformation to hollow metal/N-doped carbon particles," *Nanoscale*, vol. 9, no. 16, pp. 5323-5328, Apr 20 2017.

[90] C. Liu *et al.*, "Noble-metal-free tungsten oxide/carbon (WOx/C) hybrid manowires for highly efficient hydrogen evolution," *Nanotechnology*, vol. 28, no. 44, p. 445403, Nov 3 2017.

[91] H. Song, Z. Wang, J. Yang, X. Jia, and Z. Zhang, "Facile synthesis of copper/polydopamine functionalized graphene oxide nanocomposites with enhanced tribological performance," *Chemical Engineering Journal*, vol. 324, pp. 51-62, 2017.

[92] X. Liu, H. Zheng, Z. Sun, A. Han, and P. Du, "Earth-Abundant Copper-Based Bifunctional Electrocatalyst for Both Catalytic Hydrogen Production and Water Oxidation," *ACS Catalysis*, vol. 5, no. 3, pp. 1530-1538, 2015.

[93] H. Zhong *et al.*, "Electrocatalytic Cobalt Nanoparticles Interacting with Nitrogen-Doped Carbon Nanotube in Situ Generated from a Metal-Organic Framework for the Oxygen Reduction Reaction," *ACS Appl Mater Interfaces*, vol. 9, no. 3, pp. 2541-2549, Jan 25 2017.

[94] Thomas Leonhard, Peter Florchinger, Alf Degen, Wolfgang Held, Soren Hinze, and E. Pott, "High-performance Ceramic Substrate for Catalytic Converters," *MTZ*, vol. 5, 2003.

[95] Ming-Yu Yen, Ching-Wen Chiu, Fu-Rong Chen, Ji-Jung Kai, Chi-Young Lee, and H.-T. Chiu, "Convergent Electron Beam Induced Growth of Copper

Nanostructures: Evidence of the Importance of a Soft Template," *Langmuir,* vol. 20, no. 2, 2004.

[96] N. Jiang, "Beam damage by the induced electric field in transmission electron microscopy," *Micron,* vol. 83, pp. 79-92, Apr 2016.

[97] Richard M. Crooks, Mingqi Zhao, Li Sun, Victor Chechik, and L. K. Yeung, "Dendrimer Encapsulated Metal Nanoparticles: Synthesis, Characterization, and Applications to Catalysis," *Accounts of Chemical Research,* vol. 34, 2001.

[98] G. Shi, S. Bao, W. Lai, Z. Rao, X. Zhang, and Z. Wang, "Electron beam induced growth of silver nanoparticles," *Scanning,* vol. 35, no. 2, pp. 69-74, Mar-Apr 2013.

[99] Michael J. Edmondson *et al.*, "Electron-Beam induced Growth of Bare Silver Nanowire from Zeolite Crystallites," *Adv. Mater.,* vol. 13, no. 21, 2001.

[100] P. A. Anderson *et al.*, "Production of Ultrafine Single-Crystal Copper Wires through Electron Beam Irradiation of Cu-containing Zeolite X," *J. Inorg. Gen. Chem,* vol. 631, no. 2-3, pp. 443-447, 2005.

[101] Ji-Jun Zou, Yue-ping Zhang, and C.-J. Liu, "Reduction of Supported Noble-Metal Ions Using Glow Discharge Plasma," *Langmuir,* vol. 22, 2006.

[102] R. F. Egerton, P. Li, and M. Malac, "Radiation damage in the TEM and SEM," *Micron,* vol. 35, no. 6, pp. 399-409, 2004.

[103] S. Lin, C. T. Chen, I. Bdikin, V. Ball, J. Gracio, and M. J. Buehler, "Tuning heterogeneous poly(dopamine) structures and mechanics: in silico covalent cross-linking and thin film nanoindentation," *Soft Matter,* vol. 10, no. 3, pp. 457-64, Jan 21 2014.

[104] V. Ball *et al.*, "Deposition Mechanism and Properties of Thin Polydopamine Films for High Added Value Applications in Surface Science at the Nanoscale," *BioNanoScience,* vol. 2, no. 1, pp. 16-34, 2011.

[105] L. Klosterman, Z. Ahmad, V. Viswanathan, and C. J. Bettinger, "Synthesis and Measurement of Cohesive Mechanics in Polydopamine Nanomembranes," *Advanced Materials Interfaces,* vol. 4, no. 10, 2017.

[106] M. J. H. Niels Holten-Andersen, Henrik Birkedal, Bruce P. Lee, Phillip B. Messersmith, Ka Yee C. Lee, J. Herbert Waite, "pH-induced metal-ligand cross-links inspired by mussel yield self-healing polymer networks with near-covalent elastic moduli," *Proceedings of the National Academy of Sciences of the United States of Ameria,* vol. 108, no. 7, 2011.

[107] Q. Li, D. G. Barrett, P. B. Messersmith, and N. Holten-Andersen, "Controlling Hydrogel Mechanics via Bio-Inspired Polymer-Nanoparticle Bond Dynamics," *ACS Nano,* vol. 10, no. 1, pp. 1317-24, 2016.

[108] W. Oliver and G. Pharr, "An improved technique for determining hardness and elastic modulus using load and displacement sensing indentation experiments," *J. Mater. Res.,* vol. 7, no. 6, 1992.

[109] Q. V. Le, F. Meftah, Q. C. He, and Y. Le Pape, "Creep and relaxation functions of a heterogeneous viscoelastic porous medium using the Mori-Tanaka homogenization scheme and a discrete microscopic retardation spectrum," *Mechanics of Time-Dependent Materials,* vol. 11, no. 3-4, pp. 309-331, 2008.

[110] H. Y. Son, J. H. Ryu, H. Lee, and Y. S. Nam, "Silver-Polydopamine Hybrid Coatings of Electrospun Poly(vinyl alcohol) Nanofibers," *Macromolecular Materials and Engineering,* vol. 298, no. 5, pp. 547-554, 2013.

[111] S. Du *et al.*, "New insights into the formation mechanism of gold nanoparticles using dopamine as a reducing agent," *J Colloid Interface Sci,* vol. 523, pp. 27-34, Aug 1 2018.

[112] J. Li and G. Zheng, "One-Dimensional Earth-Abundant Nanomaterials for Water-Splitting Electrocatalysts," *Adv Sci (Weinh),* vol. 4, no. 3, p. 1600380, Mar 2017.

[113] Z. Du, Y. Wang, J. Li, and J. Liu, "Facile fabrication of Pt–Ni alloy nanoparticles supported on reduced graphene oxide as excellent electrocatalysts for hydrogen evolution reaction in alkaline environment," *Journal of Nanoparticle Research,* vol. 21, no. 1, 2019.

[114] J. Greeley, T. F. Jaramillo, J. Bonde, I. B. Chorkendorff, and J. K. Norskov, "Computational high-throughput screening of electrocatalytic materials for hydrogen evolution," *Nat Mater,* vol. 5, no. 11, pp. 909-13, Nov 2006.

[115] L. Yang *et al.*, "Transition-metal-ion-mediated polymerization of dopamine: mussel-inspired approach for the facile synthesis of robust transition-metal nanoparticle-graphene hybrids," *Chemistry,* vol. 20, no. 25, pp. 7776-83, Jun 16 2014.

[116] Yong Zhang *et al.*, "Microstructures and properties of high-entropy alloys," *Prog. Mater. Sci.,* vol. 61, p. 93, 2014.